



University of Catania,
Faculty of Mathematical, Physical and Natural Sciences
Department of Physics and Astronomy

Marco Berritta

Coherent Nanostructures

Dynamics control and noise

**Thesis presented for the degree of
Doctor of Philosophy**

XXIV Cycle

SUPERVISOR: Prof. Giuseppe Falci

REFEREE: Prof. Giuseppe Angilella

Dedicated to
To my family

Acknowledgment

I would like to express my gratitude to Professor G. Falci, who was my Ph.D supervisor, for his support and guidance throughout the past four years. I'm also grateful to my father for his love and endless support during the years of my study and education and for all the encouragement he has always given me. I'm also grateful to Adriana for her patience and support during bad and good times.

Abstract

In the last three decades the scientific community has been attracted by the possibility of controlling quantum system, for example for quantum computing or quantum simulators. Initially this idea was exploited only in microscopic quantum system as atoms and molecules. However these systems present difficulties on the large scale application due to the extreme laboratory condition that they need, for example ultra low temperature $T \sim 1\mu K$. On the other hand, great progress has been made with superconducting nanodevices, that can be more easily scaled. One of the most important problems that arise in quantum control is decoherence. We will study quantum control for coherent superconducting nanodevices. This devices are affected by a Broad Band Colored and Structured (BBCS) noise, which is qualitatively different to what encountered in atomic physics, since it is characterized by a strong non-Markovian low-frequency component with a characteristic power spectrum $S(\omega) \propto \frac{1}{\omega}$. In this thesis we will present a roundup of physical situations, involving both undriven and externally driven open quantum systems, which need to be analyzed in the perspective of quantum control. Promising applications to superconducting nanodevices, as the implementation of Λ systems, possibly allowing control of microwave photons, are discussed in detail.

The thesis is structured as follows. Chapter 1 is an overview of the theoretical background of quantum control and quantum computation. In chapter 2 an archetypical problem for driven quantum systems, namely the Rabi problem, is studied in the presence of BBCS low-frequency noise¹, which is not accounted for in standard Master Equation treatments based on the Markovian assumption. In chapter 3 a protocol named STImulated Raman Adiabatic passage (STIRAP) is studied in the presence of BBCS noise, in view of its implementation in a class of superconducting nanodevices named Cooper Pair Box². This is done in chapter where Design and control requirements to achieve large efficiency are discussed, and a new figure of merit is introduced to characterize the tradeoff between efficient coupling of the control and noise. Actually selection rules due to charge-parity symmetry make impossible operate STIRAP in these device in the regime of maximum protection from noise. Therefore in chapter 5 we propose¹ a new implementation of STIRAP with superconductive device that allows us to circumvent selection rules, based on three-photon coherent processes and suitable crafted pulses compensating the Stark shifts. In chapter 6 we will study the problem of the tunneling of a quantum particle with strongly coupled environment in a bistable potential³. Finally in chapter 7 the study of the motion of a chiral quasiparticle in graphene affected by white noise will be presented⁴⁻⁶.

References

- (1) G. Falci, M. Berritta, et. al., "Driven superconducting nanodevices in the presence of low-frequency noise", *Physica Scripta*, **2012**, p.T151, (2012).
- (2) G. Falci, A. La Cognata, M. Berritta, A. D'Arrigo, B. Spagnolo, E. Paladino, "Optimizing STIRAP in a Cooper Pair Box", *subm. to Phys. Rev. B*.
- (3) P. Caldarà, A. La Cognata, D. Valenti, B. Spagnolo, M. Berritta, E. Paladino, G. Falci, *International Journal of Quantum Information (IJQI)*, **9**, p.119 (2011).
- (4) G. Falci, M. Morello, M. Berritta, A. D'Arrigo, E. Paladino, *Physica E*, **42**, p.584 (2010).
- (5) M. Berritta, E. Paladino, A. D'Arrigo and G. Falci, In: *Physics and Control*, IPACS Library p. 1987. (6) Talk presented at the International Conference "PHYSCON 2009", Catania, Sept. 1-4 2009.

Introduction

One of the biggest challenge for the scientific community nowadays is to achieve the controlled dynamics of quantum systems. This would have astonishing implication from the technological point of view. For example, achieving control of a sufficiently complex systems could pave the way to quantum simulators (hundreds of quantum bits) and quantum computer (thousand of quantum bits). A quantum control protocol can be performed only if the coherence time of the systems to be controlled is longer than the duration of the protocol.

Motivation: the superconducting nanodevices.

There are several class of systems that have been proposed for the implementation of quantum control protocols. Amongst them superconducting quantum devices[1] may offer advantages since fabrication techniques allow for scalability (at least in principle) to a large number of coupled qubits. In addition the possibility to apply the protocols used in the quantum optic realm[2, 3] for the photonics in the range of hundreds of GHz regime suggest the possibility of manipulating single photons in a completely different regime ($\sim 10GHz$) than optical(see for an example[4]).

Part of the work described in this thesis concern the study of the implementation of some quantum manipulation protocol in superconducting nanocircuit. As in all the systems proposed for control of quantum dynamics, the main source of decoherence (loss of coherence) is the noise[1].

The Broad Band Colored Structured (BBCS) noise

In particular superconducting nanodevice are subject to noise that extends over several decades with a power spectrum often of the kind $S(f) \sim 1/f$, which has a strong low-frequency component[5]. The origin of this spectrum is far to be completely understood. For example it may come from charged impurities in the so called “charge-based” superconducting device, but also pinned flux tubes in the totally different class of “flux-based” device show the same behavior. Several standard approaches, studied in the context of atomic and nuclear magnetic resonance systems, used to explain effects of noise are based on perturbative (Born approximation) schemes suited for Markovian noise. These approach can be used also in the case of superconducting nanodevices dynamics when studying the effects of the high-frequency part of the noise spectrum[3]. However they generally fail for the low frequency part of the noise spectra, which is not important in atomic systems but paramount in superconducting devices. Several stud-

ies had been made to tackle the problem of nonperturbative noise[6]. One of the purposes of this thesis is to apply a systematic procedure to take in account the effect of the whole spectrum of the broadband noise in the implementation of quantum control in superconducting devices.

The model: multistage approach.

It is well known that the noise can be modeled using an *environment* interacting with the system to be manipulated or controlled[6]. In this framework we will apply systematically a multistage approach [7, 5], consist in integrating the separate treatment of different parts of the noise spectrum. The first step consist in accounting the fast part of the noise spectrum with an appropriate master equation approach, that give us a first estimate of the purely exponential part of the decay of the coherences and of the relaxation of the quantum populations. The second step consists in applying the average over all the realization of the dynamics of the slow degrees of freedom of the environment. In particular it has been demonstrated that in solid state physics the zero order sampling of the stochastic process (the approximation of the different realization of stochastic processes with a single stochastic variable) despite its simplicity shows a very good agreement with experiments [5, 8]. We will refer to this approximation as the Static Path Approximation (SPA).

First step toward quantum control: Rabi oscillation.

Several control and computational protocol are based on the possibility to drive a quantum system with an *AC* field with appropriate frequency, that, if resonant with an energy splitting of the system, can generate the so called *Rabi oscillation*. The Rabi oscillations are a purely coherent effect that is cancelled by the noise. We calculated the limitation, due to broadband noise, of observing this phenomenon in superconducting devices, showing when they can be observed. Our results show a good agreement with the experimental results [7, 8].

Stimulated Raman adiabatic passage

A process that attracted a great interest in the last years is the so called STImulated Raman Adiabatic Passage process (STIRAP) [9]. This protocol allows to transfer population between two quantum levels using coupling with a third level that remains empty during the whole dynamics. More in detail, STIRAP consists in addressing a deeply anharmonic three level system ($|0\rangle, |1\rangle, |2\rangle$) prepared in the $|0\rangle$ state with two *AC* gaussian pulses,

called Stokes (in resonance with the $|1\rangle \leftrightarrow |2\rangle$ transition) and the Pump (in resonance with the $|0\rangle \leftrightarrow |2\rangle$ transition). For the success and the stability of the protocol two conditions have to be filled:

Adiabaticity of the pulses the pulses have to have a slow modulation to guarantee the adiabatic evolution of the *dressed states*

Counterintuitive sequence the pump pulse has to be switched on when the intensity of the Stokes pulse begins to decrease.

Under this condition during the process a trapped state (Dark state) belonging to the subspace $|0\rangle, |1\rangle$ is created. The Dark state evolves adiabatically from the state $|0\rangle$ to the state $|1\rangle$. In general the criticality of this protocol is related with the adiabaticity (which absence would populate the intermediate level $|2\rangle$ subject to decay) and to the perfect resonance of the driving pulses with the respective transition that is not fully guaranteed from the presence of low frequency (adiabatic) noise. The dynamics become more adiabatic increasing the peak amplitude of the driving pulses.

STIRAP in superconducting quantum devices.

In superconducting devices the symmetry that allows to define the most protected working point from noise is also the symmetry that cancels the coupling of the system with the pump pulse [10]. A problem addressed in this thesis is to find a compromise between noise protection and efficiency of coupling with the driving pulse. In particular we found a specific design and a specific setup for a class of superconducting nanodevices that should be capable to perform the STIRAP [10].

Toward the implementation of STIRAP at the optimal working point.

The possibility of generating Rabi oscillation in a multilevel system using a *two photon* coupling of two levels via a dispersive coupling with a third level has been experimentally demonstrated in superconducting devices [11, 12]. This opens the possibility of seeking the implementation of STIRAP with an improved scheme using a two-photon pump pulse allowing us to operate at an optimal working point minimizing the decoherence, even if the direct coupling is prevented by parity selection rules. We showed that this idea is applicable to obtain the transfer using the STIRAP. However some compensation is needed in order to cancel the Stark shift generated from the two-photon pump coupling in the system and then maintaining the correct condition of detuning [7]. We found that this is obtained by a

frequency modulation of the Stokes pulse profile. Using some optimal control theory tools, as in particular the so called Average Hamiltonian theory [13], we found an analytical form of pulses required. On the other hand the STIRAP process, especially in this configuration, need some care also to guarantee that the driving pulses satisfy the resonant condition only with the wanted level in order to evitate that the population go to level out from the *computational space*.

Dynamics of metastable states.

An other problem studied in the optics of quantum control in this thesis is a numerical study of the generalized master equation that describe the dynamics of a quantum particle in a tilted bistable potential[14]. We showed that, in agreement with the Zeno effect, the noise suppress the tunneling, generating a delay on the decay of metastable state populations.

Coherent dynamics of graphene quasi-particle.

In the last years several condensed matter systems, as for example graphene, showed interesting characteristic that can in principle be used in quantum computation and quantum control. Graphene has been isolated for the first time in 2004 [15]. The quasi-particle in graphene shows a peculiar behaviour related to the particular form of their Hamiltonian. The Hamiltonian of quasi-particle in graphene infact is reminiscent of the Hamiltonian of the zero mass Dirac Fermion[16]. This quasiparticle are characterized by a momentum and a pseudospin. As in the case of zero mass relativistic fermion they are chiral i.e. the momentum and pseudospin operator do not commute each other. This fact imply that the coherence in pseudospin spaces reflect in peculiar phenomena in the position dynamics as for example the *zitterbewegung*, that in principle have, in this context, a mesoscopic amplitude[17]. Also, the chirality suggest the possibility that the control over the pseudospin degree of freedom reflect in a control of the quasi-particle current[18]. For this reason we performed the calculation of the effect of the noise on the dynamics of wave packet and in particular on the *zitterbewegung*, showing that this phenomenon have also in this case mesoscopic amplitude, though partially suppressed.

Contents

1	Quantum Dynamics, Control, Noise	1
1.1	Representation and Dynamics	2
1.1.1	Representation of quantum systems	3
1.1.2	Time evolution	7
1.1.3	Transformations and picture for the dynamics	10
1.1.4	Quantum Computation and Advanced Control	12
1.2	Quantum hardware	14
1.2.1	Atoms, molecules, photons	14
1.2.2	Artificial atoms	14
1.2.3	Driven artificial atoms	17
1.3	Open quantum system	17
1.3.1	System-environment Hamiltonian	17
1.3.2	A roadmap to Broadband noise	19
1.3.3	Adiabatic noise and the SPA	21
1.3.4	Quantum noise and the Master Equation	22
1.3.5	Multistage elimination	24
1.4	Summary and general formalism	24
	Bibliography	25
2	Broadband noise effect on Rabi oscillation	29
2.1	The Rabi problem	30
2.1.1	Quasi resonant and transvers approximation (TR).	31
2.1.2	Rotating Wave Approximation (RWA).	31
2.1.3	Density matrix in the rotating frame.	32
2.1.4	Dynamics of Rabi oscillation	32
2.2	Rabi oscillation in Cooper pair box	33
2.3	Multistage elimination	34
2.3.1	Adiabatic noise effect	35
	Bibliography	39

3	STIRAP and other coherent process	41
3.1	Three level system	43
3.1.1	Scheme for a three level system in an external field	43
3.1.2	General Hamiltonian	43
3.1.3	Effective Hamiltonian and RWA	44
3.2	Coherent trapping and STIRAP	46
3.2.1	Coherent trapping in a Dark state	46
3.2.2	Population transfer	47
3.2.3	Coherent transfer and STIRAP	48
3.3	Adiabaticity condition for STIRAP	50
3.3.1	STIRAP on adiabatic representation	50
3.3.2	Adiabaticity: global and local criteria	50
3.3.3	General Hamiltonian	51
3.4	Phenomena involved in the STIRAP	51
3.5	Resilience to parameters	52
3.5.1	Resilience to delay	53
3.5.2	Symmetry of external field	54
3.5.3	Resilience to detuning	55
3.5.4	Correlaated detunings = $P(t_f \delta, a\delta)$	56
3.6	Conclusion	57
	Bibliography	57
4	Broadband noise effect on STIRAP protocol	59
4.1	Introduction	60
4.2	STIRAP in the Cooper Pair Box.	61
4.2.1	Implementation of the Λ system	61
4.3	Symmetries, decoherence, selection rules	63
4.3.1	Symmetries	63
4.3.2	Decoherence	64
4.3.3	Model for charge noise	65
4.3.4	Effective model for low-frequency noise in Λ configuration	67
4.4	Typical pattern of adiabatic eigenstate	68
4.5	Broadband noise in the CPB	69
4.6	Effects of low-frequency noise	70
4.6.1	Effect of high-frequency noise	71
4.6.2	STIRAP in the Quantronium	73
4.7	Optimal design of the device	74
4.8	Comparison of different mechanisms of dephasing	76
4.9	Conclusions	79
	Bibliography	80

5	STIRAP protocol with a two photon pump pulse	85
5.1	A two photon pump pulse	86
5.1.1	Adiabatic elimination	86
5.2	Three-photon STIRAP process	89
5.2.1	Model Hamiltonian	89
5.2.2	Doubly rotating frame	90
5.2.3	Stokes pulse optimization	90
5.2.4	Model Hamiltonian	92
5.3	Sensitivity to parameters	93
5.4	Toward implementation of three-photon STIRAP process in superconductive device	95
5.4.1	Validity of three level model	95
	Bibliography	96
6	Tunneling in a bistable potential with strong dissipation	99
6.1	The model	100
6.1.1	The Feynmann-Vernon approach	101
6.1.2	Discrete Variable Representation	103
6.2	Results	104
6.3	Conclusions	106
	Bibliography	107
7	Chiral quasiparticles in an environment	109
7.1	Introduction	110
7.1.1	Spin separation and Zitterbewegung	111
7.2	Model.	112
7.2.1	Dynamics in the QP-supported frame	113
7.2.2	Master equation.	114
7.2.3	One dimensional wavepacket	115
7.3	Results	116
7.3.1	Exact solution for longitudinal noise	116
7.3.2	Transverse white noise	117
7.4	Further remarks and conclusions	120
	Bibliography	120
A	Superconductin devices	123
A.1	The Quantronium	124
A.2	Transmon	125
	Bibliography	127

B	Average Hamiltonian theory for three photon STIRAP	129
B.1	Appropriate reference frame for the model Hamiltonian . . .	130
B.2	Time evolution operator	130
	Bibliography	132

List of Figures

1.1	The Cooper pair box	16
1.2	Graphene lattice	16
2.1	$\hat{\mathcal{S}}$ and $\hat{\mathcal{Z}}$ direction in the Bloch sphere	31
2.2	Rabi oscillation	32
2.3	Samples of Rabi oscillation in CPB with broadband noise . .	36
2.4	Linewidth for Rabi oscillation	38
3.1	Schemi Lambda, Vee e Ladder per sistema a tre livelli	43
3.2	Three level energetic spectra and detuning	45
3.3	Five stages of <i>STIRAP</i> process	53
3.4	Sensitivity of STIRAP to deley	54
3.5	Sensitivity of STIRAP to simmetry	55
3.6	Linewidth	56
3.7	Sensitivity to detunings	57
4.1	Counterintuitive sequence	62
4.2	SQUID geometry implementation of CPB	63
4.3	Energy spectrum of CPB and matrix element involved in Λ scheme	64
4.4	Characterization of the Landau-Zener (LZ) patterns of instantaneous eigenvalues	68
4.5	Population histories in the Quantronium in presence of low frequency noise.	71
4.6	Effect of high-frequency noise on STIRAP in Quantronium. .	73
4.7	Effect of slow noise in the Quantronium	75
4.8	Figure of merit of adiabaticity in function of the designs and working point.	75
4.9	Efficiency of STIRAP for different designed qubit	77
4.10	Motional narrowing	78
5.1	Lambda scheme for three-photon STIRAP process	89
5.2	STIRAP three-photons	91

5.3	Resiliency vs δ_2 3-STIRAP	93
5.4	Resilience vs τ/T 3-STIRAP	94
5.5	Resilience vs κ_p and vs κ_s 3-STIRAP	95
5.6	Efficiency of three photon STIRAP process for different design	96
6.1	102
6.2	Position representation	105
6.3	Energy representation	106
7.1	Reticolo della <i>graphene</i>	110
7.2	Autovalori di spin-separation per environment trasversale . .	116
7.3	Spin separation di un pacchetto d'onda in presenza di rumore	118
7.4	Spin separation of a wave packet in presence of noise	118
7.5	119
A.1	The Quantronium	125
A.2	Energy splitting in Transmon (perturbative estimate)	126
A.3	Energy splitting in Transmon (numerical estimate)	126

Chapter 1

Quantum Dynamics, Control and Noise

This chapter contains a general description of the theoretical tools necessary to address problems of quantum dynamics and quantum control. It also contains a description of some superconducting nanodevices and some material that are used, or are strong candidate, for the implementation of quantum control and quantum computation protocols.

In section 1.1 the mathematical structures used to describe the quantum systems and their dynamics will be briefly discussed. Here I will focus on the *density matrix* description of quantum dynamics [1, 2]. The density matrix description allows to study the *open quantum system* by introducing the concept of *reduced density matrix* that is used to take in account *decoherence* [3, 4, 5].

In section 1.2 some physical systems that show coherent behaviour are described. These systems are strong candidate for quantum control. In particular we will focus on the implementation of *artificial atoms* with superconducting nanodevices [6].

Section 1.3 describe a framework used to study the effect of noise on coherent dynamics that take in account the effect of broadband noise in a simple way [6, 7].

1.1 Representation and Dynamics

Quantum networks [3] are systems S , modeled as a collection of *nodes* s_μ , coupled by mutual *interactions*. Quantum nodes are n -state system, pure states being vectors $|\psi\rangle$ of a n -dimensional Hilbert space \mathbb{H} , whose basis are denoted by $\{|i\rangle; i = 0, \dots, n - 1\}$. The associated operators form also an Hilbert vector space, called the Liouville space \mathbb{L} .

This description of S may be convenient in physical situations where the interaction between nodes is weak or can be switched off. Localized (nuclear or electronic) spins in molecular and condensed-matter systems, or confined electrons in complex nanostructures can be naturally viewed as quantum networks. Quantum computers, where the interaction between nodes should be switchable and the dynamics should involve only few nodes at once, are another example.

The advantage of this description is that the general structure of the Hamiltonian, which includes control fields and external environment, and the algebraic structure of the time evolution can be formulated in a very effective way.

1.1.1 Representation of quantum systems

States

We consider a quantum node, the basis $\{|i\rangle; i = 1, \dots, n\}$ spanning \mathbb{H} . For a quantum node representing a nanodevice with Hamiltonian H_0 the associated eigenstates form a convenient reference basis, which we call “local basis” [6]. In this basis an arbitrary state is decomposed as

$$|\psi\rangle = \sum_{i=1}^n c_i |i\rangle$$

Operators

The set \mathbb{L} of all linear operators on \mathbb{H} is a vector space on the complex field, isomorphic to $\mathbb{C}^{n \times n}$, the set of all $n \times n$ matrices [3]. This *Liouville space* has therefore dimension $\dim(\mathbb{L}) = n^2$, as it can also be seen directly, by noticing that the n^2 *transition operators* [3, §2.2.1]

$$Q_k \equiv P_{ij} = |i\rangle \langle j| \quad (1.1)$$

are linearly independent and form a basis of \mathbb{L} . We denote the generic basis of \mathbb{L} by $\{Q_l : l = 0, \dots, s\}$, where $s = n^2 - 1$.

Density matrix

In order to deal with partial coherence of physical states the formalism of QM has to be extended. First of all Quantum Mechanics can be entirely reformulated in terms of statistical mixtures as stated by a theorem due to von Neumann (1927) and Wigner (1932), associating each state $|\psi\rangle$ of the projective space \mathbb{H} to a density operator $\rho = |\psi\rangle \langle \psi|$ [4, 8, 1, 2]. Physical systems¹ are more in general statistical mixtures represented by

$$\rho = \sum_{\alpha} p_{\alpha} |\phi_{\alpha}\rangle \langle \phi_{\alpha}| \quad , \quad p_{\alpha} \geq 0 \quad \& \quad \sum_{\alpha} p_{\alpha} = 1$$

where $\{|\phi_{\alpha}\rangle\}$ is an arbitrary set of states. From the density operator it is possible to define a density matrix as

$$\rho_{ij} = \langle i | \hat{\rho} | j \rangle \quad (1.2)$$

where $\{|n\rangle\}$ is a basis for the Hilbert space \mathbb{H} . Then it is possible to represent the density operator using the transition operators

$$\hat{\rho} = \sum_{ij} P_{ij} \rho_{ij} \quad (1.3)$$

¹Actually *ensembles* S of physical systems of the same kind.

The expectation values of Hermitian operators, in density matrix formalism have the simple form

$$\langle \hat{A} \rangle = \text{Tr}[\hat{A}\hat{\rho}] \quad (1.4)$$

Inner product and orthonormal basis An inner product in the Liouville space is defined via the trace

$$(A|B) = \text{Tr}(A^\dagger B) \quad (1.5)$$

showing that \mathbb{L} has the structure of an Hilbert space. In particular the norm is the Hilbert-Schmidt norm [9] of the operator, $\|A\| = \sqrt{\text{Tr}(A^\dagger A)}$. Graham-Schmidt lemma allows orthonormalization yielding an *orthonormal operator basis* for \mathbb{L} [3]

$$\{Q_l; l = 0, \dots, s; s = n^2 - 1\} \quad ; \quad (Q_l|Q_k) = \delta_{lk} \quad (1.6)$$

Since $(P_{ij}|P_{mn}) = \text{Tr}(P_{ji}P_{mn}) = \delta_{im}\delta_{jn}$ transition operators form an orthonormal basis.

Operator Decomposition (OD) Any $A \in \mathbb{L}$ can be decomposed as [3]

$$A = \sum_{k=0}^s a_k Q_k \quad ; \quad a_k = \text{Tr}(Q_k^\dagger A) \quad (1.7)$$

which is verified by left multiplying Q_k^\dagger and taking the trace. In particular the OD for the density matrix (DM) reads

$$\rho = \sum_{k=0}^s \text{Tr}(Q_k^\dagger \rho) Q_k \quad ; \quad \text{Tr}(Q_k^\dagger \rho) = \langle Q_k \rangle^* \quad (1.8)$$

showing that the state of the system is fully specified by the averages of all basis operators.

Operator basis

Transition operators As already noticed transition operators Eq.(1.1) form an orthonormal basis of \mathbb{L} . The OD Eq.(1.7) of any $A \in \mathbb{L}$ in this basis is the standard decomposition of operators in QM, expressed by matrix elements in a basis of \mathbb{H}

$$\text{Tr}(P_{ij}^\dagger A) = \langle i|A|j\rangle \quad \longrightarrow \quad A = \sum_{ij=1}^n \langle i|A|j\rangle |i\rangle \langle j| \quad (1.9)$$

For instance a static Hamiltonian, in the eigenbasis reads $H_0 = \sum_i E_i |i\rangle \langle i| = \sum_i E_i P_{ii}$.

Operators $P_{ii} =: P_i$ are the *projection operators*, $P_i |\psi\rangle = c_i |i\rangle$. Off diagonal operators produce transitions $P_{ij} |\psi\rangle = c_j |i\rangle$. From the definition the following property holds

$$P_{ij}^\dagger = P_{ji} \quad (1.10)$$

therefore P_i are Hermitian, while off diagonal P_{ij} are not. Notice that all pairs of conjugate operators appear in the basis.

Pauli Matrices It is sometimes convenient to choose different basis sets. For instance for two-state-nodes (TSN) one often uses Pauli matrices, which greatly simplify the OD, since they are Hermitian, unitary and traceless. Their standard form gives the matrix representation in the local basis

$$\begin{aligned} \sigma_1 = P_{01} + P_{10} &= \begin{bmatrix} 0 & 1 \\ 1 & 0 \end{bmatrix} & \sigma_2 = -i(P_{01} - P_{10}) &= \begin{bmatrix} 0 & -i \\ i & 0 \end{bmatrix} \\ \sigma_3 &= P_{00} - P_{11} = \begin{bmatrix} 1 & 0 \\ 0 & -1 \end{bmatrix} \end{aligned}$$

And the orthonormal basis is given by $\frac{1}{\sqrt{2}}(\mathbb{1}, \sigma_1, \sigma_2, \sigma_3)$. Another convenient basis is formed by the operators $(\frac{1}{\sqrt{2}}, \frac{\sigma_3}{\sqrt{2}}, P_{01}, P_{10})$.

Unitary operator basis for multistate nodes For $n > 2$ basis with all the properties of Pauli matrices do not exist [3]. There are choices of basis for multistate nodes whose elements exhibit at least some of the properties of the Pauli matrices [3]. For several purposes it is useful to consider a unitary generalization of Pauli matrices and introduce the *generalized spin matrices* [3]. The generalized Pauli matrices are defined by the relations

$$\hat{U}_{ab} |j\rangle = \omega^{jb} |(j+a) \bmod n\rangle \quad (1.11)$$

where

$$\omega = 1^{\frac{1}{N}} = e^{\frac{2\pi i}{N}}$$

The representation of such operator in terms of transition operator is

$$\hat{U}_{ab} = \sum_{l=0}^{N-1} \omega^{lb} \hat{P}_{(l+a) \bmod N, l} \quad (1.12)$$

It is possible to prove that these operator are unitary

$$\hat{U}_{ab}^\dagger \hat{U}_{ab} = \mathbb{1} \quad (1.13)$$

and orthogonal

$$Tr[\hat{U}_{ab} \hat{U}_{cd}^\dagger] = n \delta_{ac} \delta_{bd} \quad (1.14)$$

Properties of $SU(N)$ representation In Hermitian basis all the operators are Hermitian. Then the decomposition of any Hermitian operator has real components [3]. Indeed $\text{Tr}(Q_k^\dagger A)^* = \text{Tr}(Q_k A^\dagger)$, and it is real if both Q_k and A are Hermitian. In such a basis both H and ρ have real components. A widely used Hermitian basis is formed by the identity and the generators of $SU(n)$. From the unitarity condition of the operator belonging the $SU(N)$ and from Hermiticity condition of the generators we know that the generators are $s = N^2 - 1$. These generators $\{\hat{\lambda}_i\}$ are defined by the relations

$$\begin{aligned} [\hat{\lambda}_i, \hat{\lambda}_j] &= 2i \sum_{k=1}^s f_{ijk} \hat{\lambda}_k \\ \text{Tr}[\hat{\lambda}_i] &= 0 \\ \text{Tr}[\hat{\lambda}_i \hat{\lambda}_j] &= 2\delta_{ij} \end{aligned} \quad (1.15)$$

where f_{ijk} is the antisymmetric tensor in $n^2 - 1$ dimensions. These equations may be satisfied by the operators

$$\hat{\lambda} = \{\hat{u}_{1 \leq i < j \leq N}, \hat{v}_{1 \leq i < j \leq N}, \hat{w}_{1 \leq i < N}\} \quad (1.16)$$

such that

$$\begin{aligned} \hat{u}_{ij} &= \hat{P}_i + \hat{P}_j \\ \hat{v}_{ij} &= i(\hat{P}_i - \hat{P}_j) \\ \hat{w}_l &= -\sqrt{\frac{2}{l(l+1)}} \left(\sum_{k=1}^l \hat{P}_k - l\hat{P}_{l+1, l+1} \right) \end{aligned} \quad (1.17)$$

Notice that for $n > 2$ the $SU(n)$ generators are not unitary.

Using the basis

$$\begin{aligned} \hat{Q}_0 &= \frac{1}{\sqrt{N}} \mathbb{1} \\ \hat{Q}_i &= \frac{1}{\sqrt{2}} \hat{\lambda}_i \end{aligned} \quad (1.18)$$

where $\hat{\lambda}$ is defined in (eqs.1.17,1.16) we can express both H and ρ can be associated to s -dimensional vectors of a real space

$$A = \frac{1}{n} A_0 \mathbb{1} + \frac{1}{2} \sum_{k=1}^{N-1} A_k \hat{\lambda}_k. \quad (1.19)$$

Indeed the component $l = 0$ is irrelevant both for the Hamiltonian, since we can choose $\text{Tr}(H) = 0$, and for for the DM, since $\text{Tr}\rho = 1$ is fixed. The

similarity transformation defined by operators of the form

$$\begin{aligned} U(\phi) &= e^{i\phi\hat{Q}_i} \\ U^\dagger(\phi)AU(\phi) \end{aligned} \quad (1.20)$$

implement a rotation in s -dimensional space around the i -th axes. For TSN's the $s = 3$ -dimensional space is the *Bloch-Poincaré space*. In the Bloch Poincaré space it is possible to perform the 3D rotation using eq.1.20

$$U(\phi) = e^{i\phi\cdot\sigma} \quad (1.21)$$

1.1.2 Time evolution

Schrödinger Equation

In the Schrödinger picture time evolution is codified in the pure state²[4], $|\Psi(t)\rangle$. The dynamics is fully determined once preparation of the system is specified $|\Psi(t_0)\rangle = |\psi_0\rangle$. For instance averages of time-independent operators

$$\langle \hat{A}(t) \rangle = \langle \Psi(t) | \hat{A} | \Psi(t) \rangle \quad (1.22)$$

The state vector solves the Schrödinger equation ($\hbar = 1$).

$$i\partial_t |\Psi(t)\rangle = H(t) |\Psi(t)\rangle \quad \text{initial condition} \quad |\Psi(t_0)\rangle = |\psi_0\rangle \quad (1.23)$$

where the Hamiltonian $\hat{H}(t)$ is a linear hermitian operator.

Evolution operator

Since the dynamics as described by Eq.(1.23) is a linear mapping [4] $|\Psi(t_0)\rangle \rightarrow |\Psi(t)\rangle$, it can be represented by the *two-times evolution operator* (or *propagator*) $U(t, t_0)$

$$|\Psi(t)\rangle = U(t, t_0)|\Psi(t_0)\rangle \quad , \quad U(t, t) = \mathbb{1} \quad (1.24)$$

which must be linear. Uniqueness of the solution of Eq.(1.23) for given initial conditions means that the mapping is injective and implies that $U(t, t_0)$ does not depend on the initial state.

²Hereafter it is intended that all state vectors are normalized.

Properties of the propagator The Eq.(1.23) imply a similar equation for the evolution operator

$$i\hbar\frac{\partial}{\partial t}U(t, t_0) = H(t)U(t, t_0) \quad (1.25)$$

Indeed Eq.(1.23) can be written as $i\partial_t U_s(t, t_0) |\psi_0\rangle = \hat{H}(t)U_s(t, t_0) |\psi_0\rangle$ and the equality is valid for arbitrary $|\psi_0\rangle$. From the initial condition follows $U(t_0, t_0) = \mathbb{1}$ that imply an integral equation of the form

$$U(t, t_0) = \mathbb{1} - \frac{i}{\hbar} \int_{t_0}^t H(t')U(t', t_0). \quad (1.26)$$

Considering the parameter t_0 that appear in $U(t, t_0)$ as a variable t' the time evolution from t' to t is

$$|\Psi(t)\rangle = U(t, t') |\Psi(t')\rangle \quad (1.27)$$

But also

$$|\Psi(t')\rangle = U(t', t_0) |\Psi(t_0)\rangle \quad (1.28)$$

Then the composition properties follows

$$U(t, t_0) = U(t, t')U(t', t_0) \quad (1.29)$$

that is the composition rule for elements of a semigroup [4, 2]. Substituting in Eq.1.29 $t = t_0$ follows

$$\mathbb{1} = U(t_0, t)U(t, t_0) \quad (1.30)$$

Multiplying Eq.1.25 by $U^\dagger(t, t_0)$ and its complex conjugate by $U(t, t_0)$

$$\begin{aligned} -iU(t, t_0)\partial_t U^\dagger(t, t_0) &= U(t, t_0)H(t)U^\dagger(t, t_0) \\ iU(t, t_0)^\dagger\partial_t U(t, t_0) &= U^\dagger(t, t_0)H(t)U(t, t_0) \end{aligned} \quad (1.31)$$

and differentiating term by term we obtain

$$\partial_t U^\dagger(t, t_0)U(t, t_0) = 0 \rightarrow U^\dagger(t, t_0)U(t, t_0) = c \quad (1.32)$$

that with the initial condition imply that $U(t, t_0)$ is also unitary

$$U(t, t_0) = U^\dagger(t_0, t) \quad (1.33)$$

A consequence of the properties listed above is that two-times propagator can be expressed in terms of the *single time propagator* $U(t) := U(t, 0)$ as

$$U(t, t_0) = U(t, 0)U(0, t_0) = U(t)U^\dagger(t_0) \quad (1.34)$$

Dynamic equation and formal solution The dynamics is solved once $U(t, t_0)$ is found.

From Eq. 1.25 follows that the solution is immediate if \hat{H} is time-independent

$$U(t, t_0) = e^{-i\hat{H}\cdot(t-t_0)} \quad (1.35)$$

as it can be verified by substitution. This structure can be extended to special problems called superadiabatic [4], such that $[\hat{H}(t), \hat{H}(t')] = 0, \forall t, t'$ and yielding

$$U(t, t_0) = e^{-i \int_{t_0}^t ds \hat{H}(s)} \quad (1.36)$$

However when $H(t)$ does not commute at different times Eq.(1.35) is not a solution as it can be verified by considering the derivative of its series expansion [4]. In general time ordering of the operators is essential and the solution can be obtained in the form of the Dyson series which is *symbolically* reexponentiated using the time ordering operator T [4]

$$U(t, t_0) = \begin{cases} \bar{T} e^{-i \int_{t_0}^t ds \hat{H}(s)} & \text{for } t < t_0 \\ T e^{-i \int_{t_0}^t ds \hat{H}(s)} & \text{for } t > t_0 \end{cases} \quad (1.37)$$

This symbolic way of writing only means that the solution is written by first expanding the exponential as it were a number, and then acting term by term with the time-ordering (antiordering) operator.

Liouville-Neumann Equation

Under the action of $H(t)$ the density operator of a closed system evolves in time according to

$$\rho(t) = U(t) W(0) U^\dagger(t)$$

and it is easy to verify that it solves the von Neumann-Liouville equation [3, 4]

$$\frac{d\rho(t)}{dt} = -i [H(t), \rho(t)] \quad (1.38)$$

Since the r.h.s. is a linear form of the entries of the density matrix, we can rewrite the equation as

$$\frac{d\rho(t)}{dt} = \mathcal{L}(t) \rho(t) \quad (1.39)$$

where now ρ is a n^2 dimensional vector and the superoperator $\mathcal{L}(t)$ called Liouvillian is a $n^2 \times n^2$ matrix, i.e. an operator of \mathbb{L} . This allows to write the formal solution for the dynamics of the density matrix in an exponential form convenient for approximations. For instance for a time-independent problem we write

$$\rho(t) = e^{\mathcal{L}t} \rho(0)$$

1.1.3 Transformations and picture for the dynamics

The freedom in the choice of the reference basis (frame) of \mathbb{H} can be used to simplify the equations for the probability amplitudes. Transformation to the rotating frame or to the Dirac (interaction) are relevant examples. The transformed equations may allow to recognize the “relevant” dynamics, and to discard the rest or treat as a perturbation.

The physical problem posed in the *laboratory frame*, corresponds to the Schrödinger picture (§1.1.2).

Time-dependent unitary transformations

The dynamics of a time dependent quantum system, as those concerning quantum control, is very hard to determine due to the presence of the *time ordering* operator in the expression for the propagator Eq.1.37. Despite this fact often it is possible to use unitary time dependent transformation to simplify the structure of the dynamics [4]. Starting from the Schrodinger equation

$$i\partial_t |\Psi(t)\rangle = H(t) |\Psi(t)\rangle$$

we can define a new state vector related to the state vector in the Schrödinger picture by

$$|\Psi(t)\rangle = U_x(t) |\Psi(t)\rangle_x \quad (1.40)$$

where $U_x(t)$ is unitary i.e. $U_x(T)U_x^\dagger(t) = I$ substituting this expression in the Schrödinger equation follows

$$i\partial_t [U_x(t)] |\Psi(t)\rangle_x + iU_x(t)\partial_t |\Psi(t)\rangle_x = H(t)U_x(t) |\Psi(t)\rangle_x$$

multiplying both sides of this equation on the left by $U_x^\dagger(t)$ and using the unitarity property of $U_x(t)$ we obtain

$$i\partial_t |\Psi(t)\rangle_x = [U_x^\dagger(t)H(t)U_x(t) - iU_x^\dagger(t)\partial_t U_x(t)] |\Psi(t)\rangle_x = \tilde{H}(t) |\Psi(t)\rangle_x. \quad (1.41)$$

With this prescriptions we achieved a new effective Hamiltonian in a different dynamical reference frame. These consideration can be used for exemple to write an Hamiltonian in another reference frame or to obtain the Dirac (or interaction) picture, in fact if we start with an Hamiltonian of the form

$$H(t) = H_0 + \lambda H_I(t)$$

using the unitary transformation $U_0(t) = e^{-iH_0 t}$ we obtain an effective Hamiltonian of the form

$$\begin{aligned} i\partial_t |\Psi(t)\rangle_I &= \tilde{H}_i(t) |\Psi(t)\rangle_I; \\ |\Psi(t)\rangle_S &= U_0(t) |\Psi(t)\rangle_I; \\ \tilde{H}_i &= U_0^\dagger(t)H_i(t)U_0(t) \end{aligned} \quad (1.42)$$

Phase transformation

Phase transformation [4] corresponds to unitary operator of the form

$$U_x(t) := U_{rf}(t) = e^{-i \sum_m \zeta_m(t) P_{mm}} \quad (1.43)$$

Where P_{mm} , already defined in Eq.1.1 are the projection operator on states $|m\rangle$ that are eigenstates of the Hamiltonian H_0 . The index stays for *rotating frame*. In particular, since $[U_{rf}(t), H_0] = 0$, the transformation is a simmetry for H_0 , it behaves as a “rotation” of the state around the “direction” of H_0 . For a two level system this picture has an immediate visualization on the Bloch space.

It is simple verify that $[P_{mm}, P_{ll}] = 0$, then it is possible write $U_{rf}(t)$ as a product of single transformation $U_{rf}(t) = \prod_m e^{-i \zeta_m P_{mm}}$. The effect on the states is

$$e^{-i \zeta_m P_{mm}} |j\rangle = e^{-i \zeta_m \delta_{mj}} |j\rangle = \begin{cases} e^{-i \zeta_m} |m\rangle & j = m \\ |j\rangle & j \neq m \end{cases}$$

then $e^{i \zeta_m P_{mm}} |j\rangle \langle j| e^{-i \zeta_m P_{mm}} = |j\rangle \langle j|$. Consequently $U_{rf}^\dagger |j\rangle \langle j| U_{rf} = |j\rangle \langle j|$. More in general these transformations leave invariate all the diagonal operators in the H_0 eigenstates basis. The off diagonal operators pick a phase from these transformation

$$U_{rf}^\dagger |m\rangle \langle n| U_{rf} = e^{i \zeta_m P_{mm}} |m\rangle \langle n| e^{-i \zeta_n P_{nn}} = e^{i(\zeta_m - \zeta_n)} |m\rangle \langle n|$$

We now apply these results to determine the effective Hamiltonian corresponding to $H_0 + H_1(t) = \sum_m E_m |m\rangle \langle m| + \sum_{mn} V_{mn}(t) |m\rangle \langle n|$

$$\begin{aligned} H_0 + H_1 &\rightarrow \tilde{H} = U_{rf}^\dagger [H_0 + H_1] U_{rf} - i U_{rf}^\dagger \partial_t U_{rf} \\ &= H_0 + \sum_{mn} V_{mn} e^{i(\zeta_m - \zeta_n)} |m\rangle \langle n| - U_{rf}^\dagger \left[\sum_m \dot{\zeta}_m |m\rangle \langle m| \right] U_{rf} \\ &= \sum_m (E_m - \dot{\zeta}_m) |m\rangle \langle m| + \sum_{mn} V_{mn}(t) e^{i(\zeta_m(t) - \zeta_n(t))} |m\rangle \langle n| \end{aligned}$$

These transformations are very useful in the case of a system driven with AC pulses. Their cancel part of all the time dependence from $H_1(t)$, and part of the energy on the time independent part, thus greatly simplifying the problem.

Transformation to adiabatic frame. We now define a unitary transformation as

$$U_{ad}(t) = \sum_i |\phi_i(t)\rangle \langle i|, \quad |\psi\rangle = U_{ad}(t) |\psi_{ad}\rangle$$

where, $|\phi_i(t)\rangle$ are the instantaneous eigenstates of a generic Hamiltonian $H_t(t)$ and $|i\rangle$ is a time-independent basis [4]. In this basis the unitary operator elements are $[U_{ad}]_{ij} = |i\rangle U_{ad}(t) \langle j| = \langle i|\phi_j(t)\rangle$. In this context we will refer to this reference frame as *adiabatic frame*.

Dynamics in adiabatic frame. The effective Hamiltonian in adiabatic frame [4] is given by the Eq. 1.41) where $U_x(t) = U_{ad}(t)$. It is convenient distinguish to contribution writing

$$\tilde{H}_t = \tilde{H}_{ad}(t) + \delta\tilde{H}(t)$$

where

$$\tilde{H}_{ad}(t) = U_{ad}^\dagger(t) \tilde{H} U_{ad}(t) = \sum_i \epsilon_i(t) |i\rangle \langle i| \quad (1.44a)$$

$$\delta\tilde{H}(t) = -i U_{ad}^\dagger(t) \partial_t U_{ad}(t) =: \sum_{i,j} |i\rangle \delta\tilde{H}_{ij}(t) \langle j| \quad (1.44b)$$

The term $\delta\tilde{H}_{ij}(t)$ gives the non adiabatic effect. His matrix elements describe transitions between adiabatic states. The matrix $\delta\tilde{H}(t)$ is called non-adiabatic coupling matrix. His elements are

$$\delta\tilde{H}_{ij} = -i \langle i| U_{ad}^\dagger(t) [\partial_t U_{ad}(t) |j\rangle] = -i \langle \phi_i(t) | \partial_t \phi_j(t) \rangle \quad (1.45)$$

This equation allows to write the non-adiabatic coupling matrix in many cases.

1.1.4 Quantum Computation and Advanced Control

Quantum dynamics has attracted large interest since the advent of NMR and Laser physics and is nowadays a still growing subject of investigation having been boosted in the last decade by efforts towards the implementation of quantum state processors [8]. This has greatly broadened the scope of the research which now involves new physical systems, as “artificial atoms” [6], and new tasks as advanced control which are the subject of this thesis. Artificial atoms are solid-state nanodevices which are expected to exhibit dynamical behavior similar to atoms. However direct detection of quantum coherence as superpositions of states, proposed of Caldeira and Leggett [10, 11] at the beginning of the eightieees, has been a for almost twenty years an elusive experimental challenge, only achieved in 1999 by Nakamura et al. [12]. Advanced control aims at controlled manipulations of quantum states. Examples in atomic and molecular systems are the faithful and selective transfer of populations and wavepackets in in different physical locations [13].

Computation

In the last years the scientific community is attracted by the possibility to manipulate quantum information. Quantum computation consist in achieving preparation (*write*), manipulation and measurement (*read*) of a set of quantum variables \hat{Q}_i , this set defining the so called computational basis $|\{q_i\}\rangle$ [6]. The manipulation consist on the possibility of desining a Hamiltonian to control the quantum state

$$|\Psi(t)\rangle = \sum_{q_1 \cdots q_n} c_{q_1 \cdots q_n}(t) |q_1 \cdots q_n\rangle \quad (1.46)$$

implementing the unitary trasformations related to specific quantum gates of a given system. Coherence means that there is a well defined reation between the $c_{q_1, \dots, q_N}(t)$ coefficients in Eq.1.46 [6]. However the Hilbert space of a superconducting nanodevice is much larger than the computational subspace and this causes *decoherence*. In other word the system interacts with the *environment* (determined by all the degree of freedom needed to complete the Hilbert space), that destroy the phase relation between $c_{\{q_i\}}(t)$.

Control

An important problem that arises in the manipulation of solid state coherent nanostructures (as those based on superconductors with respect to microscopic system as atoms) is the loss of coherence due to noise. One of the most important aims of quantum control is to find strategy to manipulate a quantum system to achieve a given target state limiting the loss of coherence. The manipulation is performed tuning the Hamiltonian (using for example laser or microwave field). The typical Hamiltonian to be stuied in control problem depends from several tunable parameters $\mathbf{q}(t)$ ³

$$H(t) = H[\mathbf{q}(t)]. \quad (1.47)$$

Being the working point defined by specific values of these parameters \mathbf{q}_0 , the problem reduced to study an Hamiltonian of the form

$$H[\mathbf{q}(t)] = H[\mathbf{q}_0 + \delta\mathbf{q}(t)] \simeq H[\mathbf{q}_0] + \delta\mathbf{q}(t) \cdot \nabla_{\mathbf{q}} H[\mathbf{q}_0] = H_0 + \delta\mathbf{q}(t) \hat{\mathbf{Q}} \quad (1.48)$$

In the next chapters we will use single-port control models, in these case the structure of the Hamiltonian is

$$H[q(t)] = H_0 + \delta q(t) \hat{Q} \quad \text{where} \quad \hat{Q} = \frac{d\hat{H}}{dq}[q_0] \quad (1.49)$$

³Here the boldface indicate vectorial quantity

1.2 Quantum hardware

1.2.1 Atoms, molecules, photons

The first attempt to implement quantum control and quantum computation has been performed with typical “microscopic” quantum system as atoms and molecules. In such system the electrons have a discrete energy spectrum. With sufficiently high intensity laser it is possible to control the dynamics of such electrons. In particular, under suitable conditions of resonance and intensity it is possible to make relevant for this dynamics only few level (for example in quantum computation two levels or more in STIRAP processes depending in which specific realization of the process).

1.2.2 Artificial atoms

Nanodevices behaving as artificial atoms have allowed the demonstration on a mesoscopic scale of coherent phenomena proper of the microscopic realm. Advances in fabrication offer the possibility of exploring several different designs of quantum bits based on semiconductors and superconductors [14, 15, 16]. In these latter mechanisms and typical features of decoherence [16, 6] are now well understood and several strategies to minimize them have been tested. This has allowed fabrication of more complex architectures which in particular have demonstrated quantum-optics on a chip [17] and to stimulate the exploration of new designs beyond atomic analogues. To proceed in this direction quantum control of coherence in driven superconducting multilevel open nanostructures is to be achieved. A key step is the understanding of how peculiar signatures of interference, as those exhibited in driven multilevel systems [14], are sensitive to the presence of environments unconventional for atomic physics.

Example: the Cooper Pair Box

An elementary unit for superconducting coherent nanodevices is the *Cooper Pair Box* (CPB) [6], whose basic design is described in fig. 1.1. It is described by the Hamiltonian

$$\mathcal{H}_{BOX} = 4E_C(\hat{q} - q_g)^2 + V_J(\hat{\varphi}) \quad (1.50)$$

where \hat{q} is the operator of the number of Cooper pair in excess in the superconducting island. The charging energy $E_C = \frac{e^2}{2C}$ is fixed by the geometry, whereas the other parameters are tunable, allowing external control. The gate voltage fixes the gate charge, $2eq_g = C_g V_x$ and improvement of basic design as the substitution of the Josephson junction with a SQUID allows

to control also $E_J(\Phi_x)$. In the basis $|q\rangle$ of the eigenstates of the charge in the island the phase acts as $e^{\pm i\hat{\varphi}}|q\rangle = |q \pm 1\rangle$. Therefore the Josephson term changes the number of Cooper pairs in units and the Cooper pair box Hamiltonian read

$$H_0 = E_C \sum_q (q - q_g)^2 |q\rangle \langle q| - \frac{E_J}{2} (|q\rangle \langle q+1| + h.c.) \quad (1.51)$$

A time-dependent voltage reflects in a time dependent gate charge. Substituting in eq. 1.51 $q_g \rightarrow q_{g0} + q_c(t)$ the Hamiltonian read

$$H(t) = H_0 + H_c(t) \\ H_0 = E_C \sum_q (q - q_g)^2 |q\rangle \langle q| - \frac{E_J}{2} (|q\rangle \langle q+1| + h.c.) \quad (1.52)$$

$$H_c(t) = -2q_c(t) \sum_q q |q\rangle \langle q|$$

Generally the control is performed on eigenstates of H_0 then it is useful to write the complete Hamiltonian as

$$H(t) = \sum E_i P_{ii} - 2E_C q_{ij} P_{ij} \quad (1.53)$$

where $P_{ij} = |i\rangle \langle j|$ are the transitions operators defined in eq.1.9, $\{|i\rangle\}$ are the eigenstates of H_0 and $q_{ij} = \langle i|\hat{q}|j\rangle$.

Mesoscopic conductors

Graphene Graphene is a recently isolated material [19]. It is constituted by carbon atoms arranged in a 2D honeycomb lattice Fig.1.2. The Honeycomb lattice can be viewed as a biatomic lattice. It has been proven that the dynamics of the *quasi-particle* in this material follows an Hamiltonian of the form

$$H = v_F(\sigma_x p_x + \sigma_y p_y) = v_F \sigma \mathbf{p} \quad (1.54)$$

reminiscent of the Hamiltonian of *Dirac-Weyl* fermions. Here $v_F = 10^6 m s^{-1}$ is the Fermi velocity and the eigenstates of σ_z represent excitation on each sublattice. In principle, in this material, it is possible to achieve the control of the pseudospin (σ) degree of freedom [20].

Topological states of condensed matter An other interesting perspective for the quantum computation is open by the existence of topological phase in some condensed matter system [21]. Topological (*invariant*) states are collective states with great correlation length as for example Laughlin states. The topological invariance guarantees a very good protection of these states from noise.

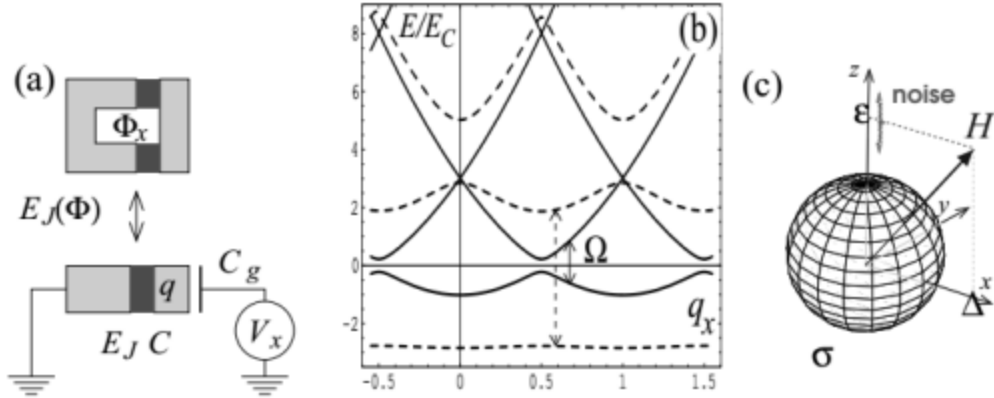


Figure 1.1: (a) Basic design of the Cooper pair box. It is a superconducting island storing the variable q and connected to a circuit via a Josephson junction and a capacitor C_g . Control is operated via V_x . Substituting the junction by a SQUID it is possible to tune also $E_J(\Phi_x)$ by changing the magnetic flux. (b) Spectrum of the box for fixed $\frac{E_J}{E_C} = 0.44$ (solid lines, corresponding to the NEC qubit [12]). In charge qubits the spectrum is very sensitive to fluctuations of q_x . Instead for $\frac{E_J}{E_C} > 1$ dashed lines, $\frac{E_J}{E_C} = 5.04$, correspond to the Quantronium [18] the splitting Ω is less sensitive to charge fluctuations. (c) The Bloch sphere and the qubit Hamiltonian. The dominant decoherence mechanism, charge noise in charge qubits, couples to σ_z .

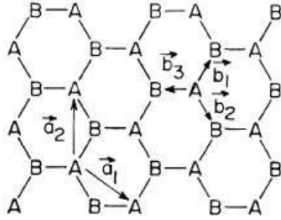


Figure 1.2: Graphene is a 2D honeycomb lattice of carbon atoms. To write the low energy effective Hamiltonian. Since the honeycomb lattice is not a Bravais lattice it is convenient to consider this lattice as constituted by two sublattices indicated with letters A and B .

Discussion

One of the main differences with usual atoms is tunability. Actually if q is a sort of electric field and also atoms may be tunable via a strong static electric field, but the dipole moment is small. On the contrary $2E_C q_{ij}$ is not that smaller than

Artificial atoms [22] are different from their natural counterpart in many respects. Indeed their properties can be engineered and they are easily tun-

able. The impact on one of the major issues for coherent dynamics, namely resilience to noise, is large and has been exploited in a twofold way. First of all devices can be tuned to optimal bias points where symmetries enforce protection from decoherence [18, 23, 24]. On the other hand the possibility of manipulating various external knobs allows to extract valuable information on the sources of decoherence. In recent years environment spectroscopy techniques which use as meters both undriven and driven (pulsed or continuously) coherent nanodevices have been developed [25, 26, 24]. Nanodevices offer the possibility of designing couplings, with external fields or between subunits, which are much stronger than what is found in atomic systems [17]. Therefore they may allow for faster operation, but on the other hand also noise may be large determining smaller decoherence times.

1.2.3 Driven artificial atoms

Starting from the Hamiltonian for artificial atoms subject to external drives, here we outline the structure of an effective Hamiltonian capturing the essence of the dynamics, and allowing for further analytical steps to be performed. The derivation is based on the assumption that the drive can be separated in a slow and a fast part and that their main contribution to the dynamics can be accounted for separately, i.e. we assume a separation of time scales. This allows to introduce in a clear way further approximations, e.g. a slow drive can be treated in the adiabatic approximation.

Although we do not give a rigorous derivation of the effective Hamiltonian, approximations we use are standard together with the assumption of scale separation. It is worth noticing that corrections can be estimated in various ways⁴, although a general way to handle them systematically is not available.

1.3 Open quantum system

1.3.1 System-environment Hamiltonian

The most important characteristic needed to perform quantum control is *coherence*. As we said above the loss of coherence is due to the interaction of the system to be controlled with an *environment*.

Therefore we should consider a *system+environment* Hamiltonian of the

⁴For instance disentangling the evolution operator and using the Average Hamiltonian Theory (App. B) to approximate leading corrections.

form

$$H(t) = H_0 + A(t)\hat{Q} + \sum_i \hat{X}_i \hat{Q}_i + H_r[\hat{X}] \quad (1.55)$$

where $H_0(t)$ describe the controlled system isolated, H_{fn} describes the environment not coupled to the degree of freedom of the system and \hat{Q}_i are the degrees of freedom of the system that couple with the degrees of freedom \hat{X}_i of the environment.

Here we assumed that the system is driven by classical fields, since this is the case for most nanodevices. In a more general treatment classical fields can be, of course, quantized.

Reduced Density Matrix and reduced dynamics

As seen in previous section, to address the problem of quantum control, it is necessary to consider a system coupled with an environment. This open system structure prevents the possibility of describing the dynamics in the computational state with pure quantum states. The goal is then to study the dynamics of the *reduced density matrix* (RDM) obtained performing a partial trace of the total density matrix of the system plus environment.

$$\rho(t) = Tr_E \rho_{S+E}(t) = \sum_i \langle r_i | \rho_{S+E}(t) | r_i \rangle \quad (1.56)$$

where $\{|r_i\rangle\}$ is a basis of the Hilbert space of the environment. Formally we can write an equation for the reduced dynamics defining a projection operator P that projects the total density operator to the Hilbert space of the relevant system $\rho(t) = P\rho_{S+E}$. For discrete systems this is the Nakajima-Zwanzig equation

$$i\partial_t \rho(t) = P\mathcal{L}\rho(t) + \int_0^t dt' P\mathcal{L} \exp[(1-P)\mathcal{L}t'](1-P)\mathcal{L}\rho(t-t') + P\mathcal{L} \exp[(1-P)\mathcal{L}t](1-P)\rho_{S+E}(0) \quad (1.57)$$

where \mathcal{L} is the Liouvillian operator defined in eq.1.39.

Ab initio and phenomenological approaches

In principle we could derive an effective Hamiltonian *ab initio*, i.e. starting from Eq.(1.55). This would require detailed knowledge of both system and environment, an information which in practice is not available [6]. Since in any case we expect that most of the microscopic details of the environment play no role in the system reduced dynamics, it is convenient to explore a less demanding strategy. An approach is to invoke weak coupling approximations which indirectly “erase” information on the environment, as

in Bloch-Redfield-Wangness Master Equation[27, 28, 29, 30], Lax Master Equation [31, 32, 33, 14] or Generalized Optical Bloch Master Equation[27, 28, 29, 30, 34]. Another point of view is to write pure phenomenological Master Equations (ME) (as Bloch ME or Optical Bloch ME)[27] whose general structure when noise is Markovian is fixed by Lindblad-Kossakowski-Gorini-Sudarshan (LKGS) theorem[35, 36, 33, 3].

The two approaches are complementary in many respects, and in several practical cases a weak coupling ME reduces to the LKGS structure. It is also worth noticing that they have the same regime of validity, which roughly requires $v\tau_c/\hbar \ll 1$, where v is the coupling between system and environment and τ_c is the correlation time of the reservoir.

This latter restriction is not met for many of the noise sources present in the solid state.

Solid state noise is broadband, i.e. the low frequency part of the spectrum of the noise cannot be treated with perturbation theory.

Multistage procedure, for eliminating parts of the environment producing qualitatively different effects on the dynamics of the system [6], was proposed. The idea is that such a procedure could be carried out from the bottom-up point of view, and the result is that different effects of the presence of noise come in a hierarchy. In particular in most nanodevices operating at low temperature and in the presence of large low-frequency noise, leading effects are the following: (a) the so called “rigid line-breadth” due to very slow modes of the environment, behaving essentially as a classical noise source; and (b) spontaneous emission (and the induced secular dephasing) triggered by quantum noise due to environmental modes quasi resonant with the Bohr frequencies of the artificial atom.

In this thesis we will adopt instead the top-down point of view, i.e. we directly use the phenomenological approach to build an effective Hamiltonian with a fictitious environment producing the same leading effects of low-frequency and quantum noise on the reduced dynamics of the system.

1.3.2 A roadmap to Broadband noise

We start from the macroscopic Hamiltonian of the device, $H_0 = H_0(q)$, which is an operator onto a n -dimensional Hilbert space \mathbb{H} . It depends on the parameter q fixing the bias (operating) point. The “local” basis of \mathbb{H} is composed by the eigenstates $\{|\phi_i(q)\rangle : i = 1, \dots, n\}$ of $H_0(q)$ [6]. In this “laboratory frame” the Hamiltonian is

$$H_0 = \sum_{i=1}^n E_i(q) |\phi_i(q)\rangle \langle \phi_j(q)| \quad (1.58)$$

External control is described by a time-dependent term. In a one-port design the driving field $A(t)$ couples to a single time-independent system operator \hat{Q}

$$H_c(t) = A(t) \hat{Q} \quad (1.59)$$

which is Hermitian and traceless. In general control is operated via the same port, i.e. by allowing the bias in $H_0(q)$ depend on time. We let $q \rightarrow q(t) + q_c(t)$ splitting in a slow $q(t)$ which includes static bias, and the fast control parameter $q_c(t)$. Accordingly we split

$$H_S = H_0[q(t) + q_c(t)] := H_0[q(t)] + H_c(t) \quad (1.60)$$

where $H_c(t)$ describes (fast) control; in relevant situations it can be linearized in $q_c(t)$, yielding the structure of Eq.(1.59). Notice that while \hat{Q} is an observable and does not depend on the local basis, its matrix representation does. The physical consequence is that the effectiveness of the fast control $q_c(t)$ in triggering transitions depends also on the slow $q(t)$, a feature of artificial atoms reflecting their ease of tunability.

The interaction with the complicated environment of microscopic degrees of freedom in the solid state can be modeled by a phenomenological Hamiltonian. We first consider classical noise, and assume that it also acts through the same control port, therefore it can be modeled by adding a stochastic component $x(t)$ to the drive. Again we split slow and fast noise, $x(t) \rightarrow x(t) + x_f(t)$, and include the slow part in H_0 . The same steps leading to Eq.(1.60) yield the noisy Hamiltonian

$$H = H_0[q(t) + x(t)] + A(t) \hat{Q} + H_{nf} \quad (1.61)$$

where H_{nf} describes Markovian high-frequency classical noise [7]. ‘‘Quantization’’ of this term, $H_{nf}(t) \rightarrow \hat{X} \hat{Q} + H_R$, yields the final system-environment Hamiltonian. Here \hat{X} operates on the environment and H_R is its Hamiltonian, plus possibly suitable counterterms.

From the physical point of view the phenomenological Hamiltonian treats on different footings environmental modes exchanging energy with the system which are treated quantum mechanically whereas slow modes responsible for pure dephasing are accounted for classically. Results of measurements involve both quantum and classical ensemble averaging. From the technical point of view effects of markovian noise alone are studied by weak coupling quantum optical Master Equations (ME). This approach fails for low-frequency noise (e.g. $1/f$) which is large in solid-state systems. To overcome this problem a multistage approach has been proposed [37] for undriven systems subject to broadband noise which quantitatively explains decoherence observed in superconducting qubits of different nature [25, 26, 24].

In these cases the leading contribution of low-frequency noise was captured by a Static-Path Approximation (SPA) i.e. approximating $x(t)$ by a suitably distributed random variable x [37, 25]. Despite of its simplicity, this approximation provides a powerful framework for applications to more complex architectures. Recently, it has been used to propose a design of optimal tuning of multiqubit systems [23, 24] and extended to the analysis of a Λ system [38]

An important feature of superconducting nanodevices is that the Hamiltonian $H_0(q)$ can be tuned in a way such that parity symmetries are enforced, where $A_i = \partial E_i / \partial q = 0$ and selection rules hold affecting matrix elements Q_{ij} in the local basis. In these parity symmetry points the device is well protected against noise.

In this work we will study AC driven nanodevices addressing the effects of low-frequency noise in the SPA. We will focus on the single-port scheme where control, noise and environmental modes all couple to the same operator \hat{Q} . Now, it is apparent that different channels for decoherence will be strongly correlated: this has consequences for quantum control. The single-port scheme provides the simplest model displaying these features, and at the same time it describes experimentally relevant devices affected by a dominant source of decoherence. A more general multiport scheme would exhibit an even richer behavior of correlation, whose essence stems from the non-markovianity of noise.

1.3.3 Adiabatic noise and the SPA

Since the adiabatic component of the environment does not produce transition in the system their can be treated performing a classical average over the realization for the stochastic process $x(t)$

$$\rho(t) = \int \mathcal{D}[x(t)] P[x(t)] \rho[t|x(t)] \quad (1.62)$$

To perform this integral we need the expression of $P[x(t)]$ that in principle can be obtained from the $n+1$ point joint probability $P(x_t, t; x_{N-1}, t_{N-1} \cdots, x_0, 0)$ of $x(t)$. The non-Markovian nature of stochastic processes of interest, does not allow to handle explicit expressions of $P[x(t)]$. However a systematic approximation scheme can be used to obtain results with the desired accuracy, by sampling better and better the interval $[0, t]$ with a finite number of mesh points. Since any specific protocol samples different properties of the stochastic problem, it is often possible to find results by considering the appropriate leading term. The lowest approximation consists on sampling all the realizations of the stochastic process with constants x with a

probability distribution $P(x)$. This is the so called Static Path approximation (SPA). Despite its simplicity the SPA showed a beautiful estimate of experimental results for free dynamics of qubits[39] and for Rabi oscillation [26].

1.3.4 Quantum noise and the Master Equation

Secular Master Equation

For a weakly coupled environment the trace of environmental degrees of freedom can be calculated in several ways at the second order in interaction. A standard approach leads to the secular master equation in the basis of the eigenstates of H_S

$$\dot{\rho}_{ij}(t) = -i\omega_{ij}\rho(t) + \sum_{kl} \mathcal{R}_{ijkl}\rho_{kl}(t) \quad (1.63)$$

where ω_{ij} is the difference in energy of eigenvalues. The relaxation tensor \mathcal{R}_{ijkl} is a combination of quantities of the kind $\int_0^\infty dt C_{ijkl}^{\lessgtr}(t)$ and may be calculated if the Green's function of the environment $G^>(t) = \langle E(t)E(0) \rangle_E$ or its Fourier transform $\frac{2S(\omega)}{1+e^{\beta\omega}}$ are known. The correlators $C_{ijkl}^{\lessgtr}(t)$ are defined by

$$\begin{aligned} C_{ijkl}^>(t) &= Tr_E[\rho_E(0) \langle i | e^{iH_E t} H_{int} e^{-iH_E t} | j \rangle \langle k | H_{int} | l \rangle] \\ C_{ijkl}^<(t) &= Tr_E[\rho_E(0) \langle i | H_{int} | j \rangle \langle k | e^{iH_E t} H_{int} e^{-iH_E t} | l \rangle]. \end{aligned} \quad (1.64)$$

Lindblad Master Equation

A phenomenological approach is based on the Gorini Kossakowski theorem [35]. This theorem asserts that the most general form for Markovian master equation is[36, 33]

$$\dot{\rho}(t) = \hat{\mathcal{L}}\rho(t) \quad (1.65)$$

here

$$\hat{\mathcal{L}}\rho = -\frac{i}{\hbar}[\hat{H}, \rho] + \frac{1}{2} \sum_{i,j=1}^s A_{ij}([\hat{L}_i, \rho \hat{L}_j^\dagger] + [\hat{L}_j, \rho \hat{L}_i^\dagger]) \quad (1.66)$$

where $(i, j = 1, 2, \dots, n^2 - 1)$

$$Tr[\hat{L}_i] = 0 \quad Tr[\hat{L}_i \hat{L}_j^\dagger] = \delta_{ij} \quad (1.67)$$

The \hat{L}_j are the *environment operator*: they describe the influence of the environment on the system. The \hat{L}_i together with the unit operator $\mathbb{1}$ may

be taken normalized, in this case they form a basis in $SU(N)$ space. The parameter matrix A_{ij} is Hermitian e positive semidefinite:

$$A_{ii} \geq 0 \quad |A_{ik}|^2 \leq A_{ii}A_{kk}. \quad (1.68)$$

The $\hat{\mathcal{L}}$ is also known as the *Lindblad operator*.

Bloch Master equation

An other phenomenological approach is the *Bloch Master Equation*. The first formulation due to Bloch [27] is for the study of relaxation in nuclear magnetic resonance. He proposed the differential equations

$$\dot{\mathbf{M}} = \gamma \mathbf{M} \times \mathbf{B}(t) - \frac{M_x}{T_2} \hat{\mathbf{x}} - \frac{M_y}{T_2} \hat{\mathbf{y}} - \frac{M_z - M_z^{eq}}{T_1} \hat{\mathbf{z}} \quad (1.69)$$

where \mathbf{M} is the polarization vector and $\mathbf{B}(t)$ is a time dependent magnetic field. The relaxation times $T_{1,2}$ was taken from experimental results. For an *AC* magnetic field

$$H_z = H_0 \quad H_x = H_1 \cos(\omega t) \quad H_y = H_1 \sin(\omega t) \quad (1.70)$$

with the substitutions

$$\begin{aligned} M_x &= u \cos(\omega t) - v \sin(\omega t) \\ M_y &= u \sin(\omega t) + v \cos(\omega t) \end{aligned} \quad (1.71)$$

the equations take the form

$$\begin{pmatrix} \dot{\hat{u}} \\ \dot{\hat{v}} \\ \dot{\hat{M}}_z \end{pmatrix} = \begin{pmatrix} -\frac{1}{T_2} & -\delta & 0 \\ \delta & -\frac{1}{T_2} & -\gamma H_1 \\ 0 & \gamma H_1 & -\frac{1}{T_1} \end{pmatrix} \begin{pmatrix} \hat{u} \\ \hat{v} \\ \hat{M}_z \end{pmatrix} + \begin{pmatrix} 0 \\ 0 \\ \frac{M_0}{T_1} \end{pmatrix} \quad (1.72)$$

Generalized Bloch Master Equation

It has proven that in case of saturation regime the Bloch equation fails [27, 28]. To avoid this problem a generalized version of the Bloch equation has been introduced [29, 34]. The Generalized Bloch Equation in term of polarization vector is

$$\begin{pmatrix} \dot{\hat{\sigma}}_x \\ \dot{\hat{\sigma}}_y \\ \dot{\hat{\sigma}}_z \end{pmatrix} = \begin{pmatrix} -\Gamma_x & -\delta & \Gamma_{xz} \\ \delta & \Gamma_y & -2\Omega_R \\ \Gamma_{zx} & 2\Omega_R & -\Gamma_z \end{pmatrix} \begin{pmatrix} \hat{\sigma}_x \\ \hat{\sigma}_y \\ \hat{\sigma}_z \end{pmatrix} + \begin{pmatrix} \gamma_x \\ 0 \\ \gamma_z \end{pmatrix} \quad (1.73)$$

here $\delta = \epsilon - \omega$ where ϵ is the splitting of the two level system and ω is the frequency of the driving field. In this equation the relaxation rates depend on the frequency and the amplitude of the driving field. Here $\Gamma_x, \Gamma_y, \Gamma_z, \Gamma_{xz}, \Gamma_{zx}$ depend on the drive characteristics. The relaxation rates differ for σ_x and σ_y ($\Gamma_x \neq \Gamma_y$).

Bloch equation in the form of Lindblad Master Equation A multistate version of Bloch equation in term of density matrix is

$$\dot{\lambda}_i - \sum_{j=1}^s \Omega_{ij} \lambda_j = \sum_{j=1}^s \xi_{ij} \lambda_j + \eta_i \quad (1.74)$$

here $\lambda_i = Tr[\rho \hat{\lambda}_i]$ being $\hat{\lambda}_i$ defined in 1.15. This is an other form of the Lindblad master equation projected on the $\hat{\lambda}_i$ component[3].

Generalized Master Equation (GME)

When the coupling between system and environmen is strong, the standard master equation approach fail. In these cases it is necessary *generalize* the master equation approach. The most general form is the Eq.1.57 that is nonlocal in time. An equation of this form will be described in chapter 6 for the study of the dynamics of the populations in a quantum bistable potential in the strong coupling limit.

1.3.5 Multistage elimination

Generally coherent superconducting devices are coupled with an environment whose operator coupled with the system have a dynamics with a power spectrum $S(\omega) \propto \frac{1}{\omega}$. Then we provide a technique to study the interplay of the fast and slow (adiabatic) component by a two stage elimination [6]. We first decompose $\hat{X}(t) \rightarrow \hat{X}_f(t) + x(t)$. Here $x(t)$ represent the slow component that can be treated as classical stochastic process (do not produce any decay or transition in the system). The component \hat{X}_f have a purely quantum effect on the system but is weak coupled with the system. Multistage approach for broadband noise consists in the equation

$$\rho(t) = \int \mathcal{D}[x(t)] P[x(t)] \rho_f^Q[t|x(t)] \quad (1.75)$$

where ρ_f^Q is the master equation obtained treating only the fast mode of the environment with a master equation approach. This expression become simpler if we use the SPA

$$\rho(t) = \int dx P(x) \rho_f^Q[t|x] \quad (1.76)$$

1.4 Summary and general formalism

We stress that the relation between tunability and resilience to noise has a special significance for solid-state nanodevices because of the central role

played by low-frequency noise in determining dephasing [37, 6] Indeed the sensitivity of qubit performances both to fabrication parameters, whose fluctuations represent a major issue for scalability of the architectures, and to external bias, whose fluctuations act as stray parameters during the operations, is well known.

The system is externally driven, using *controls*, both local (acting on an s_μ only) and nonlocal. Moreover S interacts with an *environment* R of uncontrollable degrees of freedom, the coupling being again local or nonlocal. On the other hand interactions, controls and coupling to environments are limited by the structure of the nodes, and often related to each others. An efficient classification of the Hamiltonian is achieved by specifying its structure in the Liouville space \mathbb{L} , which is the collection of linear operators A acting on the states of \mathbb{H} .

Bibliography

- [1] J. J. Sakurai. *Modern Quantum Mechanics (Revised Edition)*. Addison Wesley, 1 edition, 1993.
- [2] Claude Cohen-Tannoudji, Bernard Diu, Frank Laloe, and Bernard Dui. *Quantum Mechanics (2 vol. set)*. Wiley-Interscience, 2006.
- [3] G. Mahler and V.A. Weberruss. *Quantum networks: dynamics of open nanostructures*. Springer, 1995.
- [4] G. Falci. Quantum dynamics. Notes for Ph.D. course on *Quantum dynamics* at the University of Palermo, 2009-2010.
- [5] Wojciech Hubert Zurek. *Rev. Mod. Phys.*, **75**:715, 2003.
- [6] R. Fazio G.Falci. *Quantum Computer, Algorithms and Chaos.*, chapter Quantum computation with Josephson qubits, pages 363–413. B.L. Altshuler and V. Tognetti IOS Press The Netherlands.
- [7] et. al. G. Falci, M. Berritta. *Physica Scripta*, **2012**(T151):014020, 2012.
- [8] Michael A. Nielsen and Isaac L. Chuang. *Quantum Computation and Quantum Information (Cambridge Series on Information and the Natural Sciences)*. Cambridge University Press, 1 edition, 2004.
- [9] William R. Frensley. *Rev. Mod. Phys.*, **62**:745, 1990.
- [10] A. O. Caldeira and A. J. Leggett. *Phys. Rev. Lett.*, **46**:211, 1981.

- [11] A.O Caldeira and A.J Leggett. *Annals of Physics*, 149(2):374, 1983.
- [12] Yu. Pashkin Y. Nakamura and J. S. Tsai. *Nature*, **398**:786, 1999.
- [13] K. Bergmann, H. Theuer, and B. W. Shore. *Rev. Mod. Phys.*, **70**:1003, 1998.
- [14] Marlan O. Scully and M. Suhail Zubairy. Cambridge University Press, 1 edition, 1997.
- [15] T. D. Ladd, F. Jelezko, R. Laflamme, Y. Nakamura, C. Monroe, and J. L. O'Brien. *Nature*, **464**:45, 2010.
- [16] J. Clarke and F.K. Wilhelm. *Nature*, **453**:1031, 2008.
- [17] R. J. Schoelkopf and S. M. Girvin. *Nature*, **451**:664, 2008.
- [18] D. Vion, A. Aassime, A. Cottet, P. Joyez, H. Pothier, C. Urbina, D. Esteve, and M. H. Devoret. *Science*, **296**:886, 2002.
- [19] K. S. Novoselov, A. K. Geim, S. V. Morozov, D. Jiang, Y. Zhang, S. V. Dubonos, I. V. Grigorieva, and A. A. Firsov. *Science*, **306**:666, 2004.
- [20] S. V. Syzranov, M. V. Fistul, and K. B. Efetov. *Phys. Rev. B*, **78**:045407, 2008.
- [21] Sankar Das Sarma, Michael Freedman, and Chetan Nayak. *Physics Today*, **59**:32, 2006.
- [22] Nori Franco You, J. Q. *Nature*, **474**:589, 2011.
- [23] E. Paladino, A. Mastellone, A. D'Arrigo, and G. Falci. *Phys. Rev. B*, **81**:052502, 2010.
- [24] F Chiarello, E Paladino, M G Castellano, C Cosmelli, A D'Arrigo, G Torrioli, and G Falci. *New Journal of Physics*, **14**:023031, 2012.
- [25] G. Ithier, E. Collin, P. Joyez, P. J. Meeson, D. Vion, D. Esteve, F. Chiarello, A. Shnirman, Y. Makhlin, J. Schrieffer, and G. Schön. *Phys. Rev. B*, **72**:134519, 2005.
- [26] Gustavsson Yan F. Yoshihara F. Harrabi K. Fitch G. Cory D. G. Nakamura Y. Tsai J. Oliver W. D. Bylander, J. *Nat Phys*, **7**:565, 2011.
- [27] F. Bloch. *Phys. Rev.*, **70**:460, 1946.
- [28] Alfred G. Redfield. *Phys. Rev.*, **98**:1787, 1955.

- [29] F. Bloch. *Phys. Rev.*, **105**:1206, 1957.
- [30] C. Cohen-Tannoudji, J. Dupont-Roc, and G. Grynberg. *Atom-Photon Interactions*. Wiley, 1998.
- [31] Melvin Lax. *Phys. Rev.*, **129**:2342, 1963.
- [32] Heinz-Peter Breuer and Francesco Petruccione. *The Theory of Open Quantum Systems*. Oxford University Press, USA, 2007.
- [33] C. W. Gardiner. *Quantum Noise: A Handbook of Markovian and Non-Markovian Quantum Stochastic Methods with Applications to Quantum Optics*. Springer Berlin Heidelberg, 2010.
- [34] E. Geva and R. Kosloff. *Journal of chemical physics*, **102**:8541, 1995.
- [35] Vittorio Gorini, Andrzej Kossakowski, and E. C. G. Sudarshan. *Journal of Mathematical Physics*, **17**:821, 1976.
- [36] G. Lindblad. *Communications in Mathematical Physics*, **48**:119, 1976.
- [37] G. Falci, A. D'Arrigo, A. Mastellone, and E. Paladino. *Phys. Rev. Lett.*, **94**:167002, 2005.
- [38] A. La Cognata, P. Caldara, D. Valenti, B. Spagnolo, A. D'Aarrigo, E. Paladino, and G. Falci. *International Journal of Quantum Information*, **09**:1, 2011.
- [39] A. B. Zorin, F.-J. Ahlers, J. Niemeyer, T. Weimann, H. Wolf, V. A. Krupenin, and S. V. Lotkhov. *Phys. Rev. B*, **53**:13682, 1996.

Chapter 2

Broadband noise effect on Rabi oscillation

Many protocols of quantum computation consist in manipulating quantum systems [1] (in our case coherent superconducting nanodevices) addressing them with AC pulses. Quantum systems subject to a near-resonant AC field show the so called *Rabi oscillations* between population. The fact that Rabi oscillation have been demonstrated for many superconducting qubits [2, 3, 4, 5, 6] opened the way for implementing examples of quantum protocol [7, 8]. In the last years measurement of Rabi oscillation had been used for spectroscopy [9, 10, 11, 12, 13, 14, 15] and for noise spectroscopy [16].

In this chapter we will briefly discuss the structure of the *Rabi problem* (sec.2.1). Then we will study the effect of the broadband noise on the *Rabi oscillation* implemented on *Cooper Pair Box* (CPB) (sec.2.3.1). The result described here are collected in an paper published on Physica Scripta [17]. Many studies have been performed on the effect of quantum noise on Rabi oscillation [18, 19] for standard Markovian noise, generalizing the Optical Bloch Equations. Here we address the effect of low-frequency adiabatic noise, which is non Markovian and find analytic results in the using the *Static Path Approximation* (SPA).

2.1 The Rabi problem

The Rabi problem is defined by the Hamiltonian

$$H(t) = -\frac{1}{2}\varepsilon\sigma_3 + \Omega_0 \cos(\omega t)\sigma_x. \quad (2.1)$$

The Hamiltonian in this form refers to two different bases in the Hilbert space and consequently in the Liouville space. The first is formed by the eigenstates of σ_3 . Typically in the language of quantum computation it is called *computational basis*. The second is that of the eigenstates of σ_x , the *pointer basis*. The relations that allow to switch from one basis to the other in the Liouville space are

$$\begin{cases} \sigma_3 = \cos \theta \sigma_z + \sin \theta \sigma_x \\ \sigma_1 = -\sin \theta \sigma_z + \cos \theta \sigma_x \\ \sigma_2 = \sigma_y \end{cases} \quad \begin{cases} \sigma_z = \cos \theta \sigma_3 - \sin \theta \sigma_1 \\ \sigma_x = \sin \theta \sigma_1 + \cos \theta \sigma_3 \\ \sigma_y = \sigma_2 \end{cases}$$

Generally the analysis of the Rabi problem is made in the rotating frame defined by the unitary transformation

$$|\Psi(t)\rangle = U_{rf}(t) |\Psi(t)\rangle_{rf}; \quad U_{rf}(t) = e^{\frac{i}{2}\phi(t)\sigma_3} \quad (2.2)$$

Substituting the state in the Schrödinger equation

$$i\partial_t |\Psi\rangle = H(t) |\Psi\rangle; \quad i\partial_t U_{rf}(t) |\Psi(t)\rangle_{rf} = H(t) U_{rf}(t) |\Psi(t)\rangle_{rf}$$

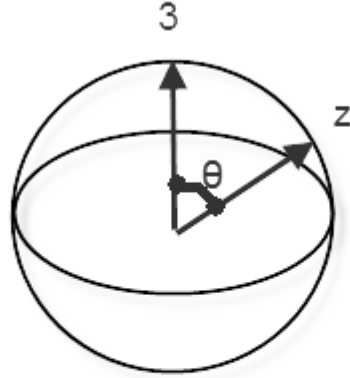


Figure 2.1: Graphical representation of the spin operator that appear in the Rabi Hamiltonian in the Bloch sphere.

with a little algebra the Hamiltonian in the rotating frame become

$$\begin{aligned}\tilde{H} &= U(t)H(t)U^\dagger(t) - iU(t)\partial_t U^\dagger(t) \\ &= -\frac{1}{2}[\delta - 2\Omega_0 \cos \theta \cos \omega t]\sigma_3 + \sin \theta \Omega_0 \cos(\omega t)(e^{-i\omega t} \sigma_+ + e^{i\omega t} \sigma_-)\end{aligned}\quad (2.3)$$

2.1.1 Quasi resonant and transvers approximation (TR).

The only field's component that generate transitions between the eigenstates of σ_3 are the quasi resonant terms that appear as the off-diagonal term of the Hamiltonian in the representation of the eigenstates of σ_3 (*transversal terms*). Then it is sufficient to retain only the *quasi-resonant transversal* terms.

2.1.2 Rotating Wave Approximation (RWA).

It is possible to simplify $H_c(t)$, using another approximation. This consists in considering only the circularly corotant polarized terms. We can obtain this approximation by writing the cosine in exponential form as $\cos x =$

$\frac{1}{2}(e^{ix} + e^{-ix})$. The term proportional to $e^{-2i\phi_p(t)}$, oscillate rapidly (in the rotating frame) and averaging them on a sufficiently small time interval Δt . This is the so called *coarse graining* procedure. Then in a coarse-grained dynamics they may be neglected. With the RWA and retaining only the transversal terms the Hamiltonian is

$$\tilde{H} = -\frac{1}{2}\delta\sigma_3 + \frac{1}{2}\Omega_R\sigma_1. \quad (2.4)$$

2.1.3 Density matrix in the rotating frame.

The transformation to the rotating frame does not affect the expectation value of the operator σ_3 . Indeed the unitary transformation $U_{rf}(t)$ does not change the σ_3 operator. We have

$$\langle\sigma_3\rangle = Tr[\sigma_3\tilde{\rho}(t)] = Tr[\sigma_3U_{rf}(t)\rho(t)U_{rf}^\dagger(t)] = Tr[\sigma_3\rho(t)] \quad (2.5)$$

where in the last step we used the cyclic properties of the trace.

2.1.4 Dynamics of Rabi oscillation

From eq.2.4 the dynamics of the Rabi oscillation is obtained

$$\rho_{10}(t) = \frac{\Omega_R}{\Omega_f} e^{-i\Omega_f t} \quad (2.6)$$

where $\Omega_f = \sqrt{\Omega_R^2 + \delta^2}$

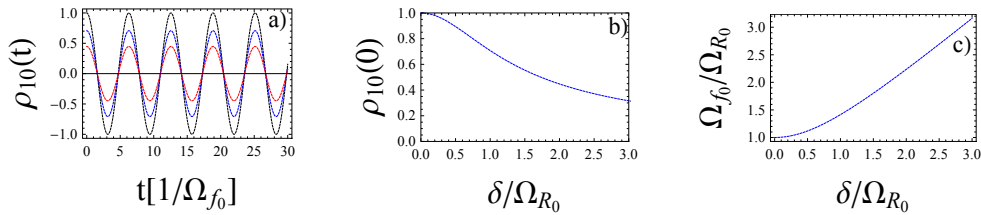


Figure 2.2: a) The dynamics of Rabi oscillations is showed for different choise of detuning δ in fuction of the time. the time units varies for different curve since $\Omega_f = \sqrt{\Omega_R^2 + \delta^2}$. Black line ($\delta = 0$), blue line ($\delta = 1$), red line ($\delta = 2$). b) Dependence of the amplitude of Rabi oscillations on detuning. c) Dependence of the frequency of Rabi oscillations on detuning.

2.2 Rabi oscillation in Cooper pair box

The main aim of this chapter is the analysis of the broadband noise effect on the dynamics of *Rabi oscillation*. We focus on the implementation of Rabi oscillation with a charge qubit.

The standard Hamiltonian for superconducting nanodevices is

$$H_C[q_g(t)] = E_C \sum_q (q - q_g(t))^2 |q\rangle \langle q| - \frac{E_J}{2} \sum_q (|q\rangle \langle q+1| + |q+1\rangle \langle q|) \quad (2.7)$$

where $E_C = \frac{e^2}{2C}$ is the charging energy, E_J is the Josephson energy and $|q\rangle$ are charge states. In particular, in a Cooper Pair Box and in general in the qubits that work in a charge regime varying the gate voltage of the device, we can control the charge of the superconducting island via q_g . Then we consider in our model

$$q_g \rightarrow q_g + q_c(t) + x(t) \quad (2.8)$$

where q_g is the bias of the CPB and determines the working point, $q_c(t)$ is the control signal of the system and $x(t)$ is, in principle, a quantum stochastic process. Following the approach described in (sec.1.3.5), we write the Hamiltonian of the driven CPB in the form

$$H = H_0[q_g + x(t)] + A(t)\hat{Q} + H_{fn} \quad (2.9)$$

in this specific case

$$\begin{aligned} H_0[q_g + x(t)] &= E_C \sum_q (q - 2q_g - 2x(t))q |q\rangle \langle q| \\ &+ \frac{E_J}{2} \sum_q (|q\rangle \langle q+1| + h.c.) \end{aligned} \quad (2.10)$$

$$\begin{aligned} A(t)\hat{Q} &= -2E_C q_c(t) \sum_q q |q\rangle \langle q| \\ H_{fn} &= \hat{Q}\hat{X} \end{aligned} \quad (2.11)$$

where we separated the purely quantum part of the noise and the slow part that can be treated as a classical stochastic process as $\hat{x} \rightarrow \hat{X}_f + x(t)$. Projecting this Hamiltonian on the first two charge states we obtain

$$H_0[q_g + x(t)] = -\frac{1}{2}\Omega[x(t)]\sigma'_3 \quad (2.12)$$

$$A(t)\hat{Q} = A_0 \cos(\omega t)\sigma_z \quad (2.13)$$

$$H_{fn} = \hat{X}\hat{Q} + H_R; \quad \hat{X} = -2E_C\hat{X}_f \quad (2.14)$$

here

$$\sigma_z = |0\rangle\langle 0| - |1\rangle\langle 1| \quad (2.15)$$

$$\sigma_x = |1\rangle\langle 0| + |0\rangle\langle 1| \quad (2.16)$$

$$\Omega[x(t)] = \sqrt{E_C^2(1 - 2q_g - 2x(t))^2 + E_J^2} \quad (2.17)$$

$$\sigma'_3 = \sigma_3 = \cos\{\theta[x(t)]\}\sigma_z + \sin\{\theta[x(t)]\}\sigma_x \quad (2.18)$$

$$(2.19)$$

the apex on σ_3 means that it depends on $x(t)$ via the angle

$$\theta[x(t)] = \arctan \frac{E_J}{E_C(1 - 2q_{g_0} - 2x(t))} \quad (2.20)$$

and q_{g_0} is the fixed gate.

2.3 Multistage elimination

To study the effect of broadband noise on the dynamics of the Rabi oscillation in the framework of the multistage elimination we have to trace away the bath quantum degree of freedom and then treat the slow component with the SPA. There are many studies in the literature on the effect of quantum noise on Rabi oscillations [18, 19], based on the master equation approach in the Bloch form and its tergeneralization. We account for the effects of the quantum noise on the Rabi oscillation dynamics with an exponential decay factor of the form $e^{\frac{\gamma}{2}t}$. We will integrate these results with the analysis of adiabatic noise in the framework of SPA [20]. As we said in 1.3.3 the SPA consist in treating the realizations of the slow stochastic process as random variable. Then we model a nanodevice in an external AC field by the Hamiltonian

$$H(t|x) = H_0(q_g + x) + A(t)\hat{Q} \quad (2.21)$$

where $A(t) = \mathcal{A} \cos \phi(t)$ is the control field with carrier frequency ω . The device is nominally biased at q_g with a random additive component x distributed with a zero average $\mathcal{P}(x)$. We consider $H_0(q_g + x)$ and for each x we define (dependence on q_g is omitted hereafter) the “ x -basis” $\{|\phi_i(x)\rangle\}$ of its eigenstates and the conditional (Schrödinger or laboratory frame) propagator $U_S(t|x)$ corresponding to $H(t|x)$. Usual protocols in nanodevices start with an imperfect (x -dependent) initialization in the lowest energy state, $\rho(0) = \int dx \mathcal{P}(x) |\phi_0(x)\rangle\langle \phi_0(x)|$. Then the system evolves conditionally to

x as $\rho(t|x) = U_S(t|x) |\phi_0(x)\rangle \langle \phi_0(x)| U_S^\dagger(t|x)$. Finally populations of the x -dependent eigenstates are measured, yielding

$$P_i(t) = \int dx \mathcal{P}(x) \langle \phi_i(x) | \rho(t|x) | \phi_i(x) \rangle \quad (2.22)$$

i.e. the simple ensemble average of conditional population histories. Averaging defocuses the coherent signal, which appears to be suppressed in time. Alternative preparations and readout of different observables may lead to further suppression of the signal, which however does not accumulate in time and in these cases Eq.(2.22) is not exact but is still a good approximation.

We now derive $U_S(t|x)$ in the Rotating Wave (RW) approximation. To this end we represent in the x -basis, $H_c(t) = A(t) \hat{Q} = \sum_{ij} A(t) Q_{ij}(x)$ and approximate this control Hamiltonian by retaining only off-diagonal quasi resonant entries, Q_{ij} such that $|E_i - E_j| \sim \omega$, and by neglecting the counterrotating part of the field. If only the lowest doublet is addressed this yields

$$H_{RW}(t|x) = \frac{\mathcal{A}}{2} e^{-i\phi(t)} Q_{10}(x) \hat{P}_{10}(x) + \text{h.c.}$$

where $\hat{P}_{ij}(x) = |\phi_i(x)\rangle \langle \phi_j(x)|$ are the transition operators. Physically the RW approximation keeps only control entries “effective” in triggering transitions between different states. Notice this effective part of the control depends on the random variable x . Terms we neglect produce a small shift in the frequencies and a small fast modulation of the signal.

2.3.1 Adiabatic noise effect

To study the adiabatic noise effect we perform a transformation to the rotating frame in RWA and the *transverse approximation* of the Hamiltonian 2.12 The relevant dynamics is described by the Hamiltonian

$$\tilde{H}(t|x) = \begin{bmatrix} 0 & \Omega_R^*(x)/2 \\ \Omega_R(x)/2 & \delta(t|x) \end{bmatrix} \quad (2.23)$$

Here, $\Omega_R(x) = \mathcal{A} Q_{10}(x)$ is the peak Rabi frequency and $\delta(x) = E_1(x) - \omega$ is the detuning for a monochromatic field $\phi(t) = \omega$ (we let $E_0 = 0$). Notice that the effect of low-frequency noise in artificial atoms, which is due to their internal fluctuations, is conveniently recast in terms of sensitivity to imperfections (both in phase and amplitude) of a fictitious drive. The corresponding populations are readily found, e.g. $P_1(t|x) = \Omega_R/(2\Omega_{fl}) [1 - \cos(\Omega_{fl}t)]$ where the flopping frequency for Rabi oscillations is $\Omega_{fl}(x) = \sqrt{\delta^2(x) + \Omega_R^2(x)}$. The average, Eq.(2.22), yields

$$P_1(t) = \bar{P}_1 - \bar{P}_1 \mathcal{R}e\langle e^{-i\Omega_{fl}(x)t} \rangle$$

where we neglect fluctuations of the amplitude, allowing to approximate

$$\bar{P}_1 \approx \Omega_{R0} / \sqrt{\delta_0^2 + \Omega_{R0}^2}$$

by values at $x = 0$ (but still depending on the bias q). This requires that fluctuations of the Rabi couplings and of the level splitting induced by fluctuations of x are small. Under the same condition we can calculate the average by expanding to second order $\Omega_{fl}(x) \approx \Omega_{fl}(0) + Ax + \frac{1}{2}Bx^2$, and assuming that $\mathcal{P}(x)$ is a Gaussian with variance σ_x , obtaining

$$\langle e^{-i\Omega_{fl}(x)t} \rangle = e^{-i\Omega_{fl}(0)t} e^{-i\Phi(t)} \quad (2.24)$$

$$e^{-i\Phi(t)} = \frac{1}{\sqrt{1 + iB\sigma_x^2 t}} \exp \left[-\frac{A^2\sigma_x^2 t^2}{2(1 + iB\sigma_x^2 t)} \right] \quad (2.25)$$

This equation describes different regimes for the decay of Rabi oscillations,

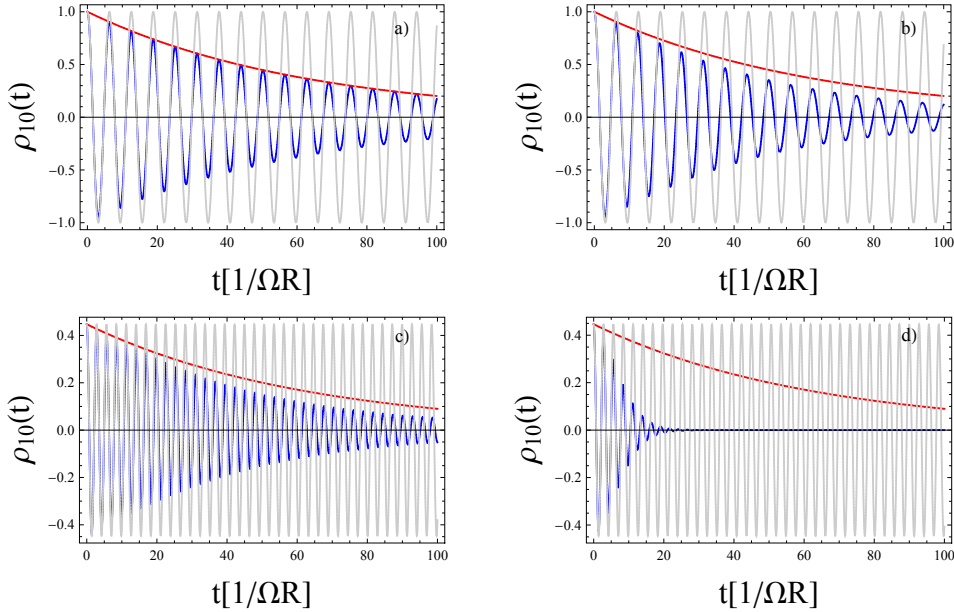


Figure 2.3: Here the dynamics of Rabi oscillation in CPB with broadband noise are shown for different working point and detuning values (blue lines). These are compared with the Rabi oscillations for same parameters without noise (grey lines), and with the decay factor due only to the fast part of the noise (red lines). a) Resonant signal at optimal working point $\delta = 0$, $q_g = 0.5$. b) Resonant signal far from optimal working point $\delta = 0$, $q_g = 0.45$. c) Non-resonant signal at optimal working point $\delta = -2$, $q_g = 0.5$. d) Non-resonant signal far from optimal working point $\delta = -2$, $q_g = 0.45$.

namely a Gaussian time decay $|e^{-i\Phi(t)}| \sim e^{-\frac{1}{2}A^2\sigma_x^2 t^2}$ when the linear term

in the expansion dominates, and power-law behavior $\sim 1/(\sigma_x\sqrt{Bt})$ when $A \rightarrow 0$. In this regime Eq.(2.25) describes the initial suppression of the signal since for physical systems decay turns to simple exponential at later times, $\sim |e^{-i\Phi(t)}| e^{\gamma t/2}$, where γ is the spontaneous decay rate not accounted for in the SPA. Manipulating the eq.2.25 it is possible to individuate two other characteristic term. A frequency shift that is present only if the drive is operated out of optimal working point $q_g = \frac{1}{2} \rightarrow A(q_g) = 0$

$$\delta\Omega_f(t) = \frac{1}{2} \frac{\sigma_x^4 A(q_g)^2 B(q_g) t^2}{1 + \sigma_x^4 B(q_g)^2 t^2} \quad (2.26)$$

and a phase shift

$$\delta\phi(t) = \frac{1}{2} \arctan(\sigma_x^2 B(q_g) t) \quad (2.27)$$

The decay law Eq. (2.25) depends on the spectrum via the series expansion of $\Omega_{fl}(x)$. We define the derivatives of the spectrum $A_i = \partial E_i / \partial q$ and $B_i = \partial^2 E_i / \partial q^2$ and the coefficients $a_R = (\partial Q_{10} / \partial q) / Q_{10}$ and $b_R = (\partial^2 Q_{10} / \partial q^2) / Q_{10}$ and expand

$$\begin{aligned} \delta(q+x) &\approx \delta_0 + A_1(q)x + \frac{1}{2} B_1(q)x^2 \\ \Omega_R(q+x) &\approx \Omega_{R0} [1 + a_R(q)x + \frac{1}{2} b_R(q)x^2] \end{aligned}$$

This makes explicit the dependence on the parameters $(q, \Omega_{R0}, \delta_0)$ which are taken as independent. We also define $(A_R, B_R) = \Omega_{R0}(a_R, b_R)$ which scale with Ω_{R0} ; notice that (A_1, B_1) scale with the much larger Bohr splitting. With this notation, the coefficients entering Eq.(2.25) read

$$\begin{aligned} A(q, \Omega_{R0}, \delta_0) &= [\delta_0 A_1 + \Omega_{R0} A_R] / \Omega_{fl} \\ B(q, \Omega_{R0}, \delta_0) &= [A_1^2 + A_R^2 - A^2 + \delta_0 B_1 + \Omega_{R0} B_R] / \Omega_{fl} \end{aligned}$$

At the resonance they reduce to $A = A_R$ and $B = A_1^2 / \Omega_{R0} + B_R$ which would imply a Gaussian time decay if fluctuations of Q_{10} were important, otherwise the decay has essentially power-law behavior. In the dispersive regime we would have $A \approx A_1$, i.e. when energy fluctuations are linear we recover the Gaussian decay law of coherent oscillations, and $B \approx (B_1 + A_R^2) / \Omega_{fl}$.

Notice that even if Eq.(2.25) describes the same regimes of the SPA for coherent oscillations of undriven systems [20], the situation is now different. In particular Eq.(2.25) quantitatively accounts for the fact that AC driving greatly reduces decoherence compared to undriven systems. This common statement is based on the intuitive expectation that an AC field may average effects of noise and is corroborated by experiments [11]. To be more specific, let us neglect, for the moment, fluctuations of Q_{ij} . At resonance, $\delta_0 = 0$, nonvanishing linear fluctuations of the spectrum, $A_1 \neq 0$, determine

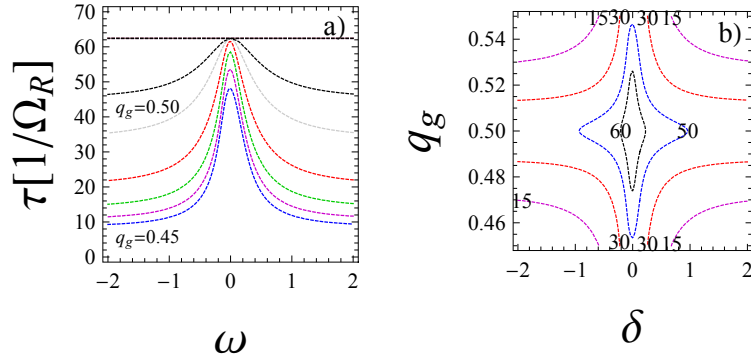


Figure 2.4: a) Decay time T_R of Rabi oscillations as a function of the nominal detuning δ , obtained from $\mathcal{I}m\Phi(T) = -1$ for a CPB in charge regime. The curve $q = 0.5$ refers to the symmetry point, whereas the others $q = 0.48, 0.46, 0.45$ refer to the devices biased off-symmetry. The constant line $T_R = \gamma/2$ is an added simple exponential decay accounting for spontaneous emission. b) Contour plot of decay time in function of the gate charge and of the detuning.

quadratic fluctuations of $\Omega_{fl}(x)$. Therefore $A = 0$ and Rabi oscillations undergo power-law decay, whereas in the absence of drive they determine the much stronger Gaussian decay $\sim e^{-\frac{1}{2}A_1^2\sigma_x^2 t^2}$ of coherent oscillations. In this regime measurements of Rabi oscillations [16] have been used to probe the environment¹ of a flux qubit. At symmetry points, where $A_1 = 0$, coherent oscillations decay with a power law, whereas Rabi oscillation are practically unaffected by low-frequency noise, and in physical systems they decay only due to spontaneous emission.

Exploiting the dependence on the detuning we find that for non-vanishing δ_0 the decay laws are the same as for coherent oscillations. In particular at symmetry points low-frequency noise determines an initial decoherence which takes over spontaneous decay. An even stronger suppression of coherence occurs off-symmetry. Therefore for increasing δ_0 we expect dephasing to interpolate between the behavior of AC driven and undriven systems, all the phenomenology depending on the single noise figure σ_x .

The above picture is applicable to many physical situations, since fluctuations of Q_{ij} are small. Indeed they correspond to a fraction of $\Omega_R \neq 0$, whereas $\delta(x)$ fluctuates on the scale of the Bohr splitting $E_1 - E_0 \gg \Omega_R$ and may be particularly relevant for $\delta_0 = 0$. However the dependence $Q_{ij}(q)$

¹In this case noise source and drive were not referring to the same port, results of this work can be easily extended to devices with many noise ports.

may lead to consequences in multilevel systems.

Bibliography

- [1] R. Fazio G.Falci. *Quantum Computer, Algorithms and Chaos.*, chapter Quantum computation with Josephson qubits, pages 363–413. B.L. Altshuler and V. Tognetti IOS Press The Netherlands.
- [2] Y. Nakamura, Yu. A. Pashkin, and J. S. Tsai. *Phys. Rev. Lett.*, **87**:246601, Nov 2001.
- [3] D. Vion, A. Aassime, A. Cottet, P. Joyez, H. Pothier, C. Urbina, D. Esteve, and M. H. Devoret. *Science*, **296**:886, 2002.
- [4] I. Chiorescu, Y. Nakamura, C. J. P. M. Harmans, and J. E. Mooij. *Science*, **299**:1869, 2003.
- [5] John M. Martinis, S. Nam, J. Aumentado, and C. Urbina. *Phys. Rev. Lett.*, **89**:117901, 2002.
- [6] Yang Yu, Siyuan Han, Xi Chu, Shih-I Chu, and Zhen Wang. *Science*, **296**:889, 2002.
- [7] A. J. Hoffman, S. J. Srinivasan, J. M. Gambetta, and A. A. Houck. *Phys. Rev. B*, **84**:184515, 2011.
- [8] Tatsuya Kutsuzawa, Hirotaka Tanaka, Shiro Saito, Hayato Nakano, Kouichi Semba, and Hideaki Takayanagi. *Applied Physics Letters*, **87**:073501, 2005.
- [9] I. Chiorescu, P. Bertet, K. Semba, Y. Nakamura, C. J. P. M. Harmans, and J. E. Mooij. *Nature*, **431**:159, 2004.
- [10] Jürgen Lisenfeld, Clemens Müller, Jared H. Cole, Pavel Bushev, Alexander Lukashenko, Alexander Shnirman, and Alexey V. Ustinov. *Phys. Rev. B*, **81**:100511, 2010.
- [11] G. Ithier, E. Collin, P. Joyez, P. J. Meeson, D. Vion, D. Esteve, F. Chiarello, A. Shnirman, Y. Makhlin, J. Schrieffer, and G. Schön. *Phys. Rev. B*, **72**:134519, 2005.
- [12] V. I. Shnyrkov, D. Born, A. A. Soroka, and W. Krech. *Phys. Rev. B*, **79**:184522, 2009.

- [13] A. Fedorov, A. K. Feofanov, P. Macha, P. Forn-D'iaz, C. J. P. M. Harmans, and J. E. Mooij. *Phys. Rev. Lett.*, **105**:060503, 2010.
- [14] S. Saito, T. Meno, M. Ueda, H. Tanaka, K. Semba, and H. Takayanagi. *Phys. Rev. Lett.*, **96**:107001, 2006.
- [15] A. Lupaşcu, P. Bertet, E. F. C. Driessen, C. J. P. M. Harmans, and J. E. Mooij. *Phys. Rev. B*, **80**:172506, 2009.
- [16] Gustavsson Yan F. Yoshihara F. Harrabi K. Fitch G. Cory D. G. Nakamura Y. Tsai J. Oliver W. D. Bylander, *J. Nat Phys*, **7**:565, 2011.
- [17] et. al. G. Falci, M. Berritta. *Physica Scripta*, **2012**(T151):014020, 2012.
- [18] E. Geva and R. Kosloff. *Journal of chemical physics*, **102**:8541, 1995.
- [19] C. Cohen-Tannoudji, J. Dupont-Roc, and G. Grynberg. *Atom-Photon Interactions*. Wiley, 1998.
- [20] G. Falci, A. D'Arrigo, A. Mastellone, and E. Paladino. *Phys. Rev. Lett.*, **94**:167002, 2005.

Chapter 3

STIRAP and other coherent process

Contents

0.8	Three level system	lix
0.8.1	Scheme for a three level system in an external field	lix
0.8.2	General Hamiltonian	lix
0.8.3	Effective Hamiltonian and RWA	lx
0.9	Coherent trapping and STIRAP	lxii
0.9.1	Coherent trapping in a Dark state	lxii
0.9.2	Population transfer	lxiii
0.9.3	Coherent transfer and STIRAP	lxiv
0.10	Adiabaticity condition for STIRAP	lxvi
0.10.1	STIRAP on adiabatic representation	lxvi
0.10.2	Adiabaticity: global and local criteria	lxvi
0.10.3	General Hamiltonian	lxvii
0.11	Phenomena involved in the STIRAP	lxvii
0.12	Resilience to parameters	lxviii
0.12.1	Resilience to delay	lxix
0.12.2	Symmetry of external field	lxx
0.12.3	Resilience to detuning	lxxi
0.12.4	Correlaated detunings = $P(t_f \delta, a\delta)$	lxxii
0.13	Conclusion	lxxiii
	Bibliography	lxxiii

The coherent dynamics of electrons in many level atoms plays a fundamental role for understanding quantum mechanics. It shows clearly interference phenomena [1], and many other effect as the dynamical formation of the Autler-Townes splitting (AT) of the spectrum or the *Electromagnetically Induced Transparency*, that allows to modify the dielectric constant of an active material using an incident laser with a appropriate frequency [1, 2]. In this chapter, that mainly follows the logic of a review paper of Vitanov [2], two phenomena will be described: *coherent population trapping in a “dark state”*. and the *Stimulated Raman Adiabatic Passage* (STIRAP) [3, 4, 5]. This material is propedeutical for the next two chapters, where new results are presented.

In the last years it was proposed that these coherent effects could be observed also in artificial atoms [6, 7, 8, 9, 10, 11]. This would imply important evolution in the application on the field of microwave manipulation ultra-fast switch device for microwave photons [12] and wavepacket transfer [13]. Other interesting applications could be the possibility to build quantum

state in nanomechanical resonator [10], electromagnetic resonators [14] and the possibility of manipulating solid state qubits [15].

3.1 Three level system

3.1.1 Scheme for a three level system in an external field

Often in atomic and molecular physics, due to selection rules, it happens that the possible transitions in a three level system involve only two couple of states. This implies that the transitions induced by external fields resonant with the Bohr's frequency could give three configuration: Lambda, Vee, Ladder configurations Fig.3.1 [5].

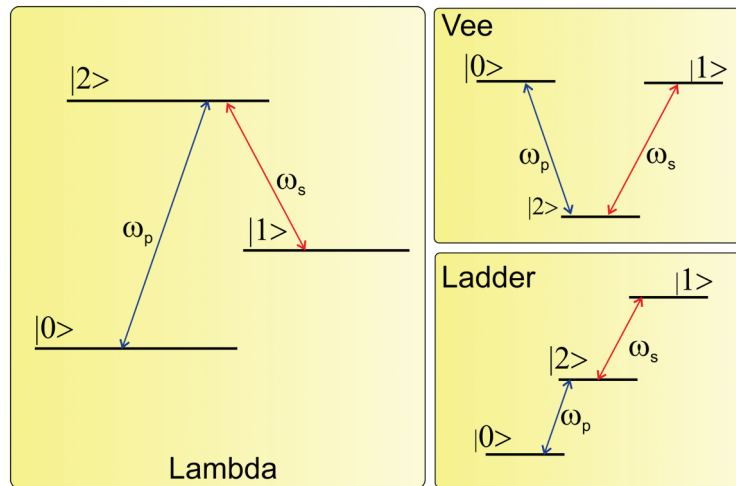


Figure 3.1: Schemi Lambda, Vee e Ladder per sistema a tre livelli

In the *Lambda* configuration, the external field couple the highest energy level $|2\rangle$ with the other two $|0\rangle$ e $|1\rangle$; in other word $|2\rangle$ is the linkage between the two state $|0\rangle$ and $|1\rangle$ in the two photon Raman process. In the *Ladder* configuration, the levels involved in the Raman process have increasing energy. In the *Vee* configuration, the intermediate state is the one with lowest energy.

3.1.2 General Hamiltonian

We start with the single *control-port* Hamiltonian

$$H(t) = H_0 + H_c(t) \quad ; \quad H_c(t) = A(t)\hat{Q} \quad (3.1)$$

where $H_0 = \sum_{i=0}^2 E_i |i\rangle \langle i|$ describes the three isolated and stationary quantum levels, $H_c(t)$ represent the effect of the external field. We make the assumption that the external control field is coupled to the system only via the operator \hat{Q} . Generally, in atomic physics \hat{Q} is the dipole moment operator and $A(t)$ is a classical electric field.

Projecting the control Hamiltonian $H_c(t)$, on the eigenstates basis of H_0 , we obtain

$$H_c(t) = A(t) \sum_{i,j=0}^2 \langle i | \hat{Q} | j \rangle P_{ij}$$

where $\langle i | \hat{Q} | j \rangle$ are the matrix element of \hat{Q} , in the eigenstates of H_0 . To obtain the Hamiltonian for the configuration discussed in (§3.1.1), we consider a two-tone control field $A(t)$

$$\begin{aligned} A(t) &= \mathcal{A}_p(t) \cos \phi_p(t) + \mathcal{A}_s(t) \cos \phi_s(t) \\ \phi_k(t) &= \omega_k t + \phi_{k0} \quad \text{per } k = p, s \end{aligned} \quad (3.2)$$

The two fields are called Pump and Stokes and have angular frequency quasi-resonant to corresponding transition. For example choosing $\omega_p \simeq E_2 - E_0$ and $\omega_s \simeq E_2 - E_1$ we obtain the *Lambda* configuration.

3.1.3 Effective Hamiltonian and RWA

Under the condition for the implementation of the STIRAP ($\delta_p \simeq E_2 - E_0$ and $\omega_s \simeq E_2 - E_1$ in *Lambda* configuration) it is possible to obtain an approximate form of the Hamiltonian, that allows to calculate analitically most of the physical features of the dynamics. Now we discuss the approximations in the case of *Lambda* configuration.

Quasi-resonant and transversal approximation The signals produce transition only between quiresonant levels, *i.e.* $p = 0 \rightarrow 2$ and $s = 1 \rightarrow 2$, then it is reasonable retain only the transversal quasi-resonant terms

$$H_c(t) \simeq Q_{02} \mathcal{A}_p(t) \cos \phi_p(t) P_{02} + Q_{01} \mathcal{A}_s(t) P_{01} \cos \phi_s(t) + h.c. \quad (3.3)$$

Rotating Wave Approximation (RWA) In the same spirit of (RWA) used for Rabi oscillation it is possible write the driving fields retaining only the circularly corotant polarized terms

$$H_c(t) \simeq H_c^{RWA}(t) = \frac{1}{2} [Q_{02} \mathcal{A}_p(t) e^{i\phi_p(t)} P_{02} + Q_{01} \mathcal{A}_s(t) e^{i\phi_s(t)} P_{01} + h.c.] \quad (3.4)$$

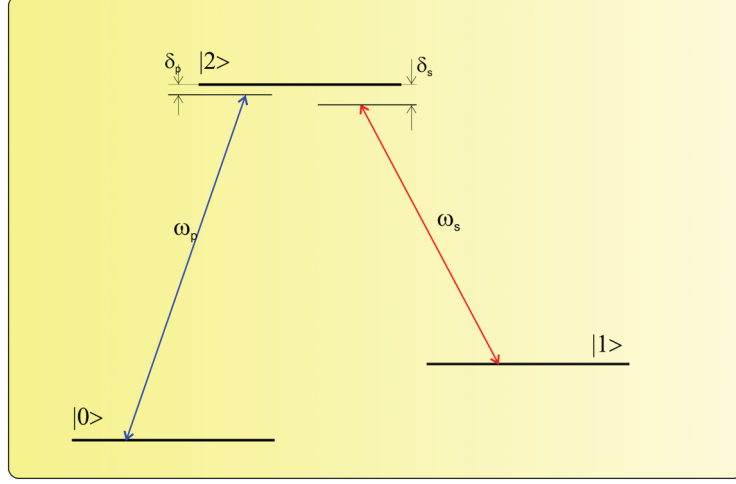


Figure 3.2: Three level energetic spectra and detuning

Effective Hamiltonian in the rotating frame. Using the approximations described above we can recast the problem in a simpler form in the *rotating frame*. Following the prescription of sec.1.1.3 we define an unitary transformation $U_{rf}(t)$.

$$U_{rf}(t) = e^{i[\phi_p(t)-\phi_{p0}]P_{00}} e^{i[\phi_s(t)-\phi_{s0}]P_{11}} \quad , \quad |\psi\rangle_S = U_{rf} |\psi\rangle \quad (3.5)$$

Then the state $|\psi(t)\rangle$ satisfies an equation with the same structure of the Schrödinger equation for $|\psi\rangle_S$, but with a new effective Hamiltonian

$$i\partial_t |\psi(t)\rangle = \tilde{H}(t) |\psi(t)\rangle \quad ; \quad \tilde{H}(t) = U_{rf}^\dagger(t) H U_{rf}(t) - iU_{rf}^\dagger(t) \partial_t U_{rf}(t) \quad (3.6)$$

In the rotating frame, the Hamiltonian $H_0 + H_{RWA}(t)$ is

$$\begin{aligned} H_0 + H_{RWA}(t) &\longrightarrow \tilde{H} = U_{rf}^\dagger [H_0 + H_{RWA}(t)] U_{rf} - iU_{rf}^\dagger \partial_t U_{rf} \\ &= [H_0 - iU_{rf}^\dagger \partial_t U_{rf}] + U_{rf}^\dagger H_{RWA}(t) U_{rf} \end{aligned}$$

The transformation cancels the time dependence of the Hamiltonian. In the diagonal term are subtracted the frequency. Defining the *detuning* of the fields δ_p , δ_s , and the *two photon detuning* $\delta = \delta_p - \delta_s$ as

$$\delta_p(t) = E_2 - \dot{\phi}_p; \quad \delta_s(t) = E_2 - E_1 - \dot{\phi}_s; \quad \delta(t) = E_1 - (\dot{\phi}_p - \dot{\phi}_s)$$

we obtain (sec. 1.1.3)

$$\begin{aligned} H(t) &= \delta(t)P_{11} + \delta_p(t)P_{22} + \\ &+ \frac{1}{2}[\mathcal{A}_p(t)e^{i\phi_{p0}}Q_{02}P_{02} + \mathcal{A}_s(t)e^{i\phi_{s0}}Q_{12}P_{12} + h.c.] \end{aligned} \quad (3.7)$$

The effective Hamiltonian may be written in matrix form as:

$$\tilde{H}(t) = \begin{bmatrix} 0 & 0 & \frac{1}{2}\Omega_p^*(t) \\ 0 & \delta(t) & \frac{1}{2}\Omega_s^*(t) \\ \frac{1}{2}\Omega_p(t) & \frac{1}{2}\Omega_s(t) & \delta_p(t) \end{bmatrix} \quad (3.8)$$

where we defined the Rabi angular frequency

$$\Omega_p(t) = e^{-i\phi_p(0)}Q_{20}\mathcal{A}_p(t); \quad \Omega_s(t) = e^{-i\phi_s(0)}Q_{21}\mathcal{A}_s(t)$$

In the case of two monocromatic field component the detunings do not depend on time and are

$$\delta_p = E_2 - E_0 - \omega_p; \quad \delta_s = E_2 - E_1 - \omega_s; \quad \delta = \delta_p - \delta_s = E_1 - E_0 - (\omega_p - \omega_s)$$

In what follows we will consider two Gaussian shaped pulse

$$\mathcal{A}_s(t) = \mathcal{A}_{s0} e^{-(t+\tau)^2/T^2}; \quad ; \quad \mathcal{A}_p(t) = \mathcal{A}_{p0} e^{-(t-\tau)^2/T^2}; \quad (3.9)$$

that describe the pulses of duration $\propto T$, with a peak value at $t = \pm\tau$.

3.2 Coherent trapping and STIRAP

3.2.1 Coherent trapping in a Dark state

Hamiltonian in an AC field

We consider the Hamiltonian Eq.3.8 in the RWA in the case of AC pulse ($\delta_k(t) = \delta_k$), $\Omega_k(t) = \Omega_k$. An important case is that of two photon resonance, $\delta = 0$, for which we have

$$\tilde{H} = \begin{bmatrix} 0 & 0 & \frac{1}{2}\Omega_p^* \\ 0 & 0 & \frac{1}{2}\Omega_s^* \\ \frac{1}{2}\Omega_p & \frac{1}{2}\Omega_s & \delta_p \end{bmatrix}$$

The stationary states are obtained solving the eigenvalues problem.

Eigenvalues. The eigenvalues are

$$\epsilon_D = 0; \quad \epsilon_{\pm} = \frac{\delta_p}{2} \pm \frac{1}{2}\sqrt{\delta_p^2 + \Omega^2}, \quad \text{where} \quad \Omega = \sqrt{|\Omega_p|^2 + |\Omega_s|^2}$$

Where Ω is the effective value of the external angular frequency. The energy spectra will be formed by a null eigenvalue and two eigenvalues named *Autler-Townes* (AT). They are separated by the (AT) splitting

$$\Omega_{AT} = \sqrt{\delta_p^2 + \Omega^2}$$

This structure of the spectra of a three level system under the effect of AC field is named AT effect.

Eigenstates. The eigenvalues are named *dressed states*. The basis $\{|i\rangle\}$ of eigenstates without field is named of *bare states*. The *Dark State* or *Trapped State* corresponding to the null eigenvalues, is given by

$$|D\rangle = \frac{\Omega_s}{\Omega} |0\rangle - \frac{\Omega_p}{\Omega} |1\rangle \quad (3.10)$$

and the AT eigenstates are

$$\begin{aligned} |+\rangle &= \frac{\Omega_p^*}{\Omega} \sin \Phi |0\rangle + \frac{\Omega_s^*}{\Omega} \sin \Phi |1\rangle + \cos \Phi |2\rangle \\ |-\rangle &= \frac{\Omega_p^*}{\Omega} \cos \Phi |0\rangle + \frac{\Omega_s^*}{\Omega} \cos \Phi |1\rangle - \sin \Phi |2\rangle \end{aligned} \quad \text{dove} \quad \tan 2\Phi = \frac{\Omega}{\delta_p} \quad (3.11)$$

A crucial point is the fact that they could be written using the *Bright state*

$$|B\rangle = \frac{\Omega_p^*}{\Omega} |0\rangle - \frac{\Omega_s^*}{\Omega} |1\rangle$$

then

$$\begin{aligned} |+\rangle &= \sin \Phi |B\rangle + \cos \Phi |2\rangle \\ |-\rangle &= \cos \Phi |B\rangle - \sin \Phi |2\rangle \end{aligned}$$

$|D\rangle$ and $|B\rangle$ represent an orthogonal basis for the subspace $\text{span}\{|0\rangle, |1\rangle\}$.

In quantum optics the name *Dark State* is referred to a particular state of an electron in atoms or molecules, for which it is not possible to have absorption or emission of photon. The trapping of a population in a specific state is an interference phenomena[2]. The *Dark* state is decoupled by the laser. It is formed by a linear combination of the initial state and final state and does not have any component along $|2\rangle$. In fact, despite the coupling between the state $|0\rangle$ and $|1\rangle$ and the states $|2\rangle$ this process interferes destructively maintaining the population on $|2\rangle$ null.

3.2.2 Population transfer

The possibility of selective and efficient transfer of population from a state to another in a quantum system is essential for application in chemistry, physics, laser spectroscopy, quantum optics and *quantum information processing*. The previously described phenomena, (§3.1), is the basis of the process named *Stimulated Raman Adiabatic Passage* (STIRAP), that allows the efficient and selective transfer, thanks to quantum coherence properties. Considering a three level system in the *Lambda* configuration addressed by two time dependent external monocromatic field, *Pump* and *Stokes*, $\Omega_s = \Omega_s(t)$ and $\Omega_p = \Omega_p(t)$. Operating the two field in sequence it is possible obtain a population transfer $|0\rangle \rightarrow |1\rangle$. This could happen in two ways:

Intuitive sequence (SEP)

The first techniques, the *Stimulated Emission Pumping* (SEP), is build by addressing the system by *pump* and *Stokes* field in the *intuitive* sequence. In this technique we address the system before with the *Pump* to transfer population from state $|0\rangle$ to the state $|2\rangle$ and then acting with the *Stokes* to transfer the population in the final state $|1\rangle$. This technique is typical for application that study the collision dynamics or in spectroscopy. It suffers of the problems related to intrinsic decay from the state $|2\rangle$. Then the efficiency of this techniques is near to 10%.

Counter intuitive sequence

When the Pump-Stokes pulse are addressed in the so called *counter intuitive* (before the Stokes pulse and then the Pump pulse) if the system is trapped in the *Dark State* it evolves adiabatically to the target, $|1\rangle$. This process is the *STIRAP* process. The adiabatic evolution of the field amplitude guarantee efficiency near 100% if the state $|2\rangle$ remain quite unpopulated during the time evolution. There exist various generalizations of the *STIRAP* that guarantee high efficiency in many level system. The problem of efficient transfer of population is one of the most important problem studied in the Optimal control theory (OCT).

3.2.3 Coherent transfer and STIRAP

We now examin in detail the ideal STIRAP process. If we consider for simplicity monocromatic fields with real envelop Ω_p and Ω_s filling the two photon resonant condition ($\delta = 0$)

$$\tilde{H}(t) = \begin{bmatrix} 0 & 0 & \frac{1}{2}\Omega_p(t) \\ 0 & 0 & \frac{1}{2}\Omega_s(t) \\ \frac{1}{2}\Omega_p(t) & \frac{1}{2}\Omega_s(t) & \delta_p \end{bmatrix} \quad (3.12)$$

Adiabatic reference frame. If the Hamiltonian written in the rotating frame present a slow dependence on time, the dynamics of the system can be described using the Adiabatic approximation. The instantaneous eigenstate of the system will depend on time and will be linear combination of *bare*

states, for $\delta = 0$ are Eqs.(3.10),(3.11) [2]

$$\begin{aligned} |D\rangle &= \cos \frac{\chi(t)}{2} |0\rangle - \sin \frac{\chi(t)}{2} |1\rangle \\ |+\rangle &= \sin \Phi(t) \left(\sin \frac{\chi(t)}{2} |0\rangle + \cos \frac{\chi(t)}{2} |1\rangle \right) + \cos \Phi(t) |2\rangle \\ |-\rangle &= \cos \Phi(t) \left(\sin \frac{\chi(t)}{2} |0\rangle + \cos \frac{\chi(t)}{2} |1\rangle \right) - \sin \Phi(t) |2\rangle \end{aligned} \quad (3.13)$$

where

$$\chi(t) = 2 \arctan \frac{\Omega_p(t)}{\Omega_s(t)}, \quad \tan 2\Phi(t) = \frac{\Omega(t)}{\delta_p}$$

The relation between the single adiabatic state and the bare state will change as a function of the *mixing angle* $\chi(t)$ and $\Phi(t)$. In function of the t variation will give the base that define the adiabatic representation. The instantaneous eigenstates and the bare states coincide at the beginning and at the ending in the STIRAP protocol. If the evolution is adiabatic (§3.3) we can neglect the transition between instantaneous eigenstates, the population of which remain unchanged. For this we need of smooth pulse and long interaction time T and high Rabi peak frequency Ω_k^{max} .

Adiabatic evolution of the Dark state The STIRAP process consist on the adiabatic evolution of the Dark state generated by a counter intuitive pulse sequence.

- At the beginning the sistem is prepared in the ground state $|0\rangle = |D(0)\rangle$.
- It evolve adiabatically $|D(0)\rangle \rightarrow |D(t)\rangle$. When only the Stokes pulse is switched on $\chi = 0$; Switching on the Pump pulse then switching off the Stokes pulse switched off we will have that $\chi = \pi$ and $|D(t)\rangle \approx |1\rangle$.
- At the end the Pump pulse is switched off $|D(t_f)\rangle = |1\rangle$.

The adiabatic evolution with the counter intuitive sequence produce then a complete population transfer $|0\rangle \rightarrow |1\rangle$.

Adiabatic evolution of AT states The other parameter $\Phi(t)$ enter only on the AT states $|\pm\rangle$, It varies cyclically during the STIRAP $\Phi(0) = \Phi(t_f) = 0$, and does not have effect on the *ideal* process. In fact in this case the AT states are not populated.

3.3 Adiabaticity condition for STIRAP

The precedent conclusions are based on the validity of the adiabatic approximation that we are going to describe.

3.3.1 STIRAP on adiabatic representation

Definition The adiabatic representation for the STIRAP is defined by the instantaneous eigenstates for $\delta = 0$. It is possible to write down explicitly the matrix $U_{ad}(t)$.

$$U_{ad}(t) = \begin{bmatrix} \cos \frac{\chi}{2} & -\sin \frac{\chi}{2} & 0 \\ \cos \Phi \sin \frac{\chi}{2} & \cos \Phi \cos \frac{\chi}{2} & -\sin \frac{\chi}{2} \\ \sin \Phi \sin \frac{\chi}{2} & \sin \Phi \cos \frac{\chi}{2} & \cos \frac{\chi}{2} \end{bmatrix}$$

The effective Hamiltonian corresponding to Eq.3.12, in the adiabatic representation is found applying Eq.1.44

$$\tilde{H}_t = \begin{bmatrix} 0 & -\frac{i}{2} \cos \Phi \dot{\chi} & -\frac{i}{2} \sin \Phi \dot{\chi} \\ \frac{i}{2} \cos \Phi \dot{\chi} & \epsilon_- & -i\dot{\Phi} \\ \frac{i}{2} \sin \Phi \dot{\chi} & i\dot{\Phi} & \epsilon_+ \end{bmatrix} \quad (3.14)$$

The new term $\delta\tilde{H}$ in the Hamiltonian, due to the time dependent part of the transformation that represents the non adiabatic correction, is given by the non-diagonal part of \tilde{H} .

3.3.2 Adiabaticity: global and local criteria

The adiabatic approximation for STIRAP[2] at $\delta = 0$ is valid if in Eq.3.14 we can neglect the nondiagonal terms. The non adiabatic transition from the *Dark state* are negligible if the elements of non adiabatic matrix are smaller then the AT splittings

$$|\langle D|\partial_t \pm\rangle| \ll |\epsilon_{\pm} - \epsilon_0| \quad (3.15)$$

This shows that the adiabaticity is guaranteed in the regime with strong laser and with $\epsilon_{\pm} \sim \Omega$ large enough.

Local criteria With $\delta = 0$ it is possible to write the previous condition Eq.(3.15), as

$$\left| \dot{\chi}(t) \frac{\cos^2 \Phi}{\sin \Phi} \right| \ll \Omega(t) \quad ; \quad \forall t$$

When $\delta_p = 0$ we have $\Phi = \pi/4$, and the inequality take the simpler form

$$|\dot{\chi}| \ll \sqrt{2}\Omega$$

It is convenient rewrite the equation in term of the Rabi frequencies

$$\frac{\dot{\Omega}_p \Omega_s - \Omega_p \dot{\Omega}_s}{\sqrt{2}\Omega^3} \ll 1 \quad (3.16)$$

it shows that a large value of Ω grows up the adiabaticity.

Global criteria When the shape's pulses is smooth, it is convenient to refer to the global adiabaticity criteria. We have that $\dot{\chi} \neq 0$ when both pulses are switched on, i.e. in a time interval $\Delta t \propto T$. In this interval we have $\dot{\chi} \rightarrow \langle \dot{\chi} \rangle \approx \pi/(\Delta t)$. This is small when $\langle \dot{\chi} \rangle \ll \Omega_0$ where Ω_0 represent the scale factor relative to the peak Rabi frequencies. Then the criteria is

$$\Omega_0 T > 10 \quad (3.17)$$

where the l.h.s. is proportional to the pulse area and the value of the r.h.s. is obtained from evaluation of results of numerical calculation.

3.3.3 General Hamiltonian

We now consider the general Hamiltonian with a finite δ . It is convenient write $\tilde{H} = \tilde{H}_0 + \delta |1\rangle \langle 1|$. Then the transformed Hamiltonian has an additional term given by

$$\delta U_{ad}^\dagger |1\rangle \langle 1| U_{ad} = \delta \cos \frac{\chi}{2} \begin{bmatrix} \tan^2 \frac{\chi}{2} & -\tan \frac{\chi}{2} \cos \Phi & -\tan \frac{\chi}{2} \sin \Phi \\ \tan \frac{\chi}{2} \cos \Phi & \cos^2 \Phi & \cos \Phi \sin \Phi \\ \tan \frac{\chi}{2} \sin \Phi & -\cos \Phi \sin \Phi & \sin^2 \Phi \end{bmatrix}$$

3.4 Phenomena involved in the STIRAP

The population transfer with the STIRAP protocol is operated preparing the system in the state $|0\rangle_S$, with the fields off ($\Omega_p = 0$ and $\Omega_s = 0$). This corresponds to $|D(0)\rangle = |0\rangle$. Despite the mathematical formulation of the problem is quite simple it is important to notice that to achieve the success of the protocol different phenomena related with the quantum coherence occur. To emphasize this, generally, the STIRAP process is described as divided in five different steges [2] (vedi fig 3.3):

Stokes-induced AT phase Switching on the Stokes pulse (the pump pulse is off) an AT splitting is generated. The mixing angle is $\chi(t) = 0$. During this phase $\Phi = \Phi(t)$ and the AT states would have component along the states $|1\rangle$ and $|2\rangle$. During this phase the adiabaticity of the system prevents *bad projection* errors, in other words, it prevents that the system prepared in $|0\rangle$ have component belonging to $|\pm\rangle$, that would evolve in an undesired way.

Stokes-induced EIT phase During this stage the Stokes pulse is at the maximum intensity and the Pump pulse is switched on. The $\chi(t)$ angle begin to grow up but the system remains in $|\psi(t)\rangle = |D(t)\rangle \approx |0\rangle$. The Stokes induced AT splitting cancel coherently the transition $|0\rangle \rightarrow |2\rangle$ that the non null Pump pulse would produce. This effect is called Electromagnetic Induced Transparency (EIT): the Pump pulse is not absorbed due to the strong Stokes field;

Adiabatic passage Switching off the Stokes pulse and incrementing the Pump pulse the mixing angle χ grow. During this phase $|\phi(t)\rangle = |D(t)\rangle$, and at the end $|\phi(t_2)\rangle = |D(t_2)\rangle \rightarrow |1\rangle$;

Pump-induced EIT phase During this phase the Pump pulse have the maximum intensity and the Stokes pulse is adiabatically switched off, This guarantee that $\chi = \pi$ and then $|\psi(t)\rangle = |D(t)\rangle \approx |1\rangle$. Now the Pump induced AT splitting cancels coherently the transition $|0\rangle \rightarrow |1\rangle$ that could be induced by the Stokes pulse;

Pump-induced AT phase In this step the Stokes pulse intensity is null and the AT splitting decrease with the Pump pulse. The *Dark state* is belong the target state $|t_f\rangle = |D(t_f)\rangle = |1\rangle$.

The five stages are represented in fig.3.3

3.5 Resilience to parameters

The efficiency of the *STIRAP* process depends from many parameters: the time delay of the pulses τ , the shape of the pulses, the ratio $\kappa = \Omega_s/\Omega_p$ between their peak amplitude, the signal detunings δ and δ_p . The analysis of efficiency dependence from these parameter is fundamental for the evaluation of optimal working condition. An important result is that STIRAP is robust against variation of all the parameters, except for a critical dependence from the two photon detuning δ .

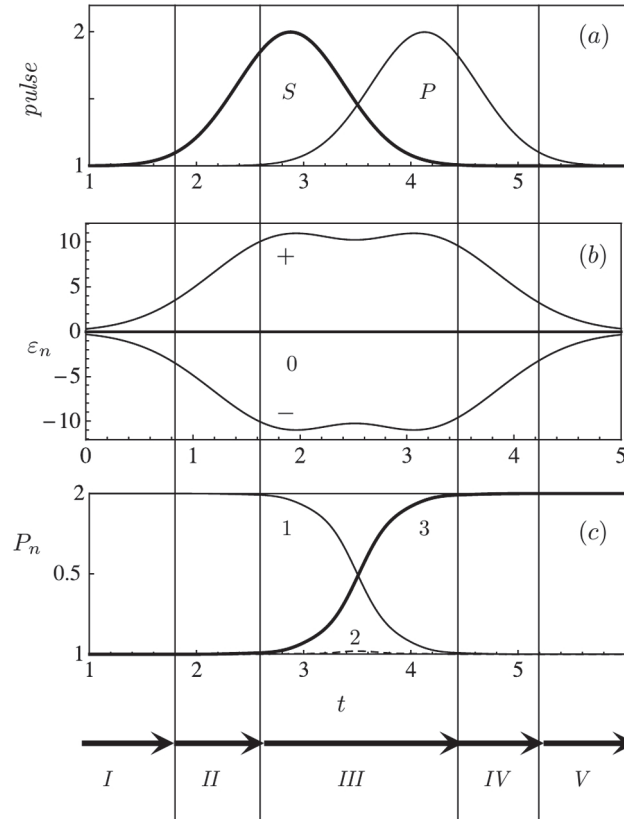


Figure 3.3: In the top figure the *Stokes* and *Pump* field are showed in counterintuitive sequence. The central figure shows the evolution of adiabatic eigenstates. The bottom figure shows the population evolution. The Roman number sign the five stages.

3.5.1 Resilience to delay

The adiabaticity is a necessary condition for the validity of the applied approximations.

The optimal value of delay τ is obtained by maximizing the adiabaticity and by imposing a smooth variation in time of $\chi(t)$ that makes the non adiabatic terms negligible. The optimal value does not depend only on the shape of the pulses and is related to the width of the pulses ($2\tau \sim T$). A quantitative study for gaussian pulses is shown in Fig. 3.4, for $\delta = 0$ e $\delta_p = 0$.

The lines refer to different values of $\Omega_0 T$. There are two main regimes. For $\tau < 0$, i.e. counter intuitive sequence, it is possible to have a great transfer efficiency $P_1(t_f) \simeq 1$, here we can observe plateaus of efficiency near 100%.

For $\tau > 0$ in the dynamics Rabi oscillation are present. In this region the final population is very sensitive to small deviations of τ . The presence

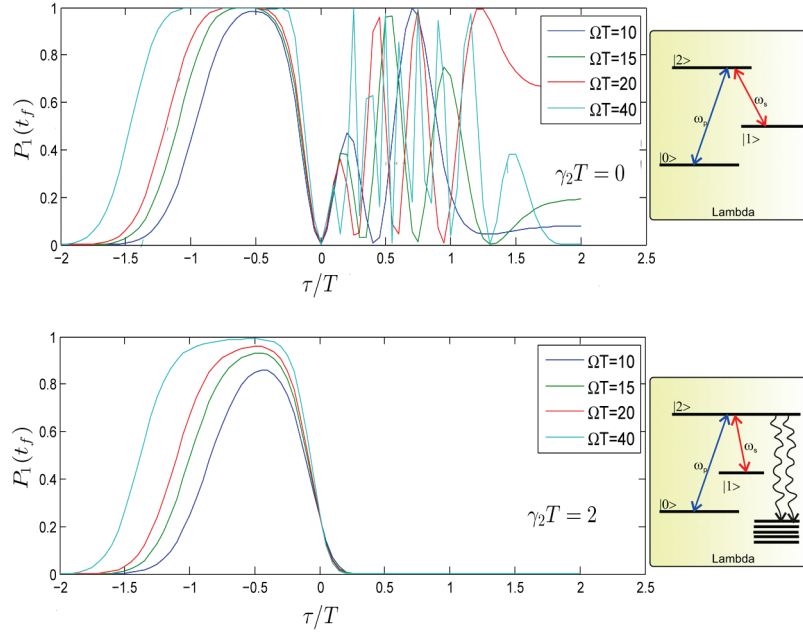


Figure 3.4: Dependence of transfer efficiency, $P_1(t_f)$, from delay τ , for different value of $\Omega_0 T = 10, 15, 20, 40$. (a) In absence of decay; (b) In presence of strong decay of intermediate state $\gamma_2 = 2/T$.

of decay could reduce the adiabaticity and force to use pulses with larger intensity to obtain an large efficiency.

3.5.2 Symmetry of external field

It is well known that the STIRAP efficiency is larger with symmetric pulse, i.e. with the same value of peak Rabi frequencies ($\Omega_s \approx \Omega_p$) and the same width T , under these condition *bad projection* error are prevented [16, pag.94]. In fig. 3.5 is reported an analysis that shows that for sufficient adiabaticity (Ω_0 big), the maximum efficiency is obtained for symmetric pulse $\kappa = 1$ where κ is the ratio between the peak amplitude of the pulses

$$\kappa = \frac{\Omega_s}{\Omega_p}$$

From fig. 3.5 we can see that for big pulses area and with null detuning $\delta = 0$ and $\delta_p = 0$, the κ are irrelevant for the STIRAP efficiency and that ($\kappa \gg 1$) could diminish efficiency.

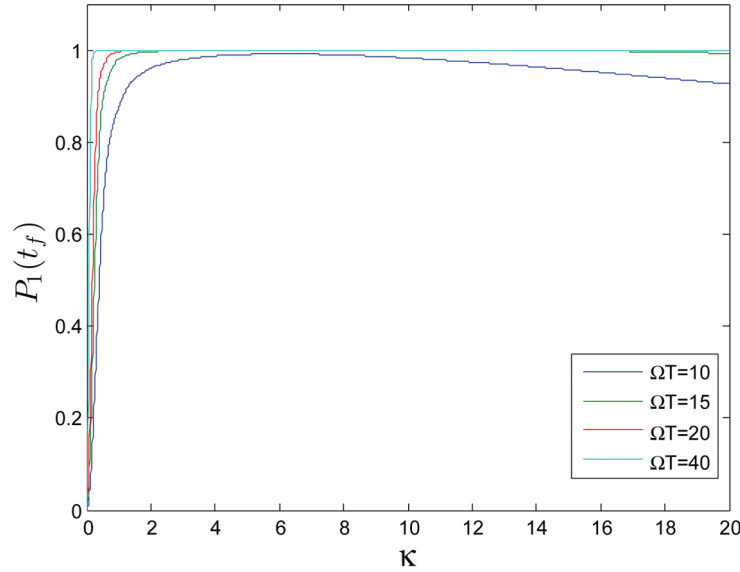


Figure 3.5: The transfer efficiency dependence on the peak Rabi frequencies for $\tau/T = 0.6$ and different values of $\Omega_0 T$

We will see that these conclusion have to be revisited for $\delta \neq 0$ (non ideal STIRAP). In this case the possibility to vary the intensity of the pulses is useful to correct "dynamically" the loss of efficiency in non ideal protocol.

3.5.3 Resilience to detuning

The use of resonant field ($\delta = \delta_p = 0$) favor the STIRAP efficiency. However often it is impossible to address the system with exactly resonant pulse. To characterize the STIRAP it is possible to performe an analisys on the dependence of the efficiency from the detuning $P_1(t_f|\delta, \delta_p)$ (Figg. 3.6 3.7). Generally two sections, called linewidths, are analized. We are interested in two case:

Single-Photon profile $P_1(t_f|0, \delta_p)$ Are varied the *one-photon detunings* mantaining constant the *two-photon detuning* δ .

In this case the destructive impact on the efficiency is not too strong because a single photon detuning does not prejudice the existence of the dark state, but make more stringent the local adiabaticity condition.

Two-Photon profile $P_1(t_f|\delta, 0)$ The frequency of the field vary such thaqt vary also the *two-photon detuning* δ .

In this case the impact on the efficiency is strong because $\delta \neq 0$ il *dark*

state is not more an instantaneous state and the population transfer isn't done with the process described for now.

This behaviour is shown in Figs. 3.6 and 3.7. In the first are reported different linewidth parametrized by ΩT . We have a small increasing in efficiency for growing up pulse area. It is important notice in Fig. 3.6 the difference of the scale on δ and δ_p axis.

In Fig. 3.7 are shown for different parameter values the level curve for efficiency of 90%. This curves allows to individue the optimal working region.

3.5.4 Correlaated detunings = $P(t_f|\delta, a\delta)$

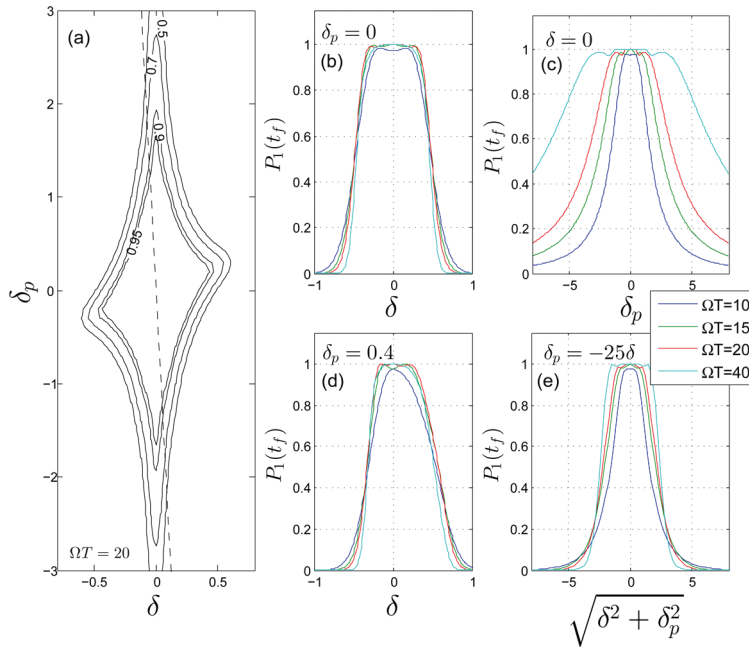


Figure 3.6: Efficiency in function of detunings. For small values of $|\delta| < \Omega_0$, instead the protocol is stable for greater values of δ_p . (a) Contour plot of $P_1(t_f|\delta, \delta_p)$; the dashed line $\delta_p = -25\delta$ correspond to correlated fluctuation of detunings. This situation presents generally for coherent nanodevices. (b)-(e) Section for different values of $\Omega T = 10, 15, 20, 40$; The width of the stability region grows with ΩT , that guarantee the adiabaticity.

The fact that the STIRAP protocol is sensible to values $\delta \neq 0$ justify the fact that correlation between δ_s and δ_p such that reduce fluctuations of $\delta = \delta_p - \delta_s$ don't reduce the efficiency of protocol.

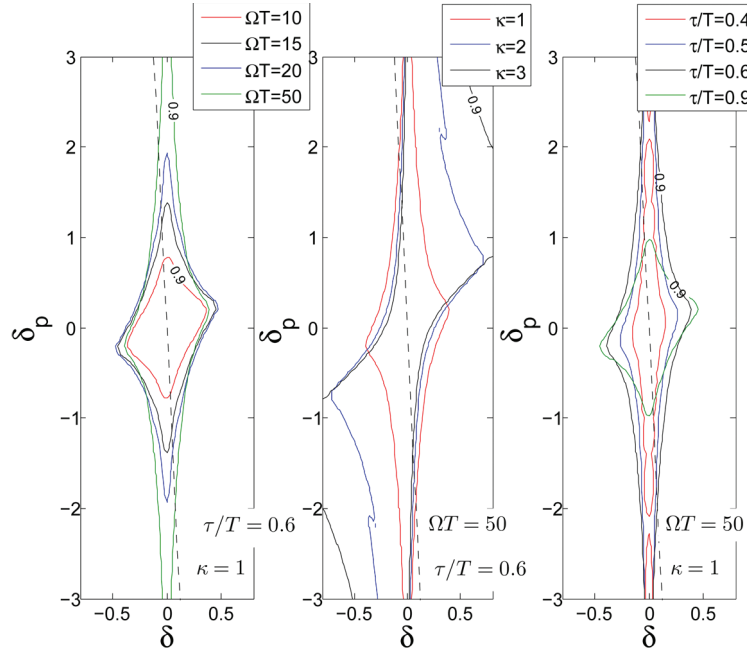


Figure 3.7: Contour plot of $P_1(t_f|\delta, \delta_p)$ (a) for different values of ΩT : amplitude of stability region grow up with ΩT , that correct especially the effects of $\delta_p \neq 0$. (b) for different values of κ : the efficiency "plateau" grows up in asymmetric way. (c) For different value of τ/T : the maximum width of the stability regions is for $\tau \sim 0.6T$.

3.6 Conclusion

In this chapter the STIRAP process was studied in general. We have seen that, in principle, a specific procedure of control performed via AC with an adiabatic modulation of the amplitude allows to perform a population transfer from a given state to a target state $|0\rangle \rightarrow |1\rangle$. This protocol present reduced sensitivity to the parameters. In the next chapter we will study the implementation of the STIRAP protocol in the superconductive device present some difficulties due to some selection rule that make impossible a direct pump coupling at the optimal working point.

Bibliography

- [1] Marlan O. Scully and M. Suhail Zubairy. Cambridge University Press, 1 edition, 1997.

- [2] N. V. Vitanov, M. Fleischhauer, B. W. Shore, and K. Bergmann. *Adv. Atom. Mol. Opt. Phys.*, **46**:55, 2001.
- [3] K. Bergmann, H. Theuer, and B. W. Shore. *Rev. Mod. Phys.*, **70**:1003, 1998.
- [4] E. Arimondo. V coherent population trapping in laser spectroscopy. volume **35** of *Progress in Optics*, page 257. Elsevier, 1996.
- [5] B. W. Shore N. V. Vitanov, T. Halfmann and K. Bergmann. *Annu. Rev. Phys. Chem.*, **52**:763, 2001.
- [6] M. H. S. Amin, A. Yu. Smirnov, and Alec Maassen van den Brink. *Phys. Rev. B*, **67**:100508, 2003.
- [7] J. Siewert and T. Brandes. *Adv. Solid State Phys.*, **44**:181, 2004.
- [8] K. V. R. M. Murali, Z. Dutton, W. D. Oliver, D. S. Crankshaw, and T. P. Orlando. *Phys. Rev. Lett.*, **93**:087003, 2004.
- [9] Yu-xi Liu, J. Q. You, L. F. Wei, C. P. Sun, and Franco Nori. *Phys. Rev. Lett.*, **95**:087001, 2005.
- [10] Jens Siewert, Tobias Brandes, and G. Falci. *Phys. Rev. B*, **79**:024504, 2009.
- [11] M. J. Storcz *et al.* M. Mariani. *arXiv:cond-mat/0509737v2*, 2005.
- [12] Katarina Cicak Fabio Altomare Jae I. Park Raymond W. Simmonds Mika A. Sillanpää Jian Li, G. S. Paraoanu and Pertti J. Hakonen. *Scientific Reports 2*, Art. num. 645, 2012. 1038/srep00645.
- [13] Ioannis Thanopoulos, Petr Král, and Moshe Shapiro. *Phys. Rev. Lett.*, **92**:113003, 2004.
- [14] F. Nori J.Q, You. **474**:589.
- [15] Yury P. Bliokh, Sergey Savel'ev, and Franco Nori. *Phys. Rev. Lett.*, **100**:244803, 2008.
- [16] Vitanov. *Manipulating Quantum Structures Using Laser Pulses*. Cambridge.

Chapter 4

Broadband noise effect on STIRAP protocol

In this chapter we propose a way to analyze the STIRAP process in presence of broadband noise. In particular we will focus on the possibility of implementing the STIRAP in the Quantronium, showing that optimizing the tradeoff between efficient coupling and protection against noise may allow to observe coherent population transfer in this nanodevice. An important result is the definition of a simple figure of merit which describes the relevant tradeoff between coupling and noise, and can serve as a first tool for optimized design and biasing of superconducting charge and flux devices. The mainly results described in this chapter are collected in a preprint submitted to Physical Review B [1].

4.1 Introduction

With the rapid technological progress in quantum-state engineering in superconducting devices there is an increasing demand for techniques of quantum control. The Stimulated Raman Adiabatic Passage (STIRAP) [2, 3], that as we have seen in the previous chapter, is a powerful method in quantum optics has remained largely unknown to solid-state physicists. Using AC fields in Λ configuration (see Fig. 4.1.a) a quantum $M > 2$ -state system is trapped into a subspace spanned by the two longest lived states. Control in this trapping subspace can be achieved by adiabatic time evolution induced by properly crafted external fields, allowing for instance to prepare a given target state [4, 5]. Adiabatic passage used in STIRAP guarantees highly efficient and selective population transfer in atomic and molecular systems [2, 6].

In the last few years it has been proposed that multilevel quantum coherent effects [5] could be observed in superconducting nanodevices, as observing Electromagnetically Induced Transparency (EIT) [7] or selective population transfer by STIRAP [8, 9, 10, 11]. This would be important also from a fundamental point of view, since coherent dynamics in multilevel atoms clearly displays beautiful interference phenomena [5]. Very recently few experiments have demonstrated features of multilevel coherence in such devices, as the Autler-Townes (AT) splitting [12, 13], EIT [14], preparation and measurement of three-state superpositions [15], dynamical AT control [16] and coherent population trapping [17].

In all the above experiments, except for the latter, the multilevel system was driven in the Ladder configuration [5]. Indeed in order to implement a Λ configuration the device Hamiltonian should not be symmetric under parity transformations, which is achieved by a proper external bias [9, 11, 18] otherwise selection rules prevent to drive efficiently the Pump transition. However the longest decoherence times in quantum bits are achieved by

biasing the devices at (or near) symmetry points therefore difficulties in operating coherent superconducting nanodevices in Λ configuration come from fundamental design issues. Indeed low-frequency noise which is known to determine the performances of nanodevices operated as quantum bits [19] plays a crucial role also for the efficiency of STIRAP. So far the effect of decoherence in multilevel artificial atoms has been studied with markovian phenomenological master equations. In this chapter we address decoherence effects due to a solid-state environment where also a strong non-markovian noise component is present in addition to markovian quantum noise. From the exquisite sensitivity of coherence to operating conditions, and design parameters of the device realistic prescriptions are determined for the demonstration of a Λ scheme in superconducting nanocircuits,

We tackle this problem by a quantitative analysis of the class of superconducting nanocircuits based on the Cooper Pair Box (CPB [20], see Fig. A.1). This is an important case-study encompassing several different coherent nanodevices which have already successfully implemented quantum bits [21, 22, 23, 24, 25] and moreover the emerging physical picture holds rather in general for nanodevices in the presence of low-frequency noise.

The main message of this chapter is twofold. First we find that observation of STIRAP should be possible with devices fabricable at present days, but only if operating conditions *and* suitable design optimize the conflicting requirements of efficient coupling of states with (approximately) the same parity and protection from low-frequency noise. Second, despite to the complications of the multilevel structure and the multidimensional space of parameters, the efficiency for STIRAP depends essentially on noise channels involving the trapping subspace (fully characterized by operating the nanodevice as a qubit). This allows to determine a simple criterion to find design prescriptions of the device favoring the observation of STIRAP.

4.2 STIRAP in the Cooper Pair Box.

4.2.1 Implementation of the Λ system

The CPB [20] is a superconducting loop interrupted by two adjacent small Josephson junctions (energy $E_J/2$) defining a superconducting island (Fig. A.1). The total capacitance C gives the charging energy $E_C = (2e)^2/2C$. The electrostatic energy is modulated by a gate voltage V_g , connected to the island via a capacitance $C_g \ll C$. The Hamiltonian reads

$$H_0(q_g) = \sum_n E_C (q - q_g)^2 |q\rangle\langle q| - \frac{E_J}{2} (|q\rangle\langle q+1| + \text{h.c.}) \quad (4.1)$$

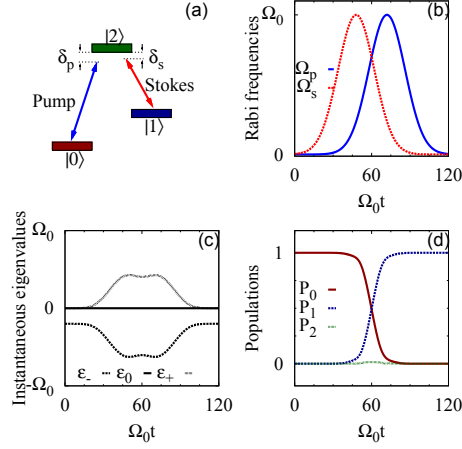


Figure 4.1: (a) Three-level system driven with AC fields in Λ configuration. (b) The counterintuitive sequence: the Stokes field is switched on *before* the pump field (here $\Omega_0 T = 20$, $\tau = 0.6 T$). (c) Instantaneous eigenvalues $\{\epsilon_0(t), \epsilon_{\pm}(t)\}$, for $\delta = 0$, $\delta_p = -0.2 \Omega_0$ and $\kappa = 1$. (d) Population histories $\rho_{ii}(t) = |\langle i | \psi(t) \rangle|^2$ for ideal STIRAP ($\delta = 0$): the system prepared in $|0\rangle$ follows the Hamiltonian along the ϵ_0 adiabatic path yielding complete population transfer to $|1\rangle$.

where $\{|q\rangle, q \in]-\infty, \infty[\}$ are eigenstates of the number operator \hat{q} of extra Cooper pairs in the island. We have defined the reduced gate charge $q_g = C_g V_g / (2e)$ polarizing the island. The spectrum can be modified by choosing a specific bias q_g (Fig. 4.3).

The parametric dependence of H_0 on q_g defines a port allowing for external control of the system: by adding an ac microwave component $q_g \rightarrow q_g + q_c(t)$ shaped in suitable pulses arbitrary rotations of the quantum state of a CPB have been demonstrated [26]. In the basis of the eigenvectors $\{|\phi_i(q_g)\rangle, i = 0, 1, 2\}$ of $H_0(q_g)$ the driven Hamiltonian reads (cf. Eq.1.48)

$$H(t) = \sum_i E_i |\phi_i\rangle \langle \phi_i| + A(t) \sum_{ij} q_{ij} |\phi_i\rangle \langle \phi_j| \quad (4.2)$$

where $q_{ij} = \langle \phi_i | \hat{q} | \phi_j \rangle$ and the control field is $A(t) = -2E_C q_c(t)$. For STIRAP we let $A(t) = \mathcal{A}_s(t) \cos \omega_s t + \mathcal{A}_p(t) \cos \omega_p t$. We then transform the Hamiltonian to the doubly rotated frame, and retain only slowly varying terms, which yields the RWA (sec. 3.1.3). By projecting onto the three lowest levels, $i, j = 0, 1, 2$, we finally obtain an effective Hamiltonian \tilde{H} implementing the Λ configuration of Eq.(3.7), with the definitions

$$\Omega_p = q_{02} \mathcal{A}_p \quad ; \quad \Omega_s = q_{12} \mathcal{A}_s. \quad (4.3)$$

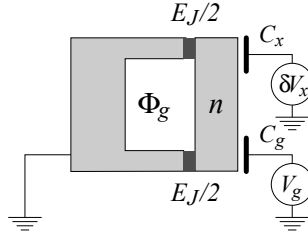


Figure 4.2: In CPB design the state of the superconducting island is represented as superpositions of states with well defined number q of extra Cooper pairs contained. The operating point of the device is biased by the gate voltage V_g ; control is operated by an ac component of V_g . Charge fluctuations are modeled by equivalent voltage fluctuations δV_x . The effective Josephson energy can be tuned via the flux Φ_g of the magnetic field threading the loop, $E_J = E_J(\Phi_g)$.

Therefore \hat{q} enters the peak Rabi angular frequencies, as the electric dipole does in atoms. Notice however that in the CPB Hamiltonian the parametric dependence on q_g (see Eq.4.2) affects “adiabatic states” and energies, and also matrix elements of \hat{q} (see Fig. 4.3). Therefore also detunings and peak Rabi frequencies in \tilde{H} will depend on q_g .

Several superconducting qubits are based on the CPB, which differ from the theoretical point of view for the values of the parameter $J = E_J/E_C$. As a consequence computational states, which are eigenstates of H_0 , are superpositions of a number of “charge states” $|q\rangle$, increasing with J , and these devices have very different energy spectra. Coherent dynamics has been observed in the charge regime [21, 23] $J \ll 1$, in the charge-phase regime [22, 24] $J \sim 1$ and in the phase regime [25] $J \gg 1$ (from several tens up to several hundreds). From the physical point of view these systems differ substantially both in the design (size, on-chip readout scheme), and in crucial properties as the ease of coupling to control fields and the resilience to noise. Therefore the CPB allows for a thorough discussion of design requirements to observe STIRAP for a wide class of nanodevices.

4.3 Symmetries, decoherence, selection rules

4.3.1 Symmetries

Charge parity is a possible symmetry of wavefunctions in charge space which is nontrivial because of the discrete nature of the momentum. Formally one may introduce operators $R_q = \sum_q |n - q\rangle \langle q|$, which implement a reflection followed by a translation in the charge space. If the parameter n is integer

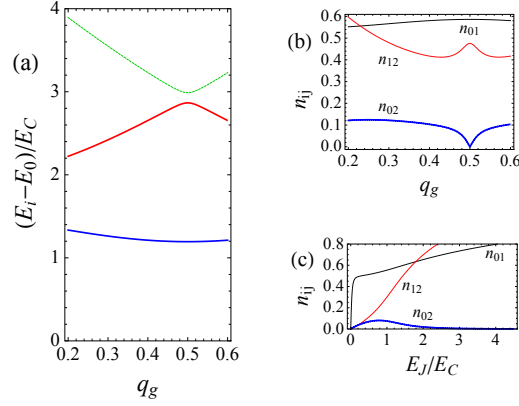


Figure 4.3: (a) Energy spectrum E_i of a charge-phase CPB (for $J = 1.32$ corresponding to the Quantronium [22]), relative to the ground state $E_0 = 0$, as a function of the bias q_g . (b) Matrix elements of \hat{q} involved in the Λ scheme as a function of q_g for $J = 1.32$; the element q_{02} vanishes at the symmetry point $q_g = 1/2$; (c) Matrix elements as a function of $J = E_J/E_C$ for $q_g = 0.48$; element q_{02} is much smaller than others (it vanishes at $q_g = 1/2$) and it has nonmonotonous behavior with J .

they onto the same Hilbert state of discrete charges. It is easy to see that

$$\Pi_n^{-1} \left[\sum_q (q - q_g)^2 |q\rangle \langle q| \right] \Pi_n = \sum_q (q - n + q_g)^2 |q\rangle \langle q|$$

whereas

$$\Pi_n^{-1} \left[\sum_q |q\rangle \langle q \pm 1| \right] \Pi_n = \sum_q |q\rangle \langle q \mp 1|$$

Therefore one can seek for the invariance of the family of Hamiltonians (4.1). Symmetry points are found for $q_g = q/2$, where $H_0(q_g)$ is invariant with respect to the respect to Π_{2q_g} . Since $\Pi_n^2 = \mathbb{1}$ one may conclude that for symmetric H_0 eigenvalues can be chosen with a well defined charge parity $\Pi_{2q_g} |\phi_j(q_g)\rangle = (-1)^j |\phi_j(q_g)\rangle$ and parity selection rules hold such that charge matrix elements $\langle \phi_j | q | \phi_i \rangle = 0$ for states of different parity.

4.3.2 Decoherence

Tunability with q_g has been exploited to find optimal points where qubit operations are well protected from low-frequency noise. For instance for $q_g = 1/2$ the Hamiltonian (4.1) is symmetric for parity transformations in the charge space, and due to this the system is well protected against external noise. This has allowed to obtain experimental dephasing times of

several hundreds of nanoseconds in charge-phase devices [22, 27] and ranging from $T_2^* > 2 \mu\text{s}$ $J \sim 50$ in the phase regime [25] up to $T_2^* \sim 0.1 \text{ ms}$ recently reported [28]. At the same time symmetry enforces a parity selection rule, which prevents transitions between states enumerated with the same parity. In particular q_{02} vanishes at $q_g = 1/2$ (see Fig. 4.3b) therefore it is not possible to implement a Hamiltonian in Λ configuration, as Eq.(3.8), since $\Omega_p = 0$. In Refs. [10, 11] it has been proposed to overcome this problem by working slightly off-symmetry (see Fig. 4.3b,c), and it has been shown that the full multilevel structure of a CPB with $E_J = E_C$ allows for coherent population transfer for $q_g \approx 0.47$, in the presence of Markovian noise.

We stress the fact that protection from noise and selection rules are connected because they stem from the same symmetry, namely charge parity. Another important property of these devices is how increasing J enforces the (approximate) selection rule in a larger and larger region close to the symmetry point $q_g = 1/2$, since it makes less effective the symmetry breaking charging energy contribution. For instance Fig. 4.3c shows that q_{02} at $q_g = 0.48$ eventually decreases for increasing J .

An important ingredient allowing selective addressing of specific transitions in CPB is the nonlinear nature of the Josephson junction making the system anharmonic. Larger J tends to suppress anharmonicity and it is also detrimental for STIRAP. However we point out that the fundamental problem is the enforcing of parity symmetry. Loss of anharmonicity is indeed related to one further symmetry of the Hamiltonian coming into play for $J \rightarrow \infty$, which charge matrix elements by the suppression of all but the ladder-type entries $q_{i,i\pm 1}$. This makes very easy to work with AC fields in ladder configuration (see q_{01} and q_{12} at $q_g = 1/2$ in Fig. 4.3c).

4.3.3 Model for charge noise

In principle each port of the device also allows injection of noise and provides a channel for decoherence. The control port associated to q_g couples to charge noise. Here we focus on this channel, which is the main source of low-frequency noise in the CPB for the regimes in which STIRAP could be observed. The structure of the coupling to noise can be obtained by allowing for fluctuations the gate charge in the Hamiltonian (Eq.4.1). Their physical origin, besides voltage fluctuations of the circuit have been recognized as the effect of switching impurities [29] located in the oxides and in the substrate close to the device. We let $q_g \rightarrow q_g + x$, where x describes stray electrical polarization of the island, and write the resulting Hamiltonian as $H = H_0(q_g) + H_{RW}(t) + \delta H$, where $H_{RW}(t)$ is the control Hamiltonian in the RWA and $\delta H = -2E_C x \hat{q}$ describes fluctuations. On a phenomenological level the structure of coupling to a quantum environment is obtained by

“quantizing” noise, i.e. by letting $\delta H = \hat{X} \hat{q} + H_R$, where \hat{X} is an environment operator and H_R describes the environment alone, possibly containing suitable counterterms [30]. In this framework Markovian noise can be studied by deriving a weak coupling quantum optical Master Equation (ME). However noise in the solid state has a large low-frequency components invalidating the ME. A multistage approach has been proposed [31] where high and low-frequency noise are separated, the latter being approximated by a classical field. Formally $\hat{X} \rightarrow \hat{X}_f - 2E_C x(t)$ where \hat{X}_f describes fast environmental degrees of freedom and $x(t)$ is a slow classical stochastic process. If we let $q_x(t) = q_g + x(t)$ the Hamiltonian is written as

$$H = H_0[q_x(t)] + H_{RW}(t) + \hat{X} \hat{q} + H_{env} \quad (4.4)$$

In many cases low-frequency noise has $1/f$ spectrum and the leading contribution of the slow dynamics of $x(t)$ is captured by a Static-Path Approximation (SPA) i.e. approximating the stochastic process by a suitably distributed random variable [31, 27] x . In this simpler scenario one should first calculate the reduced density matrix $\hat{\rho}(t|x)$ for a given stray bias x obtained by tracing out high-frequency (quantum) noise, and then average over the distribution $P(x)$. In particular population histories are given by $P_i(t) = \int dx P(x) \rho_{ii}(t|x)$; notice that for each realization x of the random variable the system is prepared and measured in the eigenbasis of $H_0(q_g + x)$, which is then conveniently used to represent ρ_{ii} .

In the case of many weakly coupled noise sources x is Gaussian distributed with width σ_x . The effect of low-frequency noise is quantified by the scale σ of the corresponding energy fluctuations. This point of view provides a simple argument explaining why the symmetry point $q_g = 1/2$ is well protected. Indeed since at this working point the energy splitting E_1 depends only quadratically on the fluctuations x , energy fluctuations are suppressed, and superpositions of the two lowest energy levels keep coherent yielding a only a power law suppression of the signal [31, 27], and longer dephasing time.

This approach has quantitatively explained the power law decoherence observed in the Quantonium [27], in flux qubits [32] and to look for optimal operating point in ultrafast driven phase qubits [33]. Recently it has been used to propose a design of optimal tuning of multiqubit systems [34]. The present extension to a Λ system of the approach of Ref. [31] enlightens the role of correlations between detunings, and provides a tool for optimal device design.

4.3.4 Effective model for low-frequency noise in Λ configuration

In order to study STIRAP the Hamiltonian (4.4) is projected onto the subspace spanned by the three lowest energy adiabatic eigenvectors of $H_0[q_x(t)]$. In doing so we assume the adiabaticity of the dynamics induced by $x(t)$, which allows to neglect effects of the time-dependence of the eigenvectors. Of course in the SPA adiabaticity of noise is automatically verified. The effective Hamiltonian is obtained starting from Eq.(2.21) and retaining in the control part only quasi resonant entries in the RW approximation

$$H_{RW}(t|x) = \frac{1}{2} \left[\mathcal{A}_p e^{-i\phi_p(t)} Q_{20}(x) \hat{P}_{20}(x) + \mathcal{A}_s e^{-i\phi_s(t)} Q_{21}(x) \hat{P}_{21}(x) \right] + \text{h.c.} \quad (4.5)$$

Then we define a doubly RF by the transformation $U_{rf}(t|x) = e^{i[\phi_p(t)\hat{P}_{00}(x) + \phi_s(t)\hat{P}_{11}(x)]}$ and project onto the lowest three-level (x -dependent) subspace, obtaining

$$\tilde{H}(t|x) = \begin{bmatrix} 0 & 0 & \Omega_p^*(t)/2 \\ 0 & \delta(x) & \Omega_s^*(t)/2 \\ \Omega_p(t)/2 & \Omega_s(t)/2 & \delta_p(x) \end{bmatrix} \quad (4.6)$$

where $\delta(x) = E_1(x) - (\omega_p - \omega_s)$ is the two-photon detuning, $\delta_p(x) = E_2(x) - \omega_p$ is the pump pulse detuning and $\Omega_i(t)$ are pulses of width T and peak Rabi frequency $\Omega_p = Q_{02} A_p$ and $\Omega_s = Q_{12} A_s$, respectively. Fluctuations of the eigenenergies translate in fluctuations of the detunings (we let $E_0 = 0$). In the SPA we have

$$\delta(x) = E_1(q_g + x) - \omega_p + \omega_s ; \delta_p(x) = E_2(q_g + x) - \omega_p \quad (4.7)$$

It is worth stressing that also the effective drive fluctuates, via the charge matrix element, and for instance $\Omega_p = q_{02}(q_g + x) A_p$. Thus the effect of low-frequency noise in solid-state devices, is conveniently recast in terms of sensitivity of the protocol to imperfections (in both phase and amplitude) of a fictitious drive. This allows to apply to solid state devices several results from the quantum optics realm. For instance the known critical sensitivity to two-photon detuning, translates in the fact that the main figure to be minimized in order to achieve efficient population transfer in nanodevices are fluctuations of the lowest energy splitting, a quantity which is well characterized from the qubit dynamics [27, 32, 33, 35].

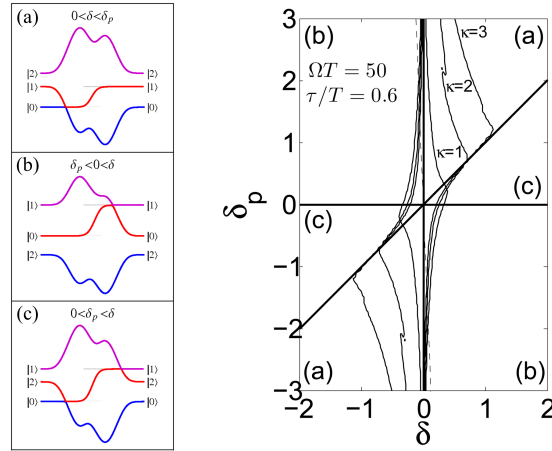


Figure 4.4: Left panel: typical LZ patterns with one crossing in the Stokes-AT phase, one crossing in the pump-AT phase, and two crossings. Right panel: efficiency diagram $P_1(t_f)$ vs. the detunings. The configurations (δ, δ_p) determines the typical LZ pattern as indicated in the regions of the phase diagram. By increasing the Stokes field amplitude (increasing κ) the efficiency in the region (a) increases, minimizing the effect of the corresponding avoided crossing.

4.4 Typical pattern of adiabatic eigenstate

Before to proceed with the procedure for studying the broadband noise effect on STIRAP we focus on the effect of the most critical parameter for the STIRAP process, the two photon detuning $\delta(x)$ [36]. The mapping of energy fluctuations onto $\delta(x)$ allows to translate to solid state devices several results from the quantum optics realm. Non-zero δ modify the whole adiabatic picture of STIRAP [3] since the dark state is not anymore an instantaneous eigenstate and there is no adiabatic connection from the initial to the target state. However non-ideal STIRAP may still take place via non-adiabatic transitions between adiabatic states. For small values of δ , narrow avoided crossings between instantaneous eigenvalues occur and the population is transferred by Landau-Zener (LZ) tunneling [3, 2] (see Fig. 4.4). Increasing δ reduces the transfer efficiency and in general the excited state $|\phi_2\rangle$ is populated during the protocol.

Nonadiabatic LZ patterns for STIRAP can be classified in three categories, namely: (a) a single (avoided) crossing is present at the beginning (Stokes-AT phase) of the protocol; (b) one crossing at the end (pump-AT phase); (c) two crossings, one in each phase (see Fig. 4.4, left panel). Each category corresponds to a specific relations between the detunings, e.g. pattern (b) is obtained for anticorrelated detunings $\text{sign}(\delta) = -\text{sign}(\delta_p)$, as

illustrated in (see Fig. 4.4b). This correspondence can be understood by inspection of the eigenvalues in the AT phases. For instance during the pump-AT phase $\Omega_s = 0$, the energy δ of $|\phi_1\rangle$ is constant whereas $\Omega_p \neq 0$ determines the further splitting (AT effect) between $|\phi_0\rangle$ and $|\phi_2\rangle$ which disappears at the end of the protocol.

This classification finds a physical counterpart when fluctuations in nanodevices are concerned. In this case stray δ and δ_p are not independent, since the corresponding energy fluctuations reflect the behavior of the spectrum as a function of the bias parameter q . For instance in CPB's charge noise determines anticorrelated fluctuations of detunings, and LZ pattern (b), whereas fluctuations of the Josephson energy would determine correlated detunings, and LZ patterns (a).

Now, since efficient STIRAP requires large LZ tunneling, a way to minimize the effect of stray detunings is to use, if possible, fields with larger amplitude closing the gap between avoided crossings. In particular a larger Ω_s increases the efficiency for patterns (a) and a larger Ω_p for patterns (b). In Fig. 4.4 (right panel) it is shown how a larger Ω_s , which is not suppressed by selection rules, may widen the stability region against correlated fluctuations (a) of the detunings.

More in general specific strategy to increase the efficiency depend on properties of the band structure, as correlations of the parametric fluctuations of the splittings. From a different point of view this result suggests that proper band structure may be engineered where effects of noise can be dynamically minimized by available control. It is worth stressing that all this picture relies on correlations enforced by the nonmarkovianity of noise. Indeed pure dephasing due to Markovian processes determines a loss of efficiency which does not depend on the external fields and therefore cannot be dynamically suppressed [37].

4.5 Broadband noise in the CPB

In this section we apply the above analysis to discuss the observability of STIRAP in a CPB in the charge-phase regime $E_J \sim E_C$, whose spectral properties are given in Fig. 4.3. An important point is that while dephasing is minimized by operating at the symmetry point $q_g = 1/2$ the selection rule $q_{02} = 0$ apparently prevents to implement STIRAP. Therefore it has been proposed to operate slightly off the symmetry point [11, 9]. On the other hand it is known that at these values of the bias decoherence due to low-frequency noise increases [27, 38]. This opens the question of the tradeoff between efficient coupling of the driving fields and dephasing due to slow excitations in the solid-state.

Since it is convenient to work with the largest possible pump Rabi peak frequency Ω_0 , we will consider its value fixed. It can be estimated as $\Omega_0 = (q_{02}/q_{01}) \Omega_R$ where Ω_R is the maximal angular frequency for Rabi oscillations between the lowest doublet. We will use frequencies corresponding to $\nu_R = 600$ MHz which are in principle achievable even if there may be technical problems in specific devices. For the Quantronium at $q_g = 0.48$ it would yield a maximum $\nu_p = 55$ MHz.

In the vicinity of the symmetry point coupling of the field with the Stokes transition is larger therefore we may choose $\kappa = \nu_s/\nu_p \sim q_{12}/q_{02} \gg 1$. However using larger ν_s does not improve the transfer efficiency in CPB's [3, 39] therefore we will let $\kappa = 1$ hereafter.

4.6 Effects of low-frequency noise

Low-frequency fluctuations σ_x of the stray gate charge x determine non-exponential dephasing in qubits [31]. They have been well characterized in the Quantronium (see Figs.A.1,4.3) by Ramsey interferometry at different bias points $q_g \in [0.4, 0.5]$ [27]. Charge noise is converted in charging energy fluctuations $\sigma_E = 2E_C \sigma_x \sim 0.01 E_1(1/2)$, which are independent on the bias point. The corresponding figure for charge noise $\sigma_x = \sigma_E/(2E_C) \approx 6 \cdot 10^{-3}$, is the integrated spectral density of the environment [31]. For $1/f$ noise σ_x also depends on details of the protocol as the total measurement time. Even if this dependence is only logarithmic one can take advantage from the fact that measuring the final population in STIRAP requires a lower statistics than Ramsey fringes. Therefore for our purposes lower values of σ_x are reasonable and hereafter we use $\sigma_x = 0.004$ as a realistic figure for CPB-based devices.

We consider STIRAP for the best conditions of nominal single and two-photon resonance, $\delta = \delta_p = 0$. According to Eq.(4.7) fluctuations x determine a distribution of stray detunings. For small σ_x we can approximate

$$\delta(x) \approx A_1 x + \frac{1}{2} B_1 x^2$$

where $A_1 = (\partial E_1/\partial q_g) = E_C a_1(q_g, J)$ and $B_1 = (\partial^2 E_1/\partial q_g^2) = E_C b_1(q_g, J)$. It is worth stressing that arbitrary small fluctuations determine $\delta(x) \neq 0$, therefore STIRAP may occur only via non-adiabatic patterns. In the same way also $\delta_p(x)$ depends on the derivatives $(\partial^n E_2/\partial q_g^n)$. Notice that since the detunings are functions of the single random variable x , their fluctuations are not independent. For CPB's they are anticorrelated, due to the shape of the spectrum (Fig. 4.3.a). This implies that non-ideal STIRAP may occur only via typical LZ patterns [36] shown in Fig. 4.4.

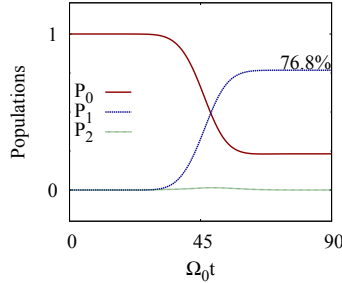


Figure 4.5: Population histories in the Quantronium at $q_g = 0.475$, averaged over fluctuations with $\sigma_x = 0.004$. Charge fluctuations determine anticorrelated stray detunings, $\delta_p = -23.5\delta$. Drives are symmetrized $\kappa = 1$, by using a lower amplitude \mathcal{A}_s .

Fluctuations of the gate charge determine in addition fluctuations of the off-diagonal elements. They can be estimated from the plots in Fig. 4.3.b. Far enough from the symmetry point, they are small. For instance for $J \sim 1$ and $q_g < 0.49$ we can estimate fluctuations of the amplitude of the pump pulse as $\sigma_p \sim a_{02} \sigma_x \Omega_0 \ll \Omega_0$, where $a_{02} = \partial n_{02} / \partial q_g$. The transfer efficiency is then calculated by averaging population histories over the distribution of correlated detunings. Fig. 4.5 shows that in a Quantronium working slightly off-symmetry low-energy fluctuations are responsible for $\sim 20\%$ efficiency loss, despite of the greatly reduced noise protection. Moreover the average population of the intermediate level is very small during the whole procedure, fulfilling the requirements for coherent population transfer. Notice on passing that in the regime where fluctuations of the off-diagonal matrix element are negligible fluctuations of the detunings are well accounted for by the linear expansion ($B_1 = B_2 = 0$).

4.6.1 Effect of high-frequency noise

High-frequency noise is studied by solving the quantum-optical master equation in the rotating frame [40] $\dot{\rho} = \frac{i}{\hbar}[\rho, \tilde{H}] - D\rho$, where ρ is the density matrix and \tilde{H} is the Hamiltonian (3.7). The structure of the dissipator $D\rho$ in the basis of the diabatic states $\{|\phi_i\rangle\}$ reads [11]

$$(D\rho)_{ij} = \frac{\gamma_i + \gamma_j}{2} \rho_{ij} - \delta_{ij} \sum_{k \neq i} \rho_{kk} \gamma_{ik} + (1 - \delta_{ij}) \tilde{\gamma}_{ij} \rho_{ij} \quad (4.8)$$

The first two terms describe emission and absorption of energy and the associated secular dephasing: $\gamma_{ij} = \gamma_{j \rightarrow i}$ are transition rates between diabatic

states, and $\gamma_i = \sum_{k \neq i} \gamma_{ki}$ are the total decay rates of states $|\phi_i\rangle$. At low temperature in an undriven system only rates corresponding to spontaneous emission between diabatic states are non negligible. In AC driven systems rates describing environment-assisted absorption are also nonzero, when the corresponding field is switched on. Finally the dissipator may include pure dephasing rates $\tilde{\gamma}_{ij} = \tilde{\gamma}_{ji}$.

In quantum optical systems STIRAP connects two ground states, $\gamma_{01} = \gamma_{10} = 0$. Therefore as long as population in $|\phi_2\rangle$ is small all the transition rates act on depopulated states, and they practically do not affect population transfer. Instead in superconducting nanocircuits the decay channel γ_{01} is active therefore it is expected to be the main source of efficiency loss due to processes involving energy exchange with the environment. This is indeed the qualitative conclusion to which we pervent, as it is shown in Fig. 4.6.

In order to simplify the physical picture in Fig. 4.6 we study separately the impact of the decay channels. First we consider only spontaneous decay in the first doublet. We take $\gamma_{01}/\Omega_0 = 1$ (it is a rather large value that we use for emphasize the effect) and we study population histories (solid lines ρ_{ii}). This channel determines a loss of population which is obviously due to decay since $\rho_{11}(t) \approx P_1(t) e^{-\gamma_{01}(t-t_i)}$, where $P_1(t)$ is the population in absence of noise. It also determines a nonvanishing population $\rho_{22} \neq 0$ which is due to loss of coherence and detrapping from the dark state.

Adding all the other decay channels (dashed lines) produces minor modifications of this picture (left panel, for fields at resonance). Notice that for nonvanishing detunings, as those produced by low-frequency fluctuations, decay γ_{01} does not determine population of $|\phi_2\rangle$ and the additional channels have no effect. For the other decay channels we consider rates which should overestimate unwanted processes, namely $\gamma_{12} = 2\gamma_{01}$, whereas $\gamma_{02} = 0.2\gamma_{01}$ (accounting for the suppression by selection rules). Notice that these emission rates become smaller when the drive amplitudes $\Omega_k(t)$ are large enough, which we do not take into account. At the same time in the weak damping Rabi regime ($T\Omega_k(t) \gg 1$ and $\delta_k \ll \Omega_k(t)$) field-induced absorption sets in even at low temperatures. We take into account this channel phenomenologically, by using the behavior of the rates obtained from the generalized (Bloch-Redfield) master equation [41] for AC driven systems undergoing Rabi oscillations. In particular we let $\gamma_{21}(t) = \gamma_{12}/4 [1 - \delta_s/(\sqrt{\delta_s^2 + \Omega_s^2(t)})]^2 g[\Omega_s(t)T]$, where $g(x) \approx 1$ only for $x \gg 1$ accounts for the requirement that field induced processes set in for underdamped Rabi oscillations. We used a similar expression for $\gamma_{20}(t)$.

Notice that the above results take into account secular dephasing but did not include pure dephasing rates, $\tilde{\gamma}_{ij} = 0$. Indeed we argue that the main contribution to pure dephasing comes from low-frequency noise, which

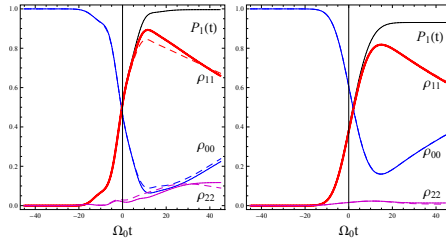


Figure 4.6: Effect of high-frequency noise on the populations $\rho_{ii}(t)$ for $\delta = \delta_p = 0$ and $\kappa = 1$. Here $\Omega_0 = 2.8 \times 10^8 \text{ rad/s}$ would be the peak pump Rabi frequency for a Quantronium operating at $q_g = 0.48$ for a drive producing Rabi oscillations with $\nu_R = 500 \text{ MHz}$ at the optimal point. We use values $\Omega_0 T = 20$, therefore $T \sim 70 \text{ ns}$ and the whole protocol takes $\sim 420 \text{ ns}$. Black curves are in absence of noise. Curves colored curves (blue, red, magenta) are obtained accounting for relaxation $1 \rightarrow 0$ only, $\gamma_{01} = 1/T_1$, and the associated secular dephasing; we use the experimental value [27] $T_1 = 500 \text{ ns}$. In dashed curves other secular decay rates γ_{ij} are included, as specified in the text.

is accounted for by classical fluctuations of x . In the next section we will study the combined effect of high and low-frequency noise. We will come back to pure dephasing in Sec. 4.8.

4.6.2 STIRAP in the Quantronium

For the CPB we take the value which has been measured in the Quantronium at $q_g = 1/2$, and does not change substantially with the bias [27].

The main conclusion of the last two sections can be summarized by stating that the leading effects reducing coherent population transfer in nanodevices mainly involve decoherence of the first doublet. On the other hand due to parity selection rules coupling to the pump pulse may be too weak. With this in mind we consider the Quantronium as a case-study and investigate the effect of fluctuations, for $q_g \leq 1/2$.

Concerning low-frequency noise, from the dependence of E_{10} and n_{02} on q_g we expect that sufficiently far from the symmetry point only linear fluctuations of the detunings matter. Fig. 4.7 shows that indeed different approximations of fluctuations yield the same result for $q_g \lesssim 0.485$, whereas by approaching $q_g = 1/2$, both quadratic fluctuations of detunings and fluctuations of q_{02} come together into play. In this latter regime fluctuations alone would lead to a non trivial behavior of the efficiency, however the effect of high-frequency noise is here dominant and leads to the suppression of the efficiency. Instead for $q_g \lesssim 0.49$ effects of low-frequency noise dominate, and

in this regime it would be possible to observe $\sim 70\%$ of population transfer in the Quantronium.

We now discuss more in detail effects of fluctuations near $q_g = 1/2$. Quadratic fluctuations of detunings alone would determine nonmonotonic behavior of the efficiency on approaching the symmetry point. Indeed for $0.49 \lesssim q_g \lesssim 0.495$ fluctuations for $x > 0$ yield smaller stray detuning $\delta(q_g + x)$ than in the linear approximation, and the efficiency increases; however sufficiently close to the symmetry point $\langle |\delta| \rangle$ exceeds the linewidth $\delta_{\frac{1}{2}}$, (which scales with Ω_0 , see next section): since $\lim_{q_g \rightarrow \frac{1}{2}} \langle |\delta| \rangle / \Omega_0 \rightarrow \infty$ the efficiency should eventually vanish. Fluctuations of n_{02} (which are also correlated to fluctuations of the detunings) spoil the above picture. Indeed, for $0.49 \lesssim q_g \lesssim 0.495$ smaller values of $\Omega_p(q_g + x)$ for $x > 0$ compensate the effect of smaller $\delta(q_g + x)$; moreover on approaching the symmetry point slow fluctuations of n_{02} provide a nonvanishing coupling which is enough to yield a nonzero efficiency. Notice that this is true even at the nominal bias $q_g = 1/2$, where the selection rule is exact, since $\lim_{q_g \rightarrow \frac{1}{2}} \langle |\delta/n_{02}| \rangle$ is finite. However in this regime efficiency is suppressed by quantum noise, in primis by spontaneous decay $|\phi\rangle_1 \rightarrow |\phi_0\rangle$. Indeed the adiabaticity condition $\Omega_s(q_g + x)T > 15$, requires for $q_g \rightarrow 1/2$ longer and longer T : when it exceeds T_1 relaxation suppresses the efficiency. This observation explains why the loss of efficiency due to high-frequency noise strongly depends on q_g even if we neglected the (weak) dependence of the rates γ_{ij} on the bias.

4.7 Optimal design of the device

Efficiency of population transfer may be improved by optimizing the parameters of the protocol. In the last section we have shown that due to the combined effect of the approximate symmetry and of spontaneous decay, efficiency is large enough if the device is biased slightly away from the symmetry point. In this section we argue that in this regime one should mainly optimize the tradeoff between coupling of the pump pulse and energy fluctuations of the lowest doublet of the device, due to low-frequency noise. Indeed the relevant figure of merit turns out to be

$$\frac{2E_C \langle n_{02} \rangle}{\sigma_\delta} \propto \frac{\Omega_p^{max}}{\sigma_\delta} \quad (4.9)$$

$\sigma_\delta = \sqrt{A_1^2 \sigma_x^2 + \frac{1}{2} B_1^2 \sigma_x^4}$ being the fluctuations of the stray two-photon detuning $\delta(x)$. Efficient population transfer requires large enough values of the quantity in Eq.(4.9), which depends on q_g and E_J/E_C , via $\langle n_{02} \rangle$ and (A_1, B_1) . This can be obtained by suitably choosing design and operating

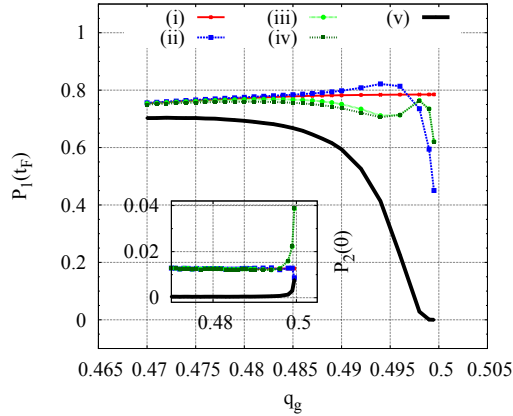


Figure 4.7: Effects of low-frequency and broadband noise for STIRAP in the Quantrium. Here $E_J/E_C = 1.32$, $\sigma_x = 0.004$, and we fix $\Omega_0 T = 15$ and $\nu_{01} = 600 \text{ MHz}$. Points represent the final population $P_1(t_f)$ for different approximations of low-frequency noise, where only fluctuations of detunings, linear (red) and quadratic (blue) are accounted for, and where fluctuations of n_{02} are considered in the linear (light green) and in the quadratic approximation (dark green). The thick line includes the effect of high-frequency noise. In the inset the population $P_2(0)$ at intermediate times.

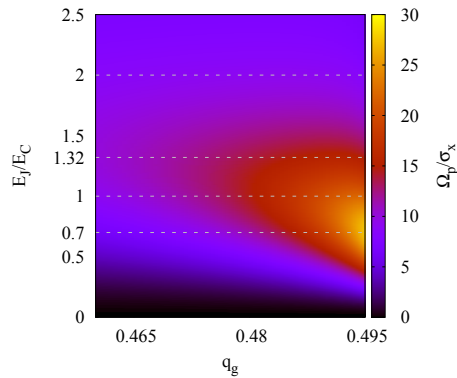


Figure 4.8: The figure of merit Ω_p/σ_δ is plotted in the $(q_g, E_J/E_C)$ expressing the tradeoff between coupling and low-frequency noise. For the plot we have chosen $\sigma_x = 0.004$ and Ω_0 produced by an external field which would determine Rabi oscillations with $\nu_R = 600 \text{ MHz}$ in the first doublet. The estimate is valid far enough from the symmetry point, where efficiency is suppressed due to selection rules. Dashed lines correspond to values of E_J/E_C checked in this paper.

conditions (see Fig.4.8). The criterion Eq.(4.9), which is clear from heuristic grounds, can be justified starting from an argument given by Vitanov et al. [3] to estimate the linewidth of population transfer for finite δ . In this case the adiabatic basis $\{|D\rangle, |\pm\rangle\}$ is not anymore formed by instantaneous eigenstates. Since still $|D\rangle$ provides a connection between the diabatic states $|\phi_0\rangle$ and $|\phi_1\rangle$, it is argued that efficiency loss depends on processes triggering transitions from $|D\rangle$ to $|\pm\rangle$. These are due to non vanishing off diagonal entries of the Hamiltonian in the adiabatic basis, being proportional to δ , therefore if $\delta \gg \min|\epsilon_{\pm}|$ population transfer does not occur. This implies that for $\delta_p = 0$ the linewidth scales linearly with amplitude of the lasers [3], $\delta_{\frac{1}{2}} = d(\tau)\sqrt{(\Omega_p^{max})^2 + (\Omega_s^{max})^2}$. In our case stray detunings $\delta(x)$ and $\delta_p(x) \neq 0$ are anticorrelated, therefore leakage from $|D\rangle$ occurs when only the pump pulse is on (see Fig. 4.4.a) and it is substantial only when $\delta_p > 2\Omega_0$. By imposing that $\delta_{\frac{1}{2}} = |\epsilon_-|$ we obtain an equation whose solution can be written as $\delta_{\frac{1}{2}} \approx d'(\tau, \kappa)\Omega_p^{max}$. Asking that fluctuations of δ does not destroy the efficiency means that we need $\sigma_{\delta} \ll \delta_{\frac{1}{2}}$, therefore we need large values of the parameter $\delta_{\frac{1}{2}}/\sigma_{\delta} \propto \Omega_p^{max}/\sigma_{\delta}$ which justifies the figure of merit defined in Eq.(4.9). Our derivation does not take into account fluctuations of the matrix elements, which are negligible in the regime where STIRAP could work. We check the optimization suggested by Fig.4.8 by looking at STIRAP for different values of E_J/E_C . It is seen that proper design allows to obtain larger efficiency as for $E_J/E_C = 0.7$ (Fig.4.9a) and $E_J/E_C = 1$ (Fig.4.9b). Instead for larger E_J/E_C , as in the Transmon design, which would guarantee best protection against noise the coupling is insufficient. Indeed $\Omega_0 T_1$ is too small, then even if the device is well protected against low-frequency charge noise coherent population transfer is limited from spontaneous decay of the first doublet (Fig.4.9c). In the opposite regime (charge qubits $E_J/E_C \ll 1$) the efficiency is also small even if large couplings could be achieved far off symmetry, due to large noise.

4.8 Comparison of different mechanisms of dephasing

Introducing a specific model for low-frequency noise in nanodevices is required by the fact that in quantum bits it gives quantitative account of striking experimental features as the peculiar non-exponential initial decoherence. Moreover this approach it provides relations between effects of noise for different bias point [27, 32, 33] and different device design uniquely explained by the parametric dependence of the energy spectrum, and this is possible only for non-markovian noise. Therefore this work complements

4.8. COMPARISON OF DIFFERENT MECHANISMS OF DEPHASING 77

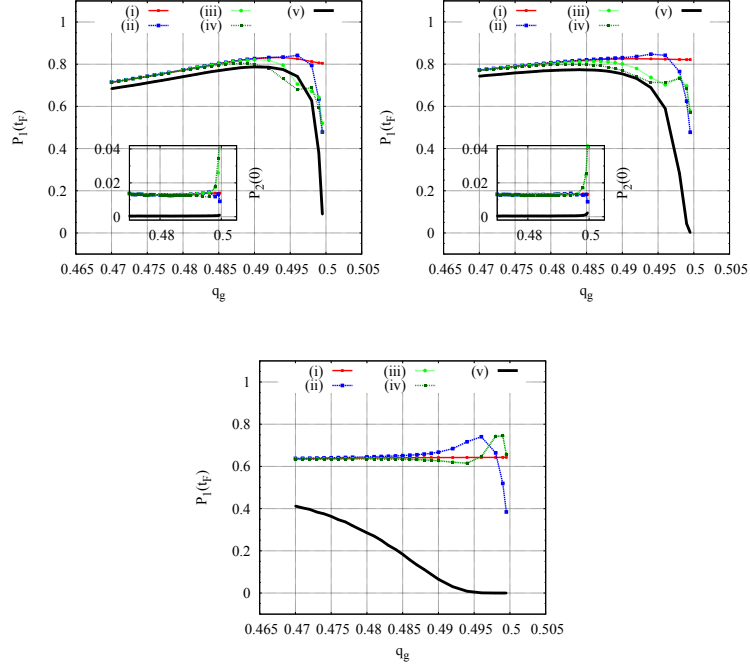


Figure 4.9: $P_1(t_f)$ vs $q_g \in [0.48, 0.5[$ for $J = 0.7, 1, 2$. Here Ω_0 corresponds to $\nu_R = 600$ Mhz and $\sigma_x = 0.004$.

previous studies in the quantum optics realm where typically the markovian master equation approach is used. Focusing on pure dephasing one considers the the dissipator Eq.4.8 with nonvanishing dephasing rates $\tilde{\gamma}_{01}$ instead of static fluctuations. This approach was pursued by Ivanov et al. [37] who derived the adiabatic solution of the Liouville equation, which interpolates between the coherent and the incoherent limit, and predicts striking behaviors as a function of the control parameters. They derived several analytic results, which have been numerically checked, and in particular for Gaussian pulses populations at the end of the protocol they found

$$\begin{aligned}\rho_{11}(\infty) &= \frac{1}{3} + \frac{2}{3}e^{-\frac{3\tilde{\gamma}_{01}T^2}{8\tau}} \\ \rho_{00}(\infty) &= \frac{1}{3} - \frac{1}{3}e^{-\frac{3\tilde{\gamma}_{01}T^2}{8\tau}}\end{aligned}\quad (4.10)$$

Notice that the efficiency is determined by the dephasing rate of the lowest doublet $\tilde{\gamma}_{01}$. The conclusion that the other dephasing channels are less relevant (for $\tilde{\gamma}_{12}, \tilde{\gamma}_{02} \gg \tilde{\gamma}_{01}$ some dependence appears in the numerical solutions of the master equation) agrees qualitatively with what we observed for the static fluctuator model. On the other hand the other striking

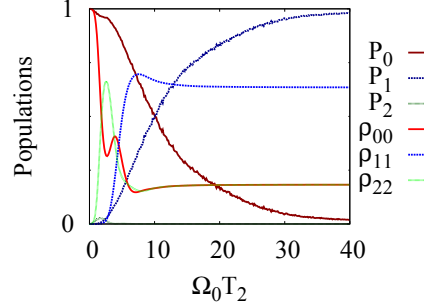


Figure 4.10: Here the efficiency vs $\Omega_0 T$ is calculated numerically for STIRAP affected by low frequency noise for $J = 1.32 q_g = 0.48$ and $\sigma_x = 0.004$. $P_1(t_f)$ is the dark blue line, $P_0(t_f)$ is the dark red line and $P_2(t_f)$ is the dark green line. This plot is compared with the numerical result obtained using the Lindblad equation for $T_2 = 57$ ns $\rho_{00}(t_f)$ is the light blue line, $\rho_{11}(t_f)$ is the light red line, $\rho_{22}(t_f)$ is the light green line,

feature of Eq.4.10, namely that losses due to dephasing are independent on the peak Rabi frequencies does not hold if low-frequency noise is taken into account. We plot in Fig. 4.10 the population $\rho_{ii}(\infty)$ obtained by numerical solution of the master equation having chosen $T = T_2^* = \frac{1}{\tilde{\gamma}_{01}}$ for increasing pulse amplitude Ω_0 compared with $P_i(\infty)$ for equivalent linear fluctuations of the detunings obtained by choosing $\sigma_x = \frac{\sqrt{2}}{A_1 T_2^*}$. It is seen that in this latter case efficiency depends on Ω_0 and improves for increasing values. The dependence on Ω_0 is natural consequence of non-ideal STIRAP via LZ patterns which occurs when low-frequency noise components are present, and which can-not be obtained accounting only for markovian noise. The situation is reminiscent of dynamical decoupling with strong AC continuous fields which is effective in eliminating dephasing due to noise of sufficiently low frequency. Another difference between markovian and non-markovian dephasing is that in this latter while decreasing transfer efficiency slightly populates the intermediate level $|\phi_2\rangle$. This is another indication of the reduced sensitivity of the protocol to low-frequency noise. On the other hand for markovian noise ρ_{22} would give direct information on $\tilde{\gamma}_{22}$ (see eq.4.10) This observation is reminiscent of the proposal of Ref [8] of using EIT on a SQUID-based nanodevice to probe decoherence of the corresponding phase qubit. Having in mind realistic noise spectra it is likely that the contribution of intermediate frequencies may determine effects similar to markovian dephasing therefore it could be interesting to cross check measurement of decoherence in two and three-level dynamics. Finally another implication of

the nonmarkovian character of noise is that correlations between the detunings exist, entirely determined by the parametric dependence of the energy spectrum. Effects of time-correlated (Ornstein Uhlenbeck) phase noise in optical systems were studied by Monte Carlo simulations, where the regime of partially correlated δ_p and δ_s was addressed. Instead for nanodevices we have in the simplest cases strongly anticorrelated (or correlated) detunings δ and δ_p and it would be interesting to investigate dynamic diffusion of phases at intermediate frequencies due to $\frac{1}{f^\alpha}$ noise.

4.9 Conclusions

In this chapter we presented a study on the combined effect of low-frequency and high-frequency charge noise on the coherence of a CPB operated as a three-level artificial atom in Lambda configuration. Observation of STIRAP should be possible in devices within present fabrication standards, provided both design and operating conditions are carefully chosen. We have shown that efficient population transfer comes from a tradeoff between large enough coupling and larger sensitivity to low-frequency noise. It may occur in a regime where low-frequency fluctuations of the energy spectrum are linear in the fluctuations x of the control parameter q_g . We have shown that noise is conveniently analyzed by mapping it onto fictitious correlated fluctuations of the detunings (see Fig. 4.3). Moreover despite of the complications brought by the multidimensional space of parameters, we have shown the efficiency for STIRAP depends essentially on noise channels relative to the trapped subspace only. These are nowadays fully characterized by operating the nanodevice as a qubit [27, 32, 33]. We have found that the tradeoff between coupling and low-frequency noise summarized by a single figure of merit Eq.4.9 indicating favorable conditions for observation of STIRAP. Its remarkable dependence on features of the three-level spectrum of the device suggests that band structure engineering plays a key role for determining optimal design solutions. This analysis, and other already available tools, as improvements in materials and control circuits, a more systematic investigation of parameters and tailoring of pulses, guarantee room for further efficiency improvement. In this work we did not consider other noise sources (as the readout circuit or critical current noise) which are possibly coupled to the device in channels “orthogonal” to the drive. This is because in the regime considered they lead to minor effects in CPB’s [27]. They can be easily accounted for by a slight generalization of our approach, allowing for independent noise sources. Notice that each of them would determine its own correlations of δ and δ_p . We remark that the physical picture which emerges from this work applies to the whole class of superconducting nanocircuits

so far used for implementing quantum bits[42]. Our analysis applies fully to flux-qubits [43, 44, 45, 46] where a coordinate-parity selection rule is active and a symmetry point exists. A proper description of actual devices should however take into account two orthogonal noise sources [32]. STIRAP in phase-qubits [47] is well described by the regime of linear fluctuations of energies are linear in the fluctuations. In all these devices the effect of low-frequency noise vs. efficient coupling can be characterized by a figure of merit analogous to Eq.4.9.

Bibliography

- [1] La Cognata A. Berritta M. D'Arrigo A. Spagnolo B. Paladino E. Falci, G. *submitted to Phys. Rev. B.*
- [2] K. Bergmann, H. Theuer, and B. W. Shore. *Rev. Mod. Phys.*, **70**:1003, 1998.
- [3] N. V. Vitanov, M. Fleischhauer, B. W. Shore, and K. Bergmann. *Adv. Atom. Mol. Opt. Phys.*, **46**:55, 2001.
- [4] E. Arimondo. V coherent population trapping in laser spectroscopy. volume **35** of *Progress in Optics*, page 257. Elsevier, 1996.
- [5] Marlan O. Scully and M. Suhail Zubairy. Cambridge University Press, 1 edition, 1997.
- [6] B. W. Shore N. V. Vitanov, T. Halfmann and K. Bergmann. *Annu. Rev. Phys. Chem.*, **52**:763, 2001.
- [7] K. V. R. M. Murali, Z. Dutton, W. D. Oliver, D. S. Crankshaw, and T. P. Orlando. *Phys. Rev. Lett.*, **93**:087003, 2004.
- [8] J. Siewert and T. Brandes. *Adv. Solid State Phys.*, **44**:181, 2004.
- [9] Yu-xi Liu, J. Q. You, L. F. Wei, C. P. Sun, and Franco Nori. *Phys. Rev. Lett.*, **95**:087001, 2005.
- [10] T. Brandes J. Siewert and G. Falci. *Opt. Comm.*, **264**:435, 2006.
- [11] Jens Siewert, Tobias Brandes, and G. Falci. *Phys. Rev. B*, **79**:024504, 2009.
- [12] Mika A. Sillanpää, Jian Li, Katarina Cicak, Fabio Altomare, Jae I. Park, Raymond W. Simmonds, G. S. Paraoanu, and Pertti J. Hakonen. *Phys. Rev. Lett.*, **103**:193601, 2009.

- [13] M. Baur, S. Filipp, R. Bianchetti, J. M. Fink, M. Göppl, L. Steffen, P. J. Leek, A. Blais, and A. Wallraff. *Phys. Rev. Lett.*, **102**:243602, 2009.
- [14] A. A. Abdumalikov, O. Astafiev, A. M. Zagoskin, Yu. A. Pashkin, Y. Nakamura, and J. S. Tsai. *Phys. Rev. Lett.*, **104**:193601, 2010.
- [15] R. Bianchetti, S. Filipp, M. Baur, J. M. Fink, C. Lang, L. Steffen, M. Boissonneault, A. Blais, and A. Wallraff. *Phys. Rev. Lett.*, **105**:223601, 2010.
- [16] Katarina Cicak Fabio Altomare Jae I. Park Raymond W. Simmonds Mika A. Sillanpää Jian Li, G. S. Paraoanu and Pertti J. Hakonen. *Scientific Reports 2*, Art. num. 645, 2012. 1038/srep00645.
- [17] William R. Kelly, Zachary Dutton, John Schlafer, Bhaskar Mookerji, Thomas A. Ohki, Jeffrey S. Kline, and David P. Pappas. *Phys. Rev. Lett.*, **104**:163601, 2010.
- [18] Nori Franco You, J. Q. *Nature*, **474**:589, 2011.
- [19] R. Fazio G.Falci. *Quantum Computer, Algorithms and Chaos.*, chapter Quantum computation with Josephson qubits, pages 363–413. B.L. Altshuler and V. Tognetti IOS Press The Netherlands.
- [20] P. Joyez D. Esteve V. Bouchiat, D. Vion and M. H. Devoret. *Physica Scripta*, **T 76**:165, 1998.
- [21] Yu. Pashkin Y. Nakamura and J. S. Tsai. *Nature*, **398**:786, 1999.
- [22] D. Vion, A. Aassime, A. Cottet, P. Joyez, H. Pothier, C. Urbina, D. Esteve, and M. H. Devoret. *Science*, **296**:886, 2002.
- [23] T. Duty, D. Gunnarsson, K. Bladh, and P. Delsing. *Phys. Rev. B*, **69**:140503, 2004.
- [24] A. Blais L. Frunzio R.-S. Huang J. Majer S. Kumar S. M. Girvin & R. J. Schoelkopf A. Wallraff, D. I. Schuster. *Nature*, **421**:162, 2004.
- [25] Jens Koch, Terri M. Yu, Jay Gambetta, A. A. Houck, D. I. Schuster, J. Majer, Alexandre Blais, M. H. Devoret, S. M. Girvin, and R. J. Schoelkopf. *Phys. Rev. A*, **76**:042319, 2007.
- [26] E. Collin, G. Ithier, A. Aassime, P. Joyez, D. Vion, and D. Esteve. *Phys. Rev. Lett.*, **93**:157005, 2004.

- [27] G. Ithier, E. Collin, P. Joyez, P. J. Meeson, D. Vion, D. Esteve, F. Chiarello, A. Shnirman, Y. Makhlin, J. Schrieffer, and G. Schön. *Phys. Rev. B*, **72**:134519, 2005.
- [28] Chad Rigetti, Jay M. Gambetta, Stefano Poletto, B. L. T. Plourde, Jerry M. Chow, A. D. Córcoles, John A. Smolin, Seth T. Merkel, J. R. Rozen, George A. Keefe, Mary B. Rothwell, Mark B. Ketchen, and M. Steffen. *Phys. Rev. B*, **86**:100506, 2012.
- [29] E. Paladino, L. Faoro, G. Falci, and Rosario Fazio. *Phys. Rev. Lett.*, **88**:228304, 2002.
- [30] Ulrich Weiss. *Quantum Dissipative Systems (Series in Modern Condensed Matter Physics)*. World Scientific Publishing Company, 2008.
- [31] G. Falci, A. D'Arrigo, A. Mastellone, and E. Paladino. *Phys. Rev. Lett.*, **94**:167002, 2005.
- [32] Gustavsson Yan F. Yoshihara F. Harrabi K. Fitch-G. Cory D. G. Nakamura Y. Tsai J. Oliver W. D. Bylander, J. *Nat Phys*, **7**:565, 2011.
- [33] F Chiarello, E Paladino, M G Castellano, C Cosmelli, A D'Arrigo, G Torrioli, and G Falci. *New Journal of Physics*, **14**:023031, 2012.
- [34] E. Paladino, A. Mastellone, A. D'Arrigo, and G. Falci. *Phys. Rev. B*, **81**:052502, 2010.
- [35] Daniel Sank, R. Barends, Radoslaw C. Bialczak, Yu Chen, J. Kelly, M. Lenander, E. Lucero, Matteo Mariantoni, A. Megrant, M. Neeley, P. J. J. O'Malley, A. Vainsencher, H. Wang, J. Wenner, T. C. White, T. Yamamoto, Yi Yin, A. N. Cleland, and John M. Martinis. *Phys. Rev. Lett.*, **109**:067001, 2012.
- [36] et. al. G. Falci, M. Berritta. *Physica Scripta*, **2012**(T151):014020, 2012.
- [37] P. A. Ivanov, N. V. Vitanov, and K. Bergmann. *Phys. Rev. A*, **70**:063409, 2004.
- [38] A. D'Arrigo G. Falci, A. Mastellone and E. Paladino. *Phys. Rev. Lett.*, **13**:323, 2006.
- [39] A. La Cognata, P. Caldara, D. Valenti, B. Spagnolo, A. D'Aarrigo, E. Paladino, and G. Falci. *International Journal of Quantum Information*, **09**:1, 2011.

- [40] T. B̃ondo A. K̃uhn, M. H̃ennrich and G. Rempe. *Appl. Phys. B*, bf 69:373, 1999.
- [41] Q. Shi and E. Geva. *Journal of chemical physics*, **119**:11773, 2003.
- [42] J. Clarke and F.K. Wilhelm. *Nature*, **453**:1031, 2008.
- [43] C. J.P. M. Harmans I. Chiorescu, Y. Nakamura and J. E. Mooij. *Science*, **299**:1869, 2003.
- [44] I. Chiorescu, P. Bertet, K. Semba, Y. Nakamura, C. J. P. M. Harmans, and J. E. Mooij. *Nature*, **431**:159, 2004.
- [45] O. Astafiev Y. Nakamura T. Yamamoto, Yu.A. Pashkin and J. S. Tsai. *Nature*, **425**:941, 2003.
- [46] A. C.J. ter Haar-C. J.P. M. Harmans J. B. Majer, F. G. Paauw and J. E. Mooij. *Phys. Rev. Lett.*, **94**:090501, 2005.
- [47] I. Chiorescu, Y. Nakamura, C. J. P. M. Harmans, and J. E. Mooij. *Science*, **299**:1869, 2003.

Chapter 5

STIRAP protocol with a two photon pump pulse

In the last chapter we have shown that it is possible to implement a Lambda configuration allowing for STIRAP in a superconducting device as the CPB biased off-symmetry in the presence of broadband noise. However the efficiency would be strongly limited and noise correlations arising from the band structure would require for dynamical suppression a larger pump coupling, which is not available. In this chapter we will propose an implementation of the Lambda scheme at the symmetry point (optimal working point) where the energy fluctuations are greatly reduced. Since the pump field cannot be directly coupled to the transition we seek for a two-photon pump coupling. These results are collected together with those on a paper published on *Physica Scripta* [1].

5.1 A two photon pump pulse

Before to proceed with the strategy for the implementation of the STIRAP process at the optimal working point in this section is discussed the main idea that allow this strategy.

5.1.1 Adiabatic elimination

One of the crucial features that suggest the possibility of performing a three-photon STIRAP process is that Rabi oscillation between a couple of quantum level in a multilevel system may be implemented with an appropriate multimode signal [2]. This *multiphoton Rabi oscillation* has been demonstrated also in superconducting devices [3, 4]. To make it clear it is possible to study a physical system described by an Hamiltonian in RWA of the form

$$\begin{aligned} \hat{H}_{Rabi}^{2-ph} = & E_1 |\phi_1\rangle \langle \phi_1| \\ & + E_2 |\phi_2\rangle \langle \phi_2| + \frac{1}{2} (\Omega_{p_1}^*(t) |\phi_1\rangle \langle \phi_0| + \Omega_{p_2}^*(t) |\phi_2\rangle \langle \phi_1| + h.c.) \end{aligned} \quad (5.1)$$

where $\Omega_{p_{1,2}}(t) = \Omega_{p_{1,2}0} e^{-i\phi_{p_{1,2}}(t)}$, that in the basis $\{|\phi_i\rangle\}$ read

$$H_{Rabi}^{2-ph} = \begin{bmatrix} 0 & \frac{1}{2}\Omega_{p_1}^* e^{i\phi_{p_1}(t)} & 0 \\ \frac{1}{2}\Omega_{p_1} e^{-i\phi_{p_1}(t)} & E_1 & \frac{1}{2}\Omega_{p_2}^* e^{i\phi_{p_2}(t)} \\ 0 & \frac{1}{2}\Omega_{p_2} e^{-i\phi_{p_2}(t)} & E_2 \end{bmatrix} \quad (5.2)$$

It will be clear later (this is the scope of this section) that, for the Three-photon STIRAP process implementation, the crucial regime is determined by:

- $\dot{\phi}_{p_1} \ll E_1$ and $\dot{\phi}_{p_2} \gg E_2 - E_1$ or $\dot{\phi}_{p_1} \gg E_1$ and $\dot{\phi}_{p_2} \ll E_2 - E_1$ that are the condition of deeply dispersive coupling of level E_1 with the levels $E_0 = 0$ and E_2

- $\delta_p \equiv E_2 - E_0 - (\dot{\phi}_{p_1} - \dot{\phi}_{p_2}) \approx 0$ that is the condition of *two-photon resonance*.

The physical features of this Hamiltonian are easy to understand in an appropriate rotating frame. For this reason an unitary transformation could be applied

$$|\Psi(t)\rangle = U_{rf}(t) |\Psi(t)\rangle_{rf}; \quad U_{rf}(t) = e^{i(\phi_{p_1} P_{11} + \phi_{p_2} P_{22})} \quad (5.3)$$

here

$$P_{ij} = |\phi_i\rangle \langle \phi_j|$$

the effective Hamiltonian for $|\Psi(t)\rangle_{rf}$ become

$$\tilde{H}_p = \begin{bmatrix} 0 & \frac{1}{2}\Omega_{p_1}^* & 0 \\ \frac{1}{2}\Omega_{p_1} & \delta_2 & \frac{1}{2}\Omega_{p_2}^* \\ 0 & \frac{1}{2}\Omega_{p_2} & \delta_p \end{bmatrix} \quad (5.4)$$

where

$$\delta_2 = E_1 - \dot{\phi}_{p_1} \quad (5.5)$$

$$\delta_p = E_2 - \dot{\phi}_{p_1} - \dot{\phi}_{p_2} \quad (5.6)$$

This scheme of coupling may allow for Rabi oscillations between states $|\phi_0\rangle$ and $|\phi_2\rangle$ which are not directly coupled. We illustrate here a standard way, named adiabatic elimination to obtain an effective Hamiltonian describing these Rabi oscillation [2]. In fact the Schrödinger equation for the dynamics of a generic state $|\Psi(t)\rangle_{rf} = c_0(t) |\phi_0\rangle + c_1(t)e^{-i\phi_{p_1}} |\phi_{p_1}\rangle + c_2(t)e^{-i\phi_{p_1}} |\phi_2\rangle$ is

$$\begin{cases} i\dot{c}_0(t) = \frac{1}{2}\Omega_{p_1}^* c_1(t) \\ i\dot{c}_1(t) = \frac{1}{2}\Omega_{p_1} c_0(t) + \delta_2 c_1(t) + \frac{1}{2}\Omega_{p_2}^* c_2(t) \\ i\dot{c}_2(t) = \frac{1}{2}\Omega_{p_2} c_1(t) + \delta_p c_2(t) \end{cases} \quad (5.7)$$

Under the assumptions $\delta_2 \gg \Omega_{k=s,p_1,p_2}$ (dispersive coupling of the the subspace $\{|\phi_0\rangle, |\phi_2\rangle\}$ with the level ϕ_1) the coarse-grained version of the second equation of eq. 5.7 with a coarse-graining time such that $\delta_2 \ll \frac{1}{\Delta t} \ll |E_i - E_j|$ is

$$\bar{c}_1(t) = -\frac{\Omega_{p_1}(t)}{2\delta_2} \bar{c}_0(t) - \frac{\Omega_{p_2}(t)}{2\delta_2} \bar{c}_2(t) \quad (5.8)$$

Substituting the expression of $\bar{c}_1(t)$ in the other two equation of the system 5.7 the effective approximate dynamics for c_0 and c_2 satisfy the equations

$$\begin{cases} i\dot{c}_0(t) = -\frac{|\Omega_{p_1}|^2}{4\delta_2} c_0(t) + \frac{\Omega_{p_1}^* \Omega_{p_2}}{4\delta_2} c_2(t) \\ i\dot{c}_2(t) = \frac{\Omega_{p_1} \Omega_{p_2}^*}{4\delta_2} c_0(t) + \frac{|\Omega_{p_2}|^2}{4\delta_2} c_2(t) \end{cases} \quad (5.9)$$

then for the dynamics in the subspace spanned by $\{|\phi_0\rangle, |\phi_2\rangle\}$ we write the effective Hamiltonian

$$\tilde{H}_{Rabi}^{ae} = \begin{bmatrix} S_1(t) & \frac{1}{2}\Omega_p^*(t) \\ \frac{1}{2}\Omega_p(t) & S_2(t) + \delta_p \end{bmatrix} \quad (5.10)$$

where

$$\Omega_p = -\frac{\Omega_{p1}(t)\Omega_{p2}^*(t)}{2\delta_2} \quad (5.11)$$

is the effective *pump pulse* and

$$S_1(t) = -\frac{|\Omega_{p1}(t)|^2}{4\delta_2}; \quad S_2(t) = -\frac{|\Omega_{p2}(t)|^2}{4\delta_2} \quad (5.12)$$

are the *Stark shifts*. In other word the system described by the Hamiltonian 5.4 could be well approximated, by an Hamiltonian of the form $\tilde{H} \simeq \tilde{H}^{ae} = H_{11} \oplus \tilde{H}_{Rabi}^{02}$ where \tilde{H}_{Rabi}^{02} is the well known Rabi Hamiltonian and $H_{11} = \delta_2 |1\rangle\langle 1|$. This means that under the condition of dispersive coupling the two *pump pulse* behaves as the *pump pulse* in the traditional STIRAP. However for the forthcoming application to STIRAP one should specify the full 3×3 structure of \tilde{H}_{ae} then is necessary account for the Stark shift of the intermediate level δH_{11}^{ae} . The Stark shifts using the second order perturbation theory (in the limit $\Omega_i \ll \delta_i$) are

$$\begin{aligned} \delta H_{00}^{ae} &= \sum_{j=1,2} \frac{|\langle \phi_0 | H_1 | \phi_j \rangle|^2}{-\delta_2} = -\frac{|\Omega_{p1}|^2}{4\delta_2} = S_1 \\ \delta H_{11}^{ae} &= \sum_{j=0,2} \frac{|\langle \phi_1 | H_1 | \phi_j \rangle|^2}{\delta_2 - E_j^0} = -\frac{|\Omega_{p1}|^2}{4\delta_2} \\ &= \frac{|\Omega_{p1}|^2}{4\delta_2} + \frac{|\Omega_{p2}|^2}{4(\delta_2 - \delta_p)} = S_1 + S_2 \\ \delta H_{22}^{ae} &= \sum_{j=0,1} \frac{|\langle \phi_2 | H_1 | \phi_j \rangle|^2}{\delta_p - \delta_2} = -\frac{|\Omega_{p2}|^2}{4(\delta_p - \delta_2)} = S_2 \end{aligned} \quad (5.13)$$

In the end we can write the effective Hamiltonian for the pump pulse terms

$$\tilde{H}_{Rabi}^{ae} = \begin{bmatrix} S_1 & 0 & \frac{1}{2}\Omega_p^* \\ 0 & \delta_2 - (S_1 + S_2) & 0 \\ \frac{1}{2}\Omega_p & 0 & S_2 \end{bmatrix}. \quad (5.14)$$

$$(5.15)$$

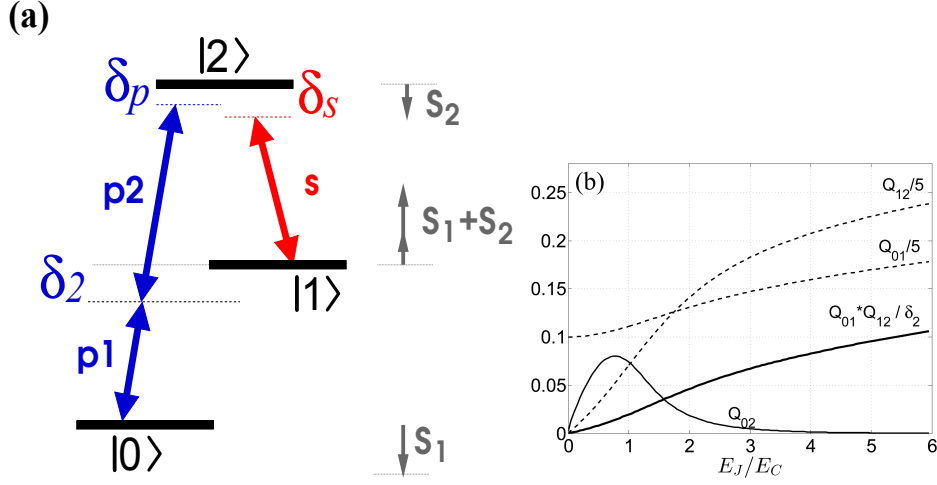


Figure 5.1: (a) Lambda scheme with a two pump fields (p_1, p_2) providing an effective $(0, 2)$ two-photon pump coupling, but producing in addition Stark shifts (S_1, S_2) of the undriven levels. (b) Off diagonal matrix element of a CPB as a function of E_J/E_C . Matrix elements Q_{01} and Q_{12} (divided by 5) are large at the symmetry point, therefore the effective coupling $\propto Q_{01}Q_{12}/\delta_2$ is large enough and increases with E_J/E_C . On the contrary Q_{02} (here off-symmetry) is non monotonic.

5.2 Three-photon STIRAP process

In this section is proposed a strategy for the implementation of the STIRAP process in superconductive device at the optimal working point using a *two-photon* pump pulse. To this end we address the three level system by a three-tone drive described schematically in Fig.5.1 a) $A(t) = \sum_k \mathcal{A}_k(t) \cos \phi_k(t)$. Here $k = s$ labels a component with carrier frequency close to the Stokes transition whereas $k = p_1, p_2$ refers to two drives implementing a two-photon pump pulse using $|\phi_1\rangle$ as the intermediate level.

5.2.1 Model Hamiltonian

We start from the single-port Hamiltonian introduced in sec.1.1.4

$$H_S(t) = H_0[\mathbf{q} + \mathbf{q}_c(t)] \simeq H_0 + q_c(t) \cdot [\nabla_{\mathbf{q}} H_0]_{\mathbf{q}(t)} = H_0 + A(t) \hat{Q} \quad (5.16)$$

where $A(t)$ is the three-tone control field described above. Retaining only the off-diagonal quasi resonant term in the RWA the Hamiltonian takes the form

$$H(t) = E_1 P_{11} + E_2 P_{22} + \{ [\Omega_{p_1}(t) e^{i\phi_{p_1}} P_{10} + (\Omega_{p_2}(t) e^{i\phi_{p_2}} P_{21} + \Omega_s(t) e^{i\phi_s} P_{21}) P_{21}] + h.c. \} \quad (5.17)$$

here

$$\begin{aligned}
H_0 |\phi_i\rangle &= E_i |\phi_i\rangle; & P_{ij} &= |\phi_i\rangle \langle \phi_j| \\
Q_{ij} &= \langle \phi_i | \hat{Q} | \phi_j \rangle; & \Omega_{p_1}(t) &= \mathcal{A}_{p_1}(t) Q_{10} \\
\Omega_{p_2}(t) &= \mathcal{A}_{p_2}(t) Q_{21}; & \Omega_s(t) &= \mathcal{A}_s(t) Q_{21}
\end{aligned} \tag{5.18}$$

5.2.2 Doubly rotating frame

The understanding of the physics described by the Hamiltonian of Eq.5.17 is simpler in a appropriate rotating frame. For this reason we apply an unitary transformation to the state of the system such that

$$|\Psi(t)\rangle = U_{rf}(t) |\Psi(t)\rangle; \quad \mathcal{U}(t) = \prod_i e^{i\zeta_i(t)P_{ii}} \tag{5.19}$$

If we choose $\zeta_0 = 0$, $\zeta_1(t) = \phi_{p_1}(t)$ and $\zeta_2(t) = \phi_{p_1}(t) + \phi_{p_2}(t)$ with the definition

$$\begin{aligned}
\delta_2(t) &= E_1 - \dot{\phi}_{p_1}(t); & \delta_p(t) &= E_2 - [\dot{\phi}_{p_1}(t) + \dot{\phi}_{p_2}(t)] \\
\delta_s(t) &= E_2 - E_1 - \dot{\phi}_s(t); & \delta(t) &= \delta_p(t) - \delta_s(t); & \dot{\phi}(t) &= \delta_t - \delta_2(t)
\end{aligned}$$

the effective Hamiltonian in the new rotating frame is

$$\begin{aligned}
\tilde{H}(t) &= \mathcal{U}^\dagger(t) H(t) \mathcal{U}(t) - i\mathcal{U}^\dagger(t) \partial_t \mathcal{U}(t) \\
&= \delta_2 P_{11} + \delta_p P_{22} \\
&+ \frac{1}{2} [\Omega_{p_1}(t) P_{10} + (\Omega_{p_2}(t) + \Omega_s(t) e^{i\phi(t)}) P_{21} + h.c.] \tag{5.20}
\end{aligned}$$

5.2.3 Stokes pulse optimization

An effective Hamiltonian for the three-photon Lambda scheme is obtained by adding to Eq.(5.4) the Stokes pulse Hamiltonian \tilde{H}_s . In the same gauge as before the Stokes term reads $\tilde{H}_s = \frac{1}{2} [\Omega_s(t) e^{-i\phi(t)} |2\rangle \langle 1| + h.c.]$, where $\phi(t) = \phi_s(t) - \phi_{p_2}(t)$; the phase is related to detunings $\dot{\phi}(t) = \delta(t) - \delta_2(t)$ therefore it is slowly varying, as well as $\Omega_s(t)$; the coarse grained version of this Hamiltonian is obtained by just substituting the nonvanishing entries of Eq.(5.14) level to those of Eq.(5.2) considering the Stark shift of the intermediate yielding

$$\tilde{H} \approx \tilde{H}_{ave} = \begin{bmatrix} S_1(t) & 0 & \Omega_p^*(t)/2 \\ 0 & \delta_2 - (S_1(t) + S_2(t)) & \Omega_s^*(t) e^{i\phi(t)}/2 \\ \Omega_p(t)/2 & \Omega_s(t) e^{-i\phi(t)}/2 & \delta_p + S_2(t) \end{bmatrix}$$

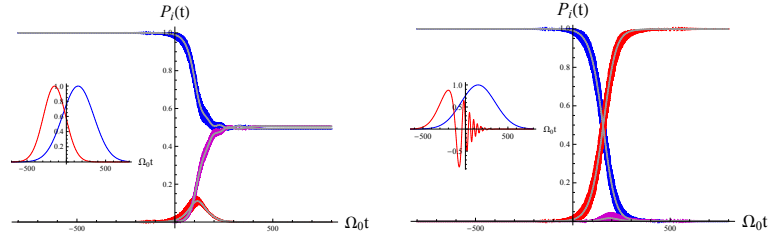


Figure 5.2: Exact population histories for a three-level system subject to a three-tone external drive (gray curves) are compared with the coarse grained version (black lines) obtained by Eq.(5.21). The agreement of the average Hamiltonian approximation is excellent. Top: population histories for monochromatic pulses at nominal two-photon resonance $\delta = 0$, where stray Stark shifts prevent efficient STIRAP. Bottom: population histories with the phase corrected Stokes field (in the inset) which allows for faithful population transfer. Here the peak Rabi frequencies are $\Omega_s = \Omega_{p1} = \Omega_{p2} =: \Omega_0$, $\Omega_0 T = 200$ and $\delta_2 = 5\Omega_0$. The relevant figure for STIRAP is $\sim \Omega_p T = 20$.

Notice that all the quantities in this equation are (slowly) time-dependent. It is convenient to perform a unitary transformation gauging away $\delta_2(t)$ and finally

$$\tilde{H}'_{ave} = \begin{bmatrix} 0 & 0 & \Omega_p^*(t)/2 \\ 0 & \delta - (2S_1(t) + S_2(t)) & \Omega_s^*(t)/2 \\ \Omega_p(t)/2 & \Omega_s(t)/2 & \delta_p(t) + (S_2(t) - S_1(t)) \end{bmatrix} \quad (5.21)$$

The Hamiltonian has now the standard structure of Eq.(4.6) apart for the Stark shifts S_i . Therefore the tree-tone drive could yield successful STIRAP also at the symmetry point, where the matrix elements Q_{01} and Q_{12} needed for coupling the two pump field are large (see Fig.5.1). However the presence of the Stark shifts requires some care, since they produce large stray detunings, comparable with amplitudes of the effective fields. In particular since $\delta - [2S_1(t) + S_2(t)] \geq \Omega_p(t)$ coherent population transfer is suppressed even for $\delta = 0$ (see Fig. 5.2, top panel). This drawback could be avoided by suitable pulse shaping, a problem to be formulated in the framework of Optimal Control Theory [5]. The fact that such a solution may exist is suggested by noticing that knowledge of the structure of the approximate average Hamiltonian allows to foresee a way to reduce the impact of the pump-induced shifts by only reshaping the Stokes pulse. In fact performing another gauge transformation to the Hamiltonian 5.21 with the unitary

operator

$$\mathcal{U}(t) = e^{i\phi'_s(t)P_{11}} \quad (5.22)$$

$$\phi'_s(t) = \int dt' (2S_1(t') + S_2(t')) \quad (5.23)$$

a new effective Hamiltonian is obtained

$$\tilde{H} = \begin{bmatrix} 0 & 0 & \frac{1}{2}\Omega_p^*(t) \\ 0 & \delta & \frac{1}{2}\Omega_s^*(t)e^{-i\phi'_s(t)} \\ \frac{1}{2}\Omega_p^*(t) & \frac{1}{2}\Omega_s(t)e^{i\phi'_s(t)} & \delta_p^{eff} \end{bmatrix} \quad (5.24)$$

$$\delta_p^{eff} = \delta_p + S_2(t) - S_1(t) \quad (5.25)$$

This new Hamiltonian is exactly the Hamiltonian for the traditional STIRAP if the traditional gaussian Stokes pulse is replaced by $\Omega_s(t) \rightarrow \Omega_s(t) e^{-i\phi'_s(t)}$. Indeed the dispersive condition means $|\Omega_{pi}(t)|^2/\delta_2 \ll \delta_2 \ll \omega_k$ implying that the approximations leading to the RWA are still valid and moreover that the new envelope (inset of Fig. 5.2, bottom) is still slowly varying on the scale of δ_2 , allowing to rederive Eq.(5.21). This expectation is confirmed by the numerical evaluation of the dynamics determined by the RWA Hamiltonian $\tilde{H}_p + \tilde{H}_s$ with the modulated Stark pulse (Fig 5.2,bottom).

5.2.4 Model Hamiltonian

Summarizing, the precedent calculation allows to write an Hamiltonian in the rotating frame where a two photon pump coupling is performed.

$$H(t) = \begin{bmatrix} 0 & \frac{1}{2}\Omega_{p1}(t) & 0 \\ \frac{1}{2}\Omega_{p1}(t) & \delta_2 & \frac{1}{2}\Omega_{p2}e^{i\delta_2 t} + \frac{1}{2}\Omega_s(t) \\ 0 & \frac{1}{2}\Omega_{p2}e^{-i\delta_2 t} + \frac{1}{2}\Omega_s^*(t) & \delta_2 \end{bmatrix} \quad (5.26)$$

where

$$\Omega_{p1} = \Omega_0 e^{\frac{[(t-\tau)/T]^2}{2}}; \quad \Omega_{p2} = \kappa_p \Omega_0 e^{\frac{[(t-\tau)/T]^2}{2}}; \quad \Omega_s = \kappa_s \Omega_0 e^{\{[(t-\tau)/T]^2 + i\phi(t)\}}$$

$$\phi(t) = -(k_p^2 + 2)A_0^2 \frac{\sqrt{\pi}T}{8\delta_2} \left[\operatorname{erf}\left(\frac{t-\tau}{T}\right) - \operatorname{erf}\left(\frac{-t_0-\tau}{T}\right) \right]$$

the modulation of the Stokes pulse with the phase $\phi(t)$ cancel the Stark shifts produced by the pump pulses. Numerical simulation confirm our estimate obtained with the effective Hamiltonian (Fig 5.2).

The study was performed for Rabi frequency $\Omega_s = \Omega_{p1} = \Omega_{p2} =: \Omega_0$, $\Omega_0 T = 200$ e $\delta_2 = 5\Omega_0$, tali da ottenere un prodotto $\Omega_p T \sim 20$. The simulations show good agreement with the final result obtained with the result obtained

with the effective Hamiltonian. The plot on the left is obtained for a Stokes pulse without the phase correction. As expected the STIRAP process does not have success. The right plot is obtained for the case of Stokes pulse corrected by the phase $\phi(t)$ (Fig 5.2, destra). In the insets are shown the pulse shape applied.

We stress about the excellent agreement between dynamics calculated with exact Hamiltonian and dynamics calculated with the effective Hamiltonian.

5.3 Sensitivity to parameters

Efficiency vs δ_2

The study of resilience is conducted considering

$$\Omega_0 = \Omega_{s0} = \Omega_{p1} = 1; \quad k_p = \frac{\Omega_{p1}}{\Omega_{p2}} = 1; \quad \tau = 0.75T;$$

We have low efficiency for non dispersive regime $\delta_2 \lesssim 1$, the plateau of efficiency near 1 become larger growing T Fig 5.3. Taking into account the

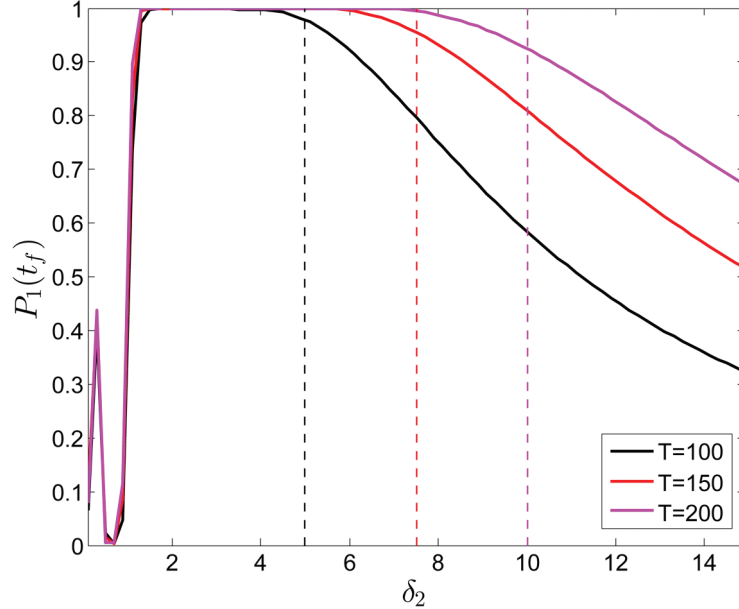


Figure 5.3: Efficiency of population transfer vs δ_2 . The dashed lines sign the limit $\Omega_p T = 10$ for every line. Here $\kappa_s = 1$, $\kappa_p = 1$ and $\tau/T = 0.75$

results showed in fig. 5.3 it is clear that with values of $\delta_2 \simeq 3.5 - 4$ the

consideration about the resilience of the parameters for traditional STIRAP are valid also for the three-photon STIRAP process with $\Omega_p(t) \rightarrow \frac{\Omega_{p1}\Omega_{p2}^*}{2\delta_2}$ and $\Omega_s(t) \rightarrow \Omega_s(t)e^{-i\phi(t)}$.

Efficiency vs τ

Considering $\Omega_{s0} = \Omega_{p10} = \Omega_{p20} = 1$ and the delay defined by

$$\frac{\tau}{T}$$

Plots are obtained varying $\Omega_p T$. The *plateau* present on the left part of the plot, become larger at the growing of T . As in the case of traditional STIRAP protocol, a counterintuitive sequence pulse guarantee an efficient transfer of population Fig.5.4.

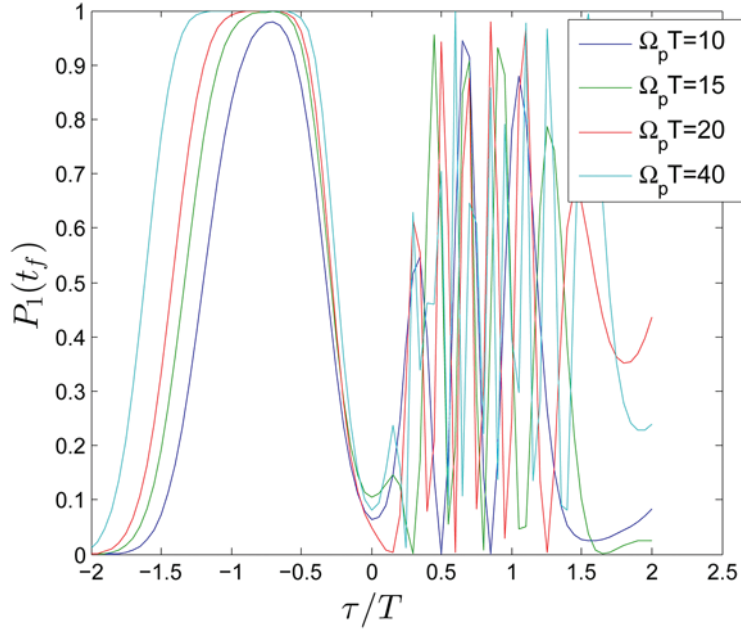


Figure 5.4: Transfer efficiency vs τ/T for $\Omega_p T = 10, 15, 20, 40$. Here $\delta_2 = 3$, $\kappa_p = 1$, $\kappa_s = 1$ e $\Omega_0 = 1$

Resilience analysis vs κ_p and κ_s

We defined

$$\kappa_s = \frac{\Omega_{p1}}{\Omega_s}; \quad \kappa_p = \frac{\Omega_{p1}}{\Omega_{p2}}; \quad \tau/T = 0.75;$$

it emerges that an asymmetry on the peak Raby frequency do not imply a better transfer. In the case of high k_p the transfer efficiency is worst.

5.4. TOWARD IMPLEMENTATION OF THREE-PHOTON STIRAP PROCESS IN SUPERCONDUCTIVE DEVICE

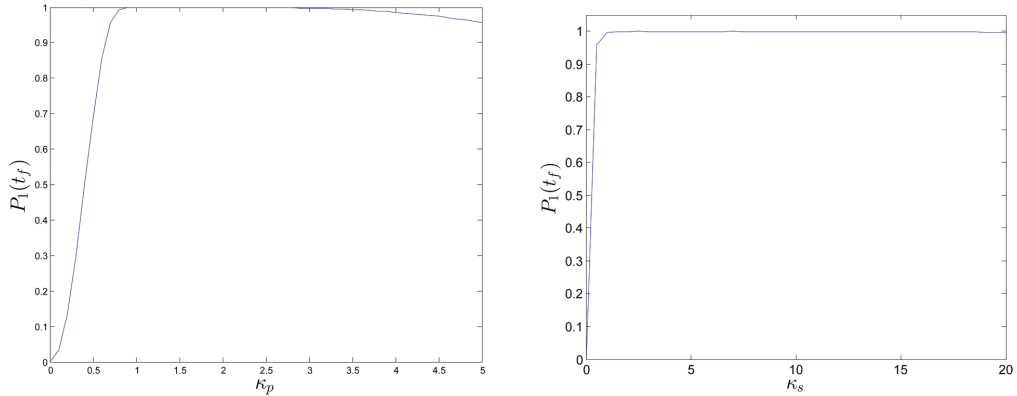


Figure 5.5: Resilience vs κ_p and vs κ_s , for $\delta_2 = 3$, $\Omega_p T = 20$ and $\tau/T = 0.75$

5.4 Toward implementation of three-photon STIRAP process in superconductive device

5.4.1 Validity of three level model

Working at the optimal working point guarantees a big suppression of the low frequency noise effect[6], however with a strong effective pulse $\Omega_p \sim |\Omega_{pi}|^2/\delta_2$. This perspective result interesting for application to nanodevices as CPB and flux qubits that, for traditional protocol need to work out from optimal working point due to the selection rule at expense of the noise immunity, and highest coupling obtained with high value of E_J/E_C . However this behaviour can decrease due to harmonicity that arise for increasing value of E_J/E_C . In fact the condition for an AC pulse with frequency ω and amplitude Ω to generate non negligible transition between levels with energy E_i and E_j is

$$||E_i - E_j| - \omega| \lesssim \Omega \quad (5.27)$$

this mean that if the spectrum of the device is near harmonic a given pulse can generate transition between undesired level. From the physical point of view working at the symmetry point ensures that decoherence due to low-frequency noise is strongly suppressed, but still large enough values of the effective $\Omega_p \sim |\Omega_{pi}|^2/\delta_2$. The appealing feature for devices as the CPB and flux qubits is that both protection from noise and coupling to the drive improve for increasing E_J/E_C , contrary to what happens for conventional STIRAP at off-symmetry bias [7] due to the behavior of matrix elements $Q_{ij}(E_J/E_C)$ (see Fig. 5.1b). This favorable trend is however expected to weaken for larger and larger E_J/E_C , as proven by Fig.5.6 (black diamonds)

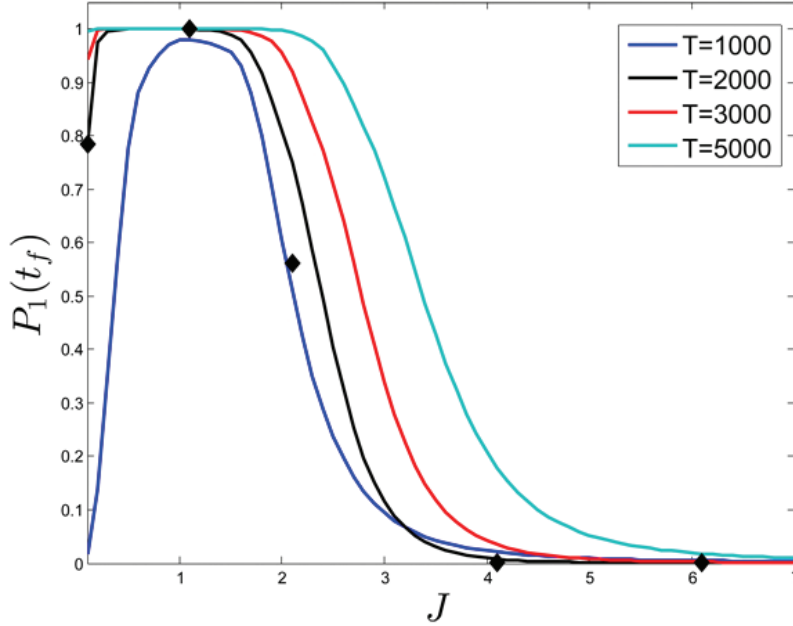


Figure 5.6: Transfer efficiency vs $J = \frac{E_J}{E_C}$ for different value of T . The continuous lines are calculated with a 3 level model Hamiltonian with the transversal approximation and RWA. The black diamonds are calculated for $T = 2000$ without approximations.

when the spectrum becomes nearly harmonic and the system may climb the ladder multilevel structure under the action of the AC drives A.

Bibliography

- [1] et. al. G. Falci, M. Berritta. *Physica Scripta*, **2012**(T151):014020, 2012.
- [2] N. V. Vitanov, M. Fleischhauer, B. W. Shore, and K. Bergmann. *Adv. Atom. Mol. Opt. Phy.*, **46**:55, 2001.
- [3] S. Saito, T. Meno, M. Ueda, H. Tanaka, K. Semba, and H. Takayanagi. *Phys. Rev. Lett.*, **96**:107001, 2006.
- [4] A. Lupaşcu, P. Bertet, E. F. C. Driessen, C. J. P. M. Harmans, and J. E. Mooij. *Phys. Rev. B*, **80**:172506, 2009.
- [5] L. M. K. Vandersypen and I. L. Chuang. *Rev. Mod. Phys.*, **76**:1037, 2005.

- [6] R. Fazio G.Falci. *Quantum Computer, Algorithms and Chaos.*, chapter Quantum computation with Josephson qubits, pages 363–413. B.L. Altshuler and V. Tognetti IOS Press The Netherlands.
- [7] La Cognata A. Berritta M. D'Arrigo A. Spagnolo B. Paladino E. Falci, G. *submitted to Phys. Rev. B.*

Chapter 6

Tunneling in a bistable potential with strong dissipation

A feature which makes a strong difference between the behaviour of a quantum system in respect to a classical one is the quantum tunneling. This effect often occurs in condensed matter physics, such as Josephson junctions and hetero-nanostructures [1]. In a dissipative quantum system interacting with a thermal bath, the quantum tunneling can play an important role on the relaxation time from a metastable state [2]. During the last years the effects of environment on quantum tunneling phenomenon have been intensively studied [3, 4, 5, 6]. Commonly, environment is modelled as a number \mathcal{N} (usually $\mathcal{N} \rightarrow \infty$) of harmonic oscillators considered at thermal equilibrium, i.e. thermal bath, interacting with the quantum system through a bilinear coupling [7, 8, 9, 10, 11]. In this context, symmetric and asymmetric quantum bistable systems are good enough to analyze superconducting quantum bits and decoherence phenomena [12, 9]. Obtaining longer coherence times in such systems, when they interact with noisy environment, is one of the major requirements in devising and manufacturing devices capable of storing quantum bits. In this respect, a main topic is to know the properties of a particle subject to an external potential, in the presence of random fluctuations. It can be also useful to study the changes occurring in the dynamics of a quantum particle affected by noisy perturbations, when different shapes of the potential profile are used. Potentials which model the interaction with laser beams have most interesting implications for quantum systems such as the coherent destruction of tunneling [13], the effect of quantum stochastic resonance [14], and the control and reduction of decoherence in open quantum systems [15]. In this chapter, in order to analyze the evolution of a quantum particle subject to time-independent asymmetric bistable potential and affected by environmental noise, we use the Caldeira-Leggett model [4], which allows to derive a quantum mechanical analogue of the generalized Langevin equation. The study is performed by using the approach of the Feynman-Vernon functional [16] in discrete variable representation (DVR) [17]. The results described in this chapter are published in a paper on the *International Journal of Quantum Information* [18].

6.1 The model

Our system consists of a quantum particle with mass M , interacting with a thermal bath which plays the role of environment. The dynamics of the particle is investigated by using the Caldeira-Leggett model [4]. In our analysis \hat{q} and \hat{p} are one-dimensional operators for position and momentum,

respectively. The unperturbed Hamiltonian of the system is

$$H_0 = \frac{\hat{p}^2}{2M} + \hat{V}_0(\hat{q}) \quad (6.1)$$

where

$$\hat{V}(\hat{q}) = \frac{M^2\omega_0^4}{64\Delta U}\hat{q}^4 - \frac{M\omega_0^4}{4}\hat{q}^2 - \epsilon\hat{q} \quad (6.2)$$

is the asymmetric bistable potential shown in Fig.6.1. Here, ϵ and ΔU are the asymmetry parameter and the barrier height, respectively, and ω_0 is the natural oscillation frequency. In our study we consider only 8 energy eigenstates. In Fig. 6.1 these energy eigenvalues are shown on the vertical axis. In the same figure, on the horizontal axis we indicate the 8 position eigenvalues, obtained by using the DVR-state $|Q_\mu\rangle$. The black circle marks the initial position of the particle, that is the system at $t = 0$ is in a state given by a proper linear combination of the 8 eigenstates $|q_\mu\rangle$ considered in our analysis. The curves shown in the figures are the eigenfunctions corresponding to the 8 energy eigenvalues. In order to describe the dynamics of the particle interacting with environment, we consider the following Hamiltonian where

$$\hat{H}_B = \sum_{j=1}^{\mathcal{N}} \frac{1}{2} \left[\frac{\hat{p}_j^2}{m_j} + m_j\omega_j^2 \left(\hat{x}_j - \frac{c_j}{m_j\omega_j^2} \hat{q} \right) \right] \quad (6.3)$$

is the Hamiltonian which describes the thermal reservoir and its interaction with the particle. As usual, the thermal bath is depicted by an ensemble of \mathcal{N} harmonic oscillators with spatial coordinate \hat{x}_j , momentum \hat{p}_j , mass m_j , and frequency ω_j . The coefficients c_j are the coupling constant between system and thermal bath. We note that, as $\mathcal{N} \rightarrow \infty$, from Eq. 6.3 a continuous spectral density is obtained. In our study we use the Ohmic spectral density characterized by an exponential cut-off ω_c

$$J(\omega) = \eta\omega e^{-\frac{\omega}{\omega_c}} \quad (6.4)$$

Here, $\eta = M\gamma$ with γ the strength of the coupling between system and heat bath. We note also that $\omega_c \gg \omega_0, \omega_j, \gamma$. Because of the bilinear coupling between the coordinate \hat{q} of the system and the coordinate \hat{x} of the thermal bath, this model is the quantum analogue of a classical system affected by a constant random force [19]. In the next two subsections we briefly summarize the mathematical approach used in this study.

6.1.1 The Feynmann-Vernon approach

In order to make our analysis independent on the properties of the heat bath, we trace out the degrees of freedom of the reservoir by using the

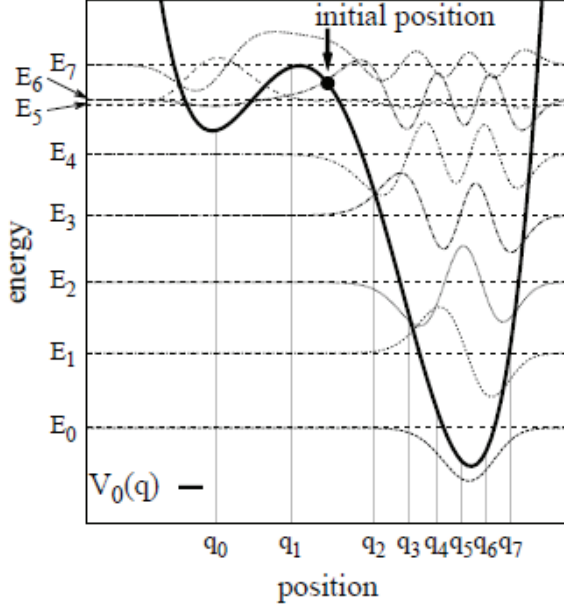


Figure 6.1: Potential profile $V_0(q)$ (see Eq.6.2) for $\Delta U = 3$ and $\epsilon = 5$. Energy level and corresponding eigenstate considered in our analysis are indicated by horizontal lines and curves, respectively. The energy eigenvalues are $E_0 = -2.01$, $E_1 = -0.92$, $E_2 = 0.11$, $E_3 = 1.08$, $E_4 = 1.97$, $E_5 = 2.69$, $E_6 = 2.76$, $E_7 = 3.27$. By using the DVR-states $|q_\mu\rangle$, eigenvalues of the position operator are obtained and shown on the horizontal axis: $q_0 = -4.17$, $q_1 = -1.38$, $q_2 = 1.71$, $q_3 = 3.02$, $q_4 = 4.05$, $q_5 = 4.97$, $q_6 = 5.86$, $q_7 = 6.81$. The initial position is $q_{start} = 0$ (black circle).

reduced density operator

$$\rho(q_f, q'_f; t) = \int dq_0 \int dq'_0 K(q_f, q'_f, t; q_0, q'_0, t_0) \rho(q_0, q'_0; t_0) \quad (6.5)$$

where the propagator K is given by

$$K(q_f, q'_f, t; q_0, q'_0, t_0) = \int_{q(t_0)=q_0}^{q(t)=q_f} \mathcal{D}q \int_{q'(t_0)=q'_0}^{q'(t)=q'_f} \mathcal{D}q' \mathcal{A}[q] \mathcal{A}^*[q'] \mathcal{F}_{FV}[q, q'] \quad (6.6)$$

and $\mathcal{A}[q] = e^{i\frac{S_S[q]}{\hbar}}$ with $S_S[q]$ being the classical action functional. In Eq. 6.6, $\mathcal{F}_{FV}[q, q'] = e^{-\frac{\phi_{FV}[q, q']}{\hbar}}$ is the Feynman-Vernon influence functional with the phase $\phi_{FV}[q, q']$ depending on the bath correlation function [19].

6.1.2 Discrete Variable Representation

By solving the eigenvalue equation connected with the Hamiltonian \hat{H}_0 (see Eq. 6.1), we get the energy eigenstates (see vertical axis in Fig. 6.2). Within the framework of the discrete variable representation (DVR) [17] it is possible to obtain the basis $|q_\mu\rangle$ of eigenstates of the position operator \hat{q} (see horizontal axis in Fig. 6.2). In this representation, applying the non-interacting cluster approximation (NICA), [3] we get the following master equation (ME)

$$\rho_{\mu\mu}(t) = \sum_{\nu=1}^N \int_{t_0}^t dt' \mathcal{H}_{\mu\nu}(t-t') \rho_{\nu\nu}(t'), \quad \mu = 1, \dots, N. \quad (6.7)$$

where N is the number of eigenstates and the kernel \mathcal{H} indicates the *cluster matrix*. [3] According to the path integral technique based on the Feynman-Vernon theory, using ME corresponds to take into account only the paths connecting diagonal elements of the reduced density matrix of the position operator \hat{q} [3]. Within NICA we neglect all intercluster interactions. We assume furthermore that the characteristic memory time τ_{mem} of the matrix elements of H in Eq. 6.7 is the smallest time scale of the problem (Markovian limit). By this assumption we obtain the following Markovian approximated master equation

$$\dot{\rho}_{\mu\mu}(t) = \sum_{\nu=1}^N \Gamma_{\mu\nu}(t) \rho_{\nu\nu}(t) \quad (6.8)$$

with the time-dependent rate coefficients

$$\Gamma_{\mu\nu}(t) = \int_0^\infty \mathcal{H}_{\mu\nu}(t, t-\tau). \quad (6.9)$$

Since the diagonal elements $\rho_{\mu\mu}(t)$ obey Eq. 6.8, the long-time dynamics is ruled by a single exponential decay. Thus, Eq. 6.8 is a set of coupled ordinary first-order differential equations, which can be decoupled via a diagonalization procedure. The diagonalized rate matrix reads

$$\sum_{k_1, k_2=1}^N (S^{-1})_{\mu k_1} \Gamma_{k_1 k_2} S_{k_2 \nu} = \Lambda_\mu \delta_{\mu\nu} \quad (6.10)$$

where $S_{\mu\nu}$ denotes the element of the transformation matrix and Λ_μ the eigenvalues of the rate matrix. The general solution of the Markov approximated ME is

$$\rho_{\mu\mu}(t) = \sum_{\nu, k=1}^N S_{\mu\nu} (S^{-1})_{\nu k} e^{\Lambda_\nu(t-t_0)} \rho_{kk}(t_0). \quad (6.11)$$

Because of the conservation probability, for the diagonal matrix elements holds

$$\Gamma_{\nu\nu}(t) = - \sum_{k \neq \nu} (t). \quad (6.12)$$

This condition implies that one eigenvalue equals zero, i.e. $\Lambda_1 = 0$. Therefore,

$$\rho_{\mu\mu}(t) = \rho_{\mu\mu}^{\infty} + \sum_{\nu=2}^N \sum_{k=1}^N S_{\mu\nu}(S^{-1})_{\mu k} e^{\Lambda_{\nu}(t-t_0)} \rho_{kk}(t_0) \quad (6.13)$$

with $\rho_{\mu\mu}^{\infty} = \sum_{k=1}^N S_{\mu,1}(S^{-1})_{1,k} \rho_{kk}(t_0)$ being the asymptotic population of the DVR-state $|q_{\mu}\rangle$. The rate which determines the dynamics over the largest time-scale is the *quantum relaxation rate*

$$\Gamma \equiv \min\{|\mathcal{R}(\Lambda_{\nu})|; \nu = 2, \dots, N\} \quad (6.14)$$

where Λ_{ν} 's are the eigenvalues of the rate matrix and $|\mathcal{R}(\Lambda_{\nu})|$ are the non-zero absolute values of the real part of Λ_{ν} . In the next section we focus our study on the medium-short time behavior of the system, using the largest Λ_{ν}^{-1} as timescale to analyze the non-equilibrium dynamics of the quantum particle in the presence of thermal fluctuations.

6.2 Results

In this section we study the time evolution of our quantum particle taking into account the 8 energy levels shown in Fig. 6.1. We restrict the study to the 8 lowest levels of the system, because we are interested in the dynamics of a particle that can not reach energy levels higher than the relative maximum of the potential. In particular, we intend to analyze the time behaviour of the populations for different values of the coupling strength, focusing on the time behaviour of the state $|q_0\rangle$ (left side well of the potential). By using the DVR-state $|q_{\mu}\rangle$, as initial condition for the particle we choose the non-equilibrium position $q_{start} = 0$. The corresponding state is given by

$$|q_{start}\rangle = c_1 |q_1\rangle + c_2 |q_2\rangle \quad (6.15)$$

with $c_1 = 0.745$ and $c_2 = 0.667$. By integrating Eq. 6.7 for different values of the parameter η , which represents the intensity of the environmental noise, for each eigenstate $|q_{\mu}\rangle$ we obtain the time behaviour of the corresponding population $\rho_{q_{\mu}} \equiv \rho_{\mu\mu}$ (see Fig. 6.2). Moreover, by a simple change of basis, we calculate the time evolution of the populations also in the energy representation (see Fig. 6.3). As one can see from Eqs. 6.8,6.9, for each value of η there are N relaxation times Λ_{μ}^{-1} . Here, we consider the maximum of

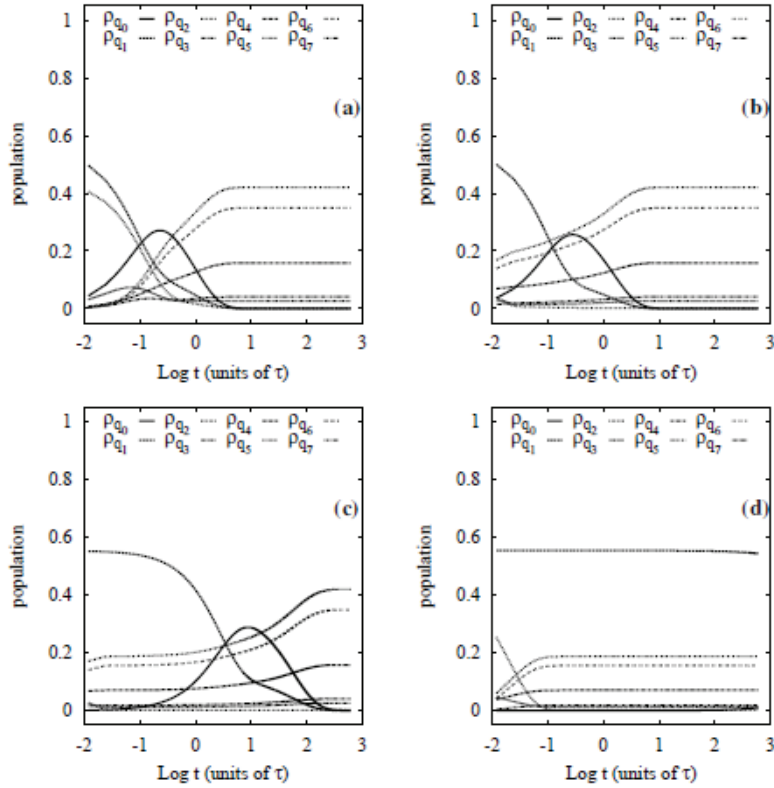


Figure 6.2: Time evolution of the populations in position representation for different values of coupling strength: a) $\eta = 0.01$, b) $\eta = 0.4$, c) $\eta = 1$ and d) $\eta = 2.8$.

these relaxation times, and note that this time increases rapidly for larger values of η . Therefore, to describe the time evolution of the system for different values of η , we choose as time scale τ the largest of the relaxation times obtained for $\eta = 0.01$ and calculate the evolution of the system for a maximum time $t = 600\tau$. This choice allows to follow the transient dynamics of the system for low and intermediate values of the coupling constant (see panels a, b, c in Figs. 6.2,6.3). For higher values of η the system can not reach the regime condition, because of the presence of relaxation times longer than the maximum time chosen to calculate the numerical solution (see panel d in Figs. 6.2,6.3). This delay in the system dynamics can be explained by the quantum Zeno effect, responsible for the suppression of the tunnel effect. Moreover, we observe in Fig. 6.2 a nonmonotonic behaviour of the population ρ_{q_0} as a function of the time. Finally, as a consequence of the quantum Zeno effect, the eigenstate $|q_0\rangle$ can be maximally populated at different times varying the coupling strength and, therefore, the value of η . This could be useful in view of placing a quantum particle in a given

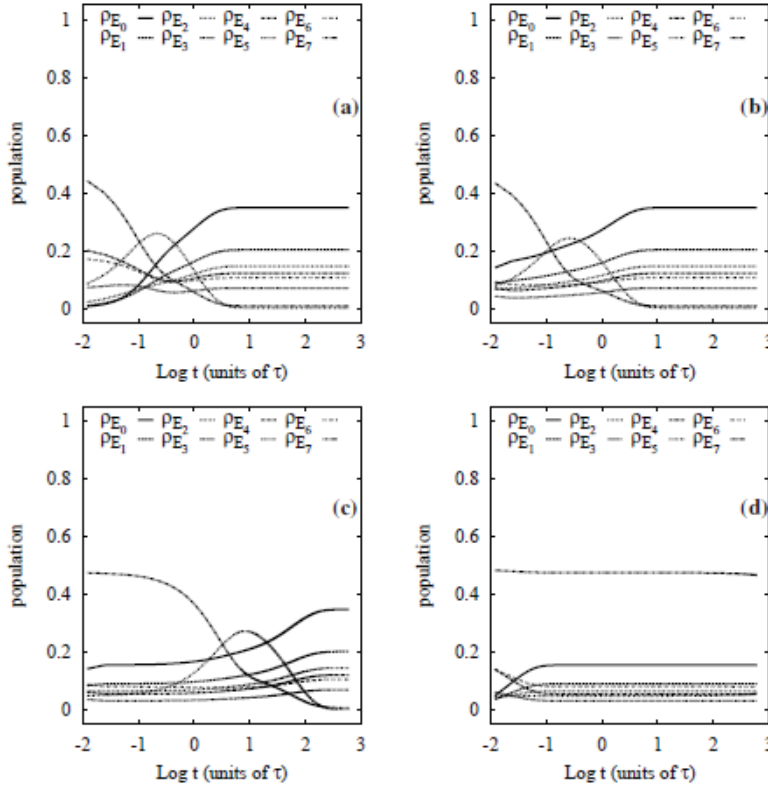


Figure 6.3: Time evolution of the populations in energy representation for different values of coupling strength: a) $\eta = 0.01$, b) $\eta = 0.4$, c) $\eta = 1$ and d) $\eta = 2.8$.

position at a fixed time.

6.3 Conclusions

In this work we analyze the dynamics of a quantum particle subject to an asymmetric bistable potential and interacting with noisy environment. The study is performed exploiting the approach of the Feynman-Vernon functional [16] within the framework of the discrete variable representation. [3, 20] By using the Caldeira-Leggett model [4], we describe the transient dynamics of the system for different values of the coupling strength between the particle and the noisy environment, modelled as a thermal bath. Due to the quantum Zeno effect, responsible for the suppression of the tunnel effect, a delayed dynamics of the system is observed for higher values of the coupling strength. We find also that the metastable state inside the left side well of the potential can be populated at different times varying the value

of the coupling strength.

Bibliography

- [1] Yu. Pashkin Y. Nakamura and J. S. Tsai. *Nature*, **398**:786, 1999.
- [2] Heer R. Strasser G. Rakoczy, D. and Smoliner J. *Physica E*, **16**:129, 2003.
- [3] M. Hanggi P. Thorwart, M. Grifoni. *Annals of physics*, **293**:15, 2001.
- [4] A. O. Caldeira and A. J. Leggett. *Phys. Rev. Lett.*, **46**:211, 1981.
- [5] S. Dorsey A. T. Fisher M. Garg A. Leggett, A. J. Chakravarty and W. Zwerger. *Rev. Mod. Phys.*, **59**:1, 1987.
- [6] M. Grifoni and P. Hanggi. *phys. Rep.*, **304**:229, 1998.
- [7] A. J. Leggett. *Phys. Rev. B*, **30**:1208, 1984.
- [8] Chung-Hsien Chou, Ting Yu, and B. L. Hu. *Phys. Rev. E*, **77**:011112, 2008.
- [9] M. Rosenau da Costa, A. O. Caldeira, S. M. Dutra, and H. Westfahl. *Phys. Rev. A*, **61**:022107, 2000.
- [10] N. V. Prokofev and P. C. E. Stamp. *Rep. Prog. Phys.*, **63**:669726, 2000.
- [11] Heinz-Peter Breuer and Francesco Petruccione. *The Theory of Open Quantum Systems*. Oxford University Press, USA, 2007.
- [12] Patel V. Chen W. Tolpygo S. K. Friedman, J. R. and J. E. Lukens. *Nature*, **406**:43, 2000.
- [13] F. Grossmann, T. Dittrich, P. Jung, and P. Hänggi. *Phys. Rev. Lett.*, **67**:516, 1991.
- [14] R. Löfstedt and S. N. Coppersmith. *Phys. Rev. Lett.*, **72**:1947, 1994.
- [15] Lorenza Viola, Emanuel Knill, and Seth Lloyd. *Phys. Rev. Lett.*, **82**:2417, 1999.
- [16] R.P Feynman and F.L Vernon Jr. *Annals of Physics*, **24**:118, 1963.
- [17] G. G. Engerholm D. O. Harris and W. D. Gwinn. *J. Chem. Phys.*, **43**:1515, 1965.

- [18] P. Caldara, A. La Cognata, D. Valenti, B. Spagnolo, M. Berritta, E. Paladino, and G. Falci. *International Journal of Quantum Information*, **09**:119, 2011.
- [19] Ulrich Weiss. *Quantum Dissipative Systems (Series in Modern Condensed Matter Physics)*. World Scientific Publishing Company, 2008.
- [20] David O. Harris, Gail G. Engerholm, and William D. Gwinn. *The Journal of Chemical Physics*, **43**:1515, 1965.

Chapter 7

Chiral quasiparticles in an environment

In this chapter, that collect the results of a paper published on *Physica E* [1], we study the dynamics of a Weyl quasi-particle coupled linearly to a bosonic environment. This model describes the dynamics of quasi-particles in graphene sheets, in the presence of noisy control, simulating external electromagnetic quantum field. Wave packets shows Spin Separation and Zitterbewegung [2] at mesoscopic scales, which are suppressed in a peculiar way by quantum fluctuations of the environment. Here we present some exact result.

7.1 Introduction

The recent discovery that individual graphene sheets can be isolated [3] has stimulated a renewed interest in carbon-based materials. Indeed graphene has distinguished mechanical and electrical properties, as the large mobility, which makes it attractive for applications in nanoelectronics. Graphene is two-dimensional carbon arranged in a honeycomb lattice. Due to the symmetries of the lattice, the (nonrelativistic) "effective mass" Hamiltonian for Quasi-Particles (QP) close to the symmetry (Dirac) points of the Brillouin zone [4, 5] is formally identical to the relativistic Hamiltonian for Quantum Electrodynamics in 2 dimensions. In a single valley QP's have a gapless linear energy-momentum dispersion and their dynamics is described by the quantum mechanical Weyl Hamiltonian for massless Dirac fermions. For a graphene sheet lying in the $x - y$ plane, and subject to a uniform electric field in the y direction $\mathbf{E} = E(t) \mathbf{e}_y$ the Hamiltonian reads

$$\mathcal{H}_W = v \hat{\mathbf{p}} \cdot \boldsymbol{\sigma} + eE(t) \hat{y} = v \left[\hat{\mathbf{p}} - \frac{e}{c} A(t) \mathbf{e}_y \right] \cdot \boldsymbol{\sigma} \quad (7.1)$$

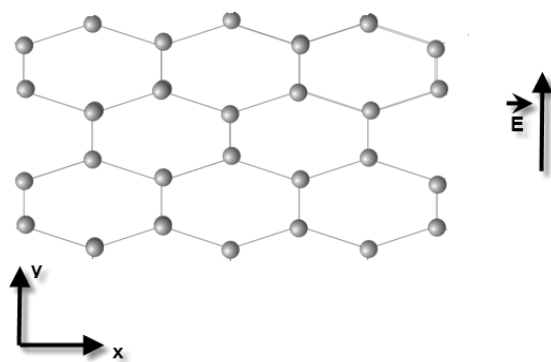


Figure 7.1: Honeycomb lattice of single graphene sheet in electric field \mathbf{E} . The electric field simulates a control port, with a deterministic time-dependent driving part, and a quantum fluctuating part.

where \hat{y} is the operator of the y-component of the QP and $E(t) = \frac{1}{c} \frac{\partial A}{\partial t}$, $A = A(t)e_y$ being the vector potential in absence of magnetic field. Here $\boldsymbol{\sigma}$ is a pseudospin operator, the eigenstates of σ_z corresponding to the QP tight-binding wavefunctions on each sublattice of the honeycomb structure (the physical spin is conserved and we ignore it), and v is the Fermi velocity, playing the role of the speed of light in the relativistic version. QP's are chiral due to spin-momentum coupling: the hamiltonian expressed in terms of the vector potential shows that quantum control of the pseudospin dynamics is possible via electric fields coupling with a QP coordinate. Therefore phototransport could be in principle modulated using quantum control protocols typical of the quantum optics realm [6]. This roadmap naturally extends to microscopic degrees of freedom one of the most fascinating experimental breakthroughs of the recent past, namely the observation of coherent pseudospin dynamics in nanodevices based on superconductors [7] and semiconductors.

7.1.1 Spin separation and Zitterbewegung

The dynamics of isolated wave-packets of Weyl QP's shows many distinct features. Contrary to massive non relativistic particles, wave-packets of Weyl QP's from a single helicity branch experience a very weak breadth, due to the linear dispersion implying that each component travels at the same velocity v . On the other hand new phenomena appear for superposition of states from different branches. Since the direction of the velocity depends on the helicity such a wave-packet will separate in two opposite moving components (SS). Interference between them gives rise to ZB. This features are usually discussed in the Heisenberg picture [2] in which the equation of motion for the speed operator are:

$$\hat{v} = i[\hat{r}, H] = v\hat{\boldsymbol{\sigma}} \quad (7.2)$$

and for instance ZB is associated to a part $\mathbf{r}_{\mathbf{ZB}}(\mathbf{t})$ of the position operator oscillating in time with angular frequency $\Omega(\mathbf{k}) = 2\mathbf{v}|\mathbf{k}|$, the energy splitting of two states $|\mathbf{k}\sigma_{\mathbf{k}}\rangle$ with the same \mathbf{k} and opposite helicity. Instead we use the Schrödinger picture, which is conveniently generalized to an open system. For the representation we use the *chiral basis* of the eigenstates of Eq.(7.1). The density matrix in the laboratory frame is given by

$$\zeta^L(t) = \sum_{\mathbf{k}\sigma\mathbf{k}'\sigma'} |\mathbf{k}\sigma_{\mathbf{k}}\rangle\langle\mathbf{k}'\sigma'_{\mathbf{k}}| \zeta_{\mathbf{k}\sigma\mathbf{k}'\sigma'}^L(\mathbf{0}) e^{-i\mathbf{v}(|\mathbf{k}|\sigma - |\mathbf{k}'|\sigma')\mathbf{t}}$$

In order to calculate averages of interest we introduce the operators $P_{\sigma} = \sum_{\mathbf{k}\sigma} |\mathbf{k}\sigma_{\mathbf{k}}\rangle\langle\mathbf{k}\sigma_{\mathbf{k}}|$ projecting on a well defined component ($\sigma = \pm 1$) of the

helicity $\sigma_{\mathbf{k}}$. Any operator \hat{A} can be decomposed in "diagonal" parts $P_\sigma \hat{A} P_\sigma$ and "off diagonal" parts $P_\sigma \hat{A} P_{-\sigma}$ these latter describing interference. In particular letting $\hat{A} = \delta(\hat{r}(t) - \mathbf{r})$ the average of the diagonal parts represent the probability densities $\varrho^\sigma(\mathbf{r}, \mathbf{t})$ of two spin-separated wave-packets, whereas the average of the interference terms yields $\varrho^{ZB}(\mathbf{r}, \mathbf{t})$, which is a spatial modulation between the two wave-packets above, oscillating with time. The associated centroid is the average of the oscillating part of the position operator

$$\langle \mathbf{r}_{ZB}(\mathbf{t}) \rangle = \sum_{\mathbf{k}\sigma} \mathbf{A}_{\sigma, -\sigma}(\mathbf{k}) \zeta_{\mathbf{k}-\sigma \mathbf{k}\sigma}^L(\mathbf{t})$$

Here $\sum_{\mathbf{k}} \rightarrow \int \frac{d\mathbf{k}}{2\pi}$ in the continuum limit (not always specified hereafter). The connection in k-space associated to the chiral basis appears $\mathbf{A}_{\sigma\sigma'}(\mathbf{k}) = \mathbf{i}\langle \sigma_{\mathbf{k}} | \nabla_{\mathbf{k}} \sigma'_{\mathbf{k}} \rangle = \sigma\sigma' \mathbf{t}_{\mathbf{k}} / (2|\mathbf{k}|)$, where the unitary vector $\mathbf{t}_{\mathbf{k}}$ is such that $\{\mathbf{k}/|\mathbf{k}|, \mathbf{t}_{\mathbf{k}}, \mathbf{z}\}$ is a left-handed reference frame for the momentum space. Notice that the density matrix enters with elements diagonal in \mathbf{k} and off diagonal in the pseudospin index σ .

7.2 Model.

The control of coherent dynamics opens ports to noise. In discussing the effect of the environment we recall that for a massive particle with ohmic damping [8] the wave-packet breadth grows only logarithmically on time, reflecting decoherence due to the environment measuring the particle position \mathbf{r} , while for finite temperatures diffusive behavior is found in the long time limit. We address the problem of noise by coupling Weyl QP's to an environment. To this end we supplement the Weyl hamiltonian with a part describing a set of quantum harmonic oscillators coupled linearly to the coordinate operator \hat{y} of the QP, as in the Caldeira-Leggett model [9, 10]

$$\begin{aligned} \delta\mathcal{H} = & -\hat{y} \sum_{\alpha} C_{\alpha} x_{\alpha} + \sum_{\alpha} \left(\frac{p_{\alpha}^2}{2m_{\alpha}} + \frac{m_{\alpha}\omega_{\alpha}^2}{2} \right) x_{\alpha}^2 \\ & + \hat{y}^2 \sum_{\alpha} \frac{C_{\alpha}^2}{2m_{\alpha}\omega_{\alpha}^2} \end{aligned} \quad (7.3)$$

The state of the system described by this hamiltonian could be described by density matrix $W(t)$; We are interested only on the dynamics of quasi-particle. To this end we consider the Reduced Density Matrix (RDM) obtained tracing over the environment degree of freedom the total density matrix: $\hat{\zeta}^L(t) = \text{Tr}_{\alpha}[W(t)]$ The relevant information on the environment is provided by the spectral density associated to X , given by $J_X(\omega) = \pi \sum_{\alpha} \frac{c_{\alpha}^2}{2m_{\alpha}\omega_{\alpha}} \delta(\omega - \omega_{\alpha})$ [11, 10].

7.2.1 Dynamics in the QP-supported frame

In order to study the dynamics we first rescale the environment coordinates and momenta $y'_\alpha \rightarrow c_\alpha y_\alpha / m_\alpha \omega_\alpha^2$ and $p'_\alpha \rightarrow m_\alpha \omega_\alpha^2 p_\alpha / c_\alpha$. Then we perform on the resulting Hamiltonian \mathcal{H}' a (polaron) transformation, represented by the unitary operator $U = \exp(-i\hat{y} \sum_\alpha \hat{p}_\alpha)$ which shifts the positions to y_α , now referred to the QP position. The effective Hamiltonian in this QP-supported frame, reads

$$\begin{aligned} \tilde{\mathcal{H}}(\hat{\mathbf{p}}) = U \mathcal{H}' U^\dagger &= v \mathbf{p} \cdot \tilde{\boldsymbol{\sigma}} - \sigma_y \mathbf{v} \sum_\alpha \mathbf{p}_\alpha + \\ &\sum_\alpha \left(\frac{p_\alpha^2}{2\mu_\alpha} + \frac{1}{2} \mu_\alpha \omega_\alpha^2 y_\alpha^2 \right) \end{aligned} \quad (7.4)$$

Therefore the coupling of the QP position \mathbf{r} with the environmental \hat{X} in Eq.(7.3) is gauged away in favor of a spin-boson like coupling of the pseudo-spin with environmental momenta. The effects of the transformation are fully defined by specifying the new spectral density

$$J_P(\omega) = \pi \sum_\alpha \frac{v^2}{2\mu_\alpha \omega_\alpha} \delta(\omega - \omega_\alpha) = \frac{v^2}{\omega^2} J_X(\omega) \quad (7.5)$$

Notice that the operator $\hat{\mathbf{p}}$, which is still the conjugate of $\hat{\mathbf{r}}$, is physically the total momentum of the system and it is conserved. Therefore the dynamics is determined by the set of Hamiltonians $\mathcal{H}_{\mathbf{K}} = \tilde{\mathcal{H}}(\mathbf{K})$ depending parametrically on the eigenvalue \mathbf{K} of \mathbf{p} . Each $\tilde{\mathcal{H}}_{\mathbf{K}}$ acts on a spin-boson system only, and the problem is mapped in a spin-boson model, with *conditional* dynamics. The evolution operator determined by the Hamiltonian (7.4) is given by $\mathcal{U}(t) = \sum_{\mathbf{K}} |\mathbf{K}\rangle \langle \mathbf{K}| \otimes e^{-i\mathcal{H}_{\mathbf{K}} t}$ and allows to express the simplified dynamics of the full density matrix $\mathcal{W}(t) = U_T W(t) U_T^\dagger$ in the QP-supported frame. In view of the simplifications brought in by the conditional dynamics it is convenient to eliminate the microscopic degrees of freedom of the *modified* environment, labeled by $\tilde{\alpha}$, to obtain

$$\hat{\zeta}(t) = \text{Tr}_{\tilde{\alpha}}[\mathcal{W}(t)] = \sum_{\mathbf{K}\sigma} |\mathbf{K}\sigma_{\mathbf{K}}\rangle \zeta_{\sigma\sigma'}^{(\mathbf{K},\mathbf{K}')} (t) \langle \mathbf{K}'\sigma'_{\mathbf{K}'}| \quad (7.6)$$

This RDM describes the *dressed* QP (polaron). It can be decomposed in a set of 2×2 operators $\zeta^{(\mathbf{K},\mathbf{K}')}$, each acting in a sector $(\mathbf{K}, \mathbf{K}')$, and evolving independently. They are structurally reminiscent to the RDM of the spin-boson model, however the parametric dependence on $(\mathbf{K}, \mathbf{K}')$ has non trivial features: for $\mathbf{K} \neq \mathbf{K}'$ the exact dynamics of $\zeta^{(\mathbf{K},\mathbf{K}')}$ is deformed [1], and it is not trace preserving.

Since the unitary transformation to the QP-supported frame preserves both the QP coordinate $\hat{\mathbf{r}}$ and the pseudo-spin, averages as the spin resolved densities $\varrho^\sigma(\mathbf{r}, \mathbf{t})$ and $\varrho^{ZB}(\mathbf{r}, \mathbf{t})$ can be calculated directly in the QP-supported frame. In particular we will evaluate

$$\begin{aligned}\varrho^\sigma(\mathbf{r}, \mathbf{t}) &= \sum_{\mathbf{K}\mathbf{K}'} \text{Tr}[\langle \mathbf{K} | \langle \mathbf{K}' | \zeta_{\sigma\sigma}^{(\mathbf{K}', \mathbf{K})}(t) \delta(\hat{\mathbf{r}} - \mathbf{r})] \\ &= \sum_{\mathbf{K}\mathbf{K}'} e^{i(\mathbf{k}-\mathbf{k}')\cdot\mathbf{r}} \langle \sigma_{\mathbf{K}} \rangle \sigma_{\mathbf{K}'} \zeta_{\sigma\sigma}^{(\mathbf{K}', \mathbf{K})}(t)\end{aligned}\quad (7.7)$$

$$\langle \mathbf{r}_{ZB}(\mathbf{t}) \rangle = - \sum_{\mathbf{K}} \frac{\mathbf{t}_{\mathbf{K}}}{|\mathbf{K}|} \Re[\zeta_{+-}^{(\mathbf{K}, \mathbf{K})}(\mathbf{t})] \quad (7.8)$$

In order to proceed we define sectors labeled by $(\mathbf{K}, \mathbf{K}')$ and projected operators, for instance $\hat{\mathcal{W}}^{(\mathbf{K}, \mathbf{K}')} = \langle \mathbf{K} | \hat{\mathcal{W}} | \mathbf{K}' \rangle$. Momentum conservation ensures that they evolve independently, undergoing a deformed dynamics

$$\hat{\mathcal{W}}^{(\mathbf{K}, \mathbf{K}')}(\mathbf{t}) = e^{-i\mathcal{H}_{\mathbf{K}}\mathbf{t}} \hat{\mathcal{W}}^{(\mathbf{K}, \mathbf{K}')}(\mathbf{0}) e^{-i\mathcal{H}_{\mathbf{K}'}\mathbf{t}}$$

7.2.2 Master equation.

Tracing out the environment one obtains the reduced operators $\tilde{\zeta}^{(\mathbf{K}, \mathbf{K}')}$ of the pseudo-spin Liouville space, appearing in Eq.(7.6). They solve an exact equation which can be written in a deformed interaction picture [1] as

$$\begin{aligned}\tilde{\zeta}^{(\mathbf{K}\mathbf{K}')}(\mathbf{t} + \Delta\mathbf{t}) - \tilde{\zeta}^{(\mathbf{K}\mathbf{K}')}(\mathbf{t}) &= \\ &- \int_t^{t+\Delta\mathbf{t}} dt' \int_t^{t'} dt'' \text{Tr}_{\bar{\alpha}} \left\{ [\tilde{\mathcal{H}}_1(t'), [\tilde{\mathcal{H}}_1(t''), \tilde{\mathcal{W}}^{(\mathbf{K}\mathbf{K}')}(\mathbf{t}'')]']' \right\}\end{aligned}$$

where $\Delta\mathbf{t}$ is a coarse graining time. Here $\tilde{\mathcal{H}}_1(\mathbf{t})$ ($\tilde{\mathcal{H}}_1'(\mathbf{t})$) is the QP-environment coupling of Eq.(7.4) in the interaction picture relative to the parameter \mathbf{K} (\mathbf{K}'). Primed commutator, reflecting deformation of the dynamics, are defined as

$$[\tilde{\mathcal{H}}_1(\mathbf{t}), \tilde{\mathcal{X}}]' = \tilde{\mathcal{H}}_1(\mathbf{t}) \tilde{\mathcal{X}} - \tilde{\mathcal{X}} \tilde{\mathcal{H}}_1'(\mathbf{t}) \quad (7.9)$$

At this stage an approximate closed equation for $\tilde{\zeta}^{(\mathbf{K}\mathbf{K}')}(\mathbf{t})$ can be obtained by first assuming factorized initial $\tilde{\mathcal{W}}^{(\mathbf{K}\mathbf{K}')}(\mathbf{0}) = \tilde{\zeta}^{(\mathbf{K}\mathbf{K}')} \otimes w_{eq}$, where w_{eq} is the equilibrium density matrix of the environment, and then following the same lines leading to the Bloch-Redfield equation [6], which govern the dynamics in the sector $\mathbf{K} = \mathbf{K}'$.

Deformation of the dynamics implies that, besides the splitting of the helicity bands $\approx 2v|\mathbf{Q}|$, where $\mathbf{Q} = (\mathbf{K} + \mathbf{K}')/2$, a new energy scale enters the problem, related to $\mathbf{q} = \mathbf{K} - \mathbf{K}'$. For a wave-packet with a dispersion $\sim \Delta$ in momentum space, the variable q may have values ranging from

Δ to zero, therefore the associated energy scale may vanish. As a consequence there will always be sectors with non-secular deformed dynamics. This structure, becomes transparent for noise with white power spectrum $J_P(\omega) \coth(\beta\omega/2) \rightarrow 2\Gamma$. In this limit the problem has an exact solution, which is very useful to capture the essential consequences of the deformed dynamics. In this case the exact master equation in the Schrödinger picture for white noise becomes

$$\begin{aligned} \partial_t \zeta^{(\mathbf{K}\mathbf{K}')} (t) &= \mathcal{L}(\mathbf{Q}, \mathbf{q}) \cdot \hat{\zeta}^{(\mathbf{K}\mathbf{K}')} (\mathbf{t}) \\ \mathcal{L}(\mathbf{Q}, \mathbf{q}) \hat{\zeta} &= -i\mathbf{v} [\mathbf{Q} \cdot \tilde{\sigma}, \hat{\zeta}] - i\frac{\mathbf{v}}{2} [\mathbf{q} \cdot \tilde{\sigma}, \hat{\zeta}]_+ \\ &\quad - \frac{\Gamma}{2} [\hat{\zeta} - \sigma_y \hat{\zeta}(t) \sigma_y] \end{aligned} \quad (7.10)$$

Notice here the presence of the anticommutator term containing \mathbf{q} . This term disappears for operators in diagonal sectors and Eq.(7.10) reduces to a standard Lindblad equation for a two-state atom with Bohr splitting $2v|\mathbf{Q}|$.

7.2.3 One dimensional wavepacket

We perform our calculation of dynamics of wave packets only in the case of one dimensional wave packets. They are, of the form:

$$g(\mathbf{k}) = \frac{\mathbf{A}}{(2\pi\sigma_{\mathbf{k}_x}^2)^{\frac{1}{4}}} e^{-\left(\frac{\mathbf{k}_x - \mathbf{k}_{x0}}{4\sigma_{\mathbf{k}_x}^2}\right)^2} \quad (7.11)$$

In order to understand motion of a one-dimensional wave-packet in an arbitrary direction \mathbf{n} , we now specify to this case the exact Master Equation for white noise, Eq.(7.10). A convenient matrix form is obtained using the decomposition $\zeta^{(\mathbf{K}\mathbf{K}')} (t) = \frac{1}{2} \sum_{i=0}^4 R_i(t) \sigma_i$, where $\{\sigma_i\} = \{\mathbb{1}, \sigma_{\mathbf{n}}, \sigma_{\mathbf{t}}, \sigma_{\mathbf{z}}\}$ is a basis of the pseudo-spin Liouville space. For each sector the master equation reads $\dot{\mathbf{R}} = \mathcal{L} \mathbf{R}$ where

$$\mathcal{L} \equiv \begin{pmatrix} 0 & -ivq & 0 & 0 \\ -ivq_n & -\Gamma c^2 & \Gamma sc & 0 \\ 0 & \Gamma sc & -\Gamma s^2 & -2vQ \\ 0 & 0 & 2vQ & -\Gamma \end{pmatrix} \quad (7.12)$$

Notice that $R_0 = \text{Tr}[\zeta^{(\mathbf{K}\mathbf{K}')}]$ and $R_1 = \text{Tr}[\zeta^{(\mathbf{K}\mathbf{K}')} \sigma_{\mathbf{n}}]$ enter the spin separated densities, whereas R_2 and R_3 determine ϱ_{ZB} . We concentrate on the explicit calculation of the dynamics of one dimensional wave packet ($Q_t, q_t = 0$). In this case it is readily verified that for longitudinal noise ($\phi_{\mathbf{n}} = \pi/2$) the result agrees with the exact solution of sec. 7.3.1. Indeed noise does not enter the components R_0 and R_1 : the two imaginary eigenvalues $\pm ivq$ of \mathcal{L} lead to SS as for the isolated QP. The other two eigenvalues, given by

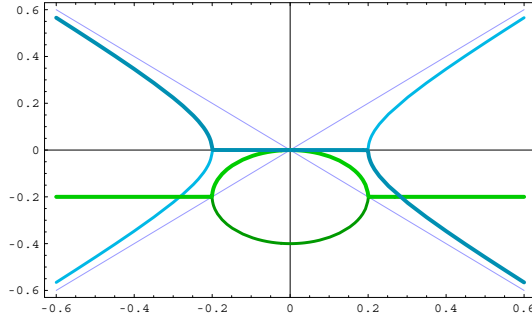


Figure 7.2: Schematic plot of the behavior of the eigenvalues $z_{0,1}$ for SS ($z_{2,3}$ for ZB) as given by Eq.(7.15) as a function of vq (vQ). Imaginary parts (blue) vanish in the overdamped regime $2vq < \Gamma$ ($4vQ < \Gamma$) whereas in the opposite limit they behave as $\sim \pm ivq$ ($\sim \pm ivQ$). In this limit real parts (green) are given by $(\Gamma/2)$ whereas in the overdamped limit, $\Re z \sim 0, \Gamma$, the zero value being associated to the Zeno effect.

$-\Gamma \pm 2ivQ$ yield damped ZB oscillations at the band splitting frequency, decaying at a rate Γ , which agrees with the proper limit of Eq.(7.14).

Instead for generic \mathbf{n} all four eigenvalues have a non vanishing real part. This indicates that both SS and ZB have components $\hat{\zeta}^{(\mathbf{K}, \mathbf{K}')}$ which are damped or even overdamped.

7.3 Results

7.3.1 Exact solution for longitudinal noise

If we set initially $K_x = 0$ the dynamics in each sector (K, K') involves the Hamiltonians of the form $\mathcal{H}_K = \mathcal{H}_{K\mathbf{e}_y}$. The helicity coincides with σ_y and it is conserved, since $[\mathcal{H}_K, \sigma_y] = 0$. Therefore eigenstates of the helicity are unaffected by longitudinal noise. Dynamics in each sector is given by

$$\zeta_{\sigma\sigma'}^{(KK')}(t) = \langle \sigma_y | \text{Tr}_{\bar{\alpha}} [e^{-i\mathcal{H}_K t} \mathcal{W}^{(KK')}(0) e^{i\mathcal{H}_{K'} t}] | \sigma_y' \rangle$$

Since it acts on its eigenstates the spin operator σ_y contained in each Hamiltonian can be replaced by a number, $\mathcal{H}_K |\sigma_y\rangle = (ivK\sigma + \mathcal{H}_\sigma) |\sigma_y\rangle$, where \mathcal{H}_σ is the Hamiltonian (7.4) for $\mathbf{K} = \mathbf{0}$ and for $\sigma_x \rightarrow \sigma = \pm 1$. Using the cyclic property of the partial trace we obtain

$$\zeta_{\sigma\sigma'}^{(KK')}(t) = e^{-i(K\sigma - K'\sigma')vt} \text{Tr}_{\bar{\alpha}} [\mathcal{W}^{(KK')}(0) e^{i\mathcal{H}_{\sigma'} t} e^{-i\mathcal{H}_\sigma t}] \quad (7.13)$$

We see that for diagonal elements the effect of the environment cancels, expressing helicity conservation. As a consequence spin resolved probability

densities $\rho_\sigma(\mathbf{r}, \mathbf{t})$ evolve as in absence of the environment, fully displaying spin separation.

Instead off diagonal elements are affected by the presence of the environment. Assuming factorized initial conditions the partial trace for $\sigma' = -\sigma$ can be written as

$$\text{Tr}_{\tilde{\alpha}}[\cdot] = \zeta_{\sigma-\sigma'}^{(KK')}(0) e^{-D(t)}$$

where $D(t)$ is a decay factor describing pure dephasing. Therefore longitudinal noise determines a suppression of interference effects in a superpositions of spin states and of ZB oscillations. For an oscillator environment one finds explicitly

$$D(t) = \int_0^\infty \frac{d\omega}{\pi} J_P(\omega) \coth \frac{\beta\omega}{2} \frac{1 - \cos \omega t}{\omega^2} \quad (7.14)$$

for an arbitrary environment spectral density.

7.3.2 Transverse white noise

If noise is transverse to the motion, $\mathbf{n} \equiv \mathbf{x}$, the Lindblad operator Eq.(7.12) is again reducible, the eigenvalues being

$$\begin{aligned} z_{0,1} &= -\frac{\Gamma}{2} \pm \frac{1}{2} \sqrt{\Gamma^2 - (2vq)^2} \\ z_{2,3} &= -\frac{\Gamma}{2} \pm \frac{1}{2} \sqrt{\Gamma^2 - (4vQ)^2} \end{aligned} \quad (7.15)$$

where $z_{0,1}$ enter the SS dynamics and $z_{0,1}$ determine ZB. The common feature of both pairs is that for increasing Γ they exhibit a crossover from an “underdamped” (secular) regime, where $\Im z_i \neq 0$, to an “overdamped” (non secular) regime where eigenvalues are real and negative (see Fig.7.2). Notice that for large Γ two of the four real eigenvalues vanish as $z \propto v^2/\Gamma$, and the corresponding dynamics is “frozen”. This is a manifestation of the Zeno effect determined by the continuous quantum measurement of the particle by the noisy field. The fact that sectors such that $\hat{\zeta}^{(\mathbf{K}, \mathbf{K}')}$ has Zeno-like eigenvalues exist, means that there may be overdamped modes of the wave-packet motion. The consequences are apparent in the behavior of SS, shown in Fig. 7.3, where we consider a gaussian wave-packet with initial width Δ in the distribution of K_x . Spin-resolved marginal probability densities are given by the simplified expression

$$\varrho_{\mathbf{x}}^\sigma(y, t) = \int \frac{dq}{2\pi} e^{-\frac{q^2}{8\Delta^2}} \chi_{\sigma\sigma}(q, t) e^{iqy} \quad (7.16)$$

where the variable Q has been integrated out. Modes corresponding to $q < \Gamma/(2v)$ are overdamped, therefore we expect a strong noise regime ($\Delta < \Gamma/v$) where all modes are overdamped, whereas only part of them are

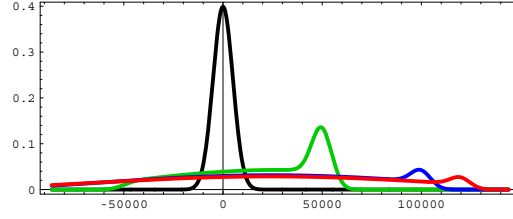


Figure 7.3: Marginal probability density $\rho_{\mathbf{x}}(x, t)$ for a 1D-wavepacket of well defined chirality. Here y is expressed in units of the lattice distance a and per $t = 0, 5, 10, 12$ in units of $10^4 a/v$. For $\Gamma/\Delta = 0.5$ (upper panel) the coherent peak and the incoherent tail are shown. For $\Gamma/\Delta = 2$ (lower panel) the incoherent peak is frozen close to the origin (notice the different spatial scale of the two figures).

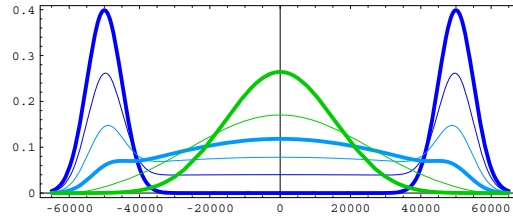


Figure 7.4: Marginal probability density $\rho_{\mathbf{x}}(x, t)$ for $t = 5 \cdot 10^4 a/v$, for a superposition of chirality states. Curves for $\Gamma/\Delta = 0, 0.2, 0.5, 1$ (blue) show SS. For $\Gamma/\Delta = 2, 5$ (green) SS is suppressed.

in the weak noise regime ($\Delta > \Gamma/v$). The dynamics of a wave-packet prepared in an eigenstate of chirality is illustrated in Fig. 7.3. In the weak noise regime (upper panel) wave-packets show a coherent component moving with constant velocity ($\pm v$) which disappears in a time $t \sim 1/\Gamma$. They leave behind an inelastic tail, due to the presence of overdamped modes. For larger Γ the inelastic processes prevail, all the modes are overdamped (Fig. 7.3, lower panel) and the peak represents an incoherent mixture of both chirality eigenstates. Wave-packets prepared in a superposition of eigenstates of the chirality are shown in Fig. 7.4 at a fixed time. In the weak noise regime they show SS, the two separated coherent peaks keeping their initial width, independently of Γ . For strong noise spin-separation is suppressed and the wave-packet shows a single incoherent peak “frozen” at the initial position. ZB oscillations are derived starting from the eigenvectors corresponding to the second pair of eigenvalues Eq.(7.15). In particular the ZB part of the position operator Eq.(7.7) is given, for a gaussian wave-packet and suitable

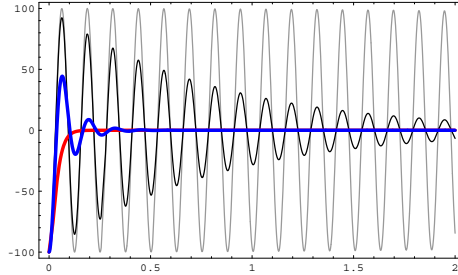


Figure 7.5: ZB component of the average position $\langle y(t) \rangle_{ZB}$ vs. time ($10^4 a/v$ units) for transverse white noise. Here a superposition of chirality states with dispersion $\Delta = 10^{-4}/a$ about $K_0 = 50\Delta$. Weak noise $\Gamma < \Delta$ has no effect on the signal (grey curve) whereas for larger values $\Gamma/(4vK_0) = 0.025, 0.25, 1$ $\langle y(t) \rangle_{ZB}$ decays exponentially (black) and eventually reaches the overdamped regime (red).

initial conditions, by the simple form

$$\langle y_{ZB}(t) \rangle = e^{-\frac{\Gamma}{2}t} \int \frac{dK}{2K} \frac{e^{-\frac{K^2}{2\Delta^2}}}{\sqrt{2\pi\Delta}} \frac{z_3 e^{i\omega t} - z_2 e^{-i\omega t}}{z_3 - z_2}$$

where $\omega = \sqrt{\Gamma^2 - (4vK)^2}$ (Fig. 7.5). In the weak damping regime $\Gamma < 4vQ$, oscillation disappear only for times $t > 2/\Gamma$, more slowly than for longitudinal noise. Instead small values of $|Q|$ determine overdamped modes in ZB.

We notice that the qualitative effect on SS and ZB of transverse and longitudinal noise is reversed: the former determines strong SS suppression, while the latter produces stronger dephasing of ZB oscillations. This is a consequence of the anisotropic coupling of noise in $\delta\mathcal{H}$, Eq.(7.3). It is related to the conservation of σ_z and it is reminiscent to the properties of certain nanodevices for quantum computation of exhibiting optimal operating points. On this basis we may argue that the same conclusions hold for general spectral density $J_P(\omega)$ of the environment.

Finally, since ZB oscillations are overdamped only if $\Gamma > 2v|Q|$, in the opposite regime $2v|Q| \gg \Gamma \sim \Delta$ noise will affect mainly SS. In these conditions weakly damped ZB oscillations may coexist with overdamped SS, or at least with a substantial incoherent tail of the wave-packet. This conclusion depends on the low-frequency behavior of the spectral density, holding for instance in the ohmic case $J_P(\omega) \sim \omega$.

7.4 Further remarks and conclusions

We have discussed the dynamics of one-dimensional wave-packets in the presence of noise, however many qualitative conclusions can be extended to an arbitrary wave-packet with any finite spread $\Delta_{\mathbf{n}}$ of $K_{\mathbf{n}}$. For instance, since small values of q , corresponding to overdamped modes (except for longitudinal noise), are always present, SS will show an incoherent tail.

An appealing property of ZB in graphene is that, contrary to the case of electron-positron superpositions, ZB oscillations of the wave-packet extend over a mesoscopic distance. For $\langle Q \rangle \gg \Delta$ the amplitude of $\langle \mathbf{r}(\mathbf{t}) \rangle_{\mathbf{ZB}}$ scales as $\sim 1/\langle Q \rangle$. Although it is suppressed for wave-packets centered in the vicinity of the Dirac points, $\langle Q \rangle \ll \Delta$, for suitable values of $\langle Q \rangle$ it may be several hundreds of lattice spacings a large. This is encouraging for possible experiments aiming at observing ZB in graphene. Our results suggest that this is still true for wave-packets with $\langle Q \rangle \ll \min[\Delta, \Gamma/(4v)]$, even in the presence of an incoherent tail.

A general feature of the problem is expressed by the transformation Eq.(7.5). It shows that the pseudo-spin dynamics is very sensitive to low-frequency fluctuations of the environment.

We finally remark that our model shows that the effect of noise on the dynamics of QP's is completely described by the effect on the dynamics of the pseudo-spin. This is also true for controls operated by electromagnetic fields. This fact may be used for studying quantum control of photocurrents in chiral many body system. In this perspective it is worth stressing that effective control of the pseudo-spin dynamics by electromagnetic fields also opens ports to noise, which will have strongly anisotropic effects on the QP's motion.

Bibliography

- [1] G. Falci, M. Morello Baganella, M. Berritta, A. D'Arrigo, and E. Paladino. *Physica E: Low-dimensional Systems and Nanostructures*, **42**(3):584, 2010.
- [2] Walter Greiner. *Relativistic Quantum Mechanics. Wave Equations*. Springer, 2000.
- [3] K. S. Novoselov, A. K. Geim, S. V. Morozov, D. Jiang, Y. Zhang, S. V. Dubonos, I. V. Grigorieva, and A. A. Firsov. *Science*, **306**:666, 2004.
- [4] Gordon W. Semenoff. *Phys. Rev. Lett.*, **53**:2449, 1984.

- [5] A. H. Castro Neto, F. Guinea, N. M. R. Peres, K. S. Novoselov, and A. K. Geim. *Rev. Mod. Phys.*, **81**:109, 2009.
- [6] C. Cohen-Tannoudji, J. Dupont-Roc, and G. Grynberg. *Atom-Photon Interactions*. Wiley, 1998.
- [7] A. Blais L. Frunzio R.-S. Huang J. Majer S. Kumar S. M. Girvin & R. J. Schoelkopf A. Wallraff, D. I. Schuster. *Nature*, **421**:162, 2004.
- [8] Vincent Hakim and Vinay Ambegaokar. *Phys. Rev. A*, **32**:423, 1985.
- [9] A. O. Caldeira and A. J. Leggett. *Phys. Rev. Lett.*, **46**:211, 1981.
- [10] Ulrich Weiss. *Quantum Dissipative Systems (Series in Modern Condensed Matter Physics)*. World Scientific Publishing Company, 2008.
- [11] E. Paladino, L. Faoro, G. Falci, and Rosario Fazio. *Phys. Rev. Lett.*, **88**:228304, 2002.

Appendix A

Superconductin devices

Many coherent superconductive nanodevice are described by an Hamiltonian of the same form.

$$H = E_C \sum_q (q - q_g)^2 |q\rangle \langle q| - \frac{E_J}{2} \sum_q (|q\rangle \langle q+1| + |q+1\rangle \langle q|) \quad (\text{A.1})$$

Is said that such device work in charge, charge-phase or phase regime depending to the ratio $J = \frac{E_J}{E_C}$ is respectively $J \ll 1$, $J \simeq 1$, $J \gg 1$ from this ratio in fact depend also the sensibility to control performed via the charge port $q_g(t)$ or the flux port $E_J(\Phi)$. In this appendix we describe two kind of these device: The transmon characterized by $J \sim 10^2 - 10^3$. The Quantronium with $J \sim 1 - 10$

A.1 The Quantronium

The qubit demonstrated by the Saclay group [1] is based on a Cooper pair box implemented by a SQUID geometry (Fig. A.1). The main difference in the design with respect to the charge qubit is the presence of an extra large Josephson junction in the loop, whose phase ϕ_t is in principle an extra dynamical quantum variable, but in practice it behaves classically . This provides a second control port for the qubit, since a current bias I_x fixes ϕ_t and consequently the total phase across the two smaller junctions connecting the island to the rest of the circuit. The effective Hamiltonian is again Eq.A.1 where $V_J(\phi) = E_j(\Phi) \cos \phi_t \cos \hat{\phi}$. This two-port design gives the possibility of using two knobs to tune optimally the device when processing and moreover it to use the large junction to measure the circulating current rather than the charge in the island. This allows efficient manipulation with AC pulses coupled to the qubit charge. The matrix element of the charge operator \hat{q} that couples with the external control are shown in Fig.A.1b At low temperatures the dynamics is restricted to at most the two lowest eigenstates $|\phi_0\rangle, |\phi_1\rangle$ and the qubit Hamiltonian is obtained by projecting Eq.A.1 onto this subspace

$$\mathcal{H}_Q = \Omega |\phi_1\rangle \langle \phi_1| = -\frac{1}{2}\Omega\sigma_3 \quad (\text{A.2})$$

where the pseudospin operator $\sigma_3 = |\phi_0\rangle \langle \phi_0| - |\phi_1\rangle \langle \phi_1|$. The energy split Ω between the two lowest eigenstates depends on the gate charge q_x and the total phase ϕ_t . The projection of the charge operator read

$$P\hat{q}P - \frac{1}{2}(q_{00} + q_{11}) = -\frac{1}{2}(q_{11} - q_{00}) + q_{01}\sigma_1 = \frac{1}{2}\bar{q}\sigma_z \quad (\text{A.3})$$

where the matrix element q_{ij} of \hat{q} in the eigenbasis can be made real for proper choice of the phases of the eigenstates. We define $\bar{q} = \sqrt{(q_{00} - q_{11})^2 + (q_{01} + q_{10})^2}$

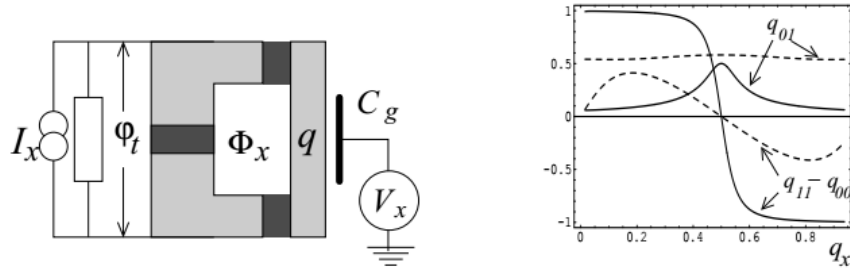


Figure A.1: (a) The two-port Cooper pair box implementing the Quantronium. External control is operated via AC pulses $V_x(t)$ during processing and via step pulses $I_x(t)$ for measurement. (b) Projected matrix elements of the charge operator. In the Quantronium (dashed lines) the first two eigenstates are less distinguishable by the different average charge than in a charge qubit (solid lines). Nonvanishing off-diagonal charge matrix elements allow coupling with an external AC control field $V_x(t)$

and the pseudo spin operator $\sigma_1 = |\phi_0\rangle\langle\phi_1| + |\phi_1\rangle\langle\phi_0|$ Eq.A.3 gives $\sigma_z = \cos\theta\sigma_3 - \sin\theta\sigma_1$ where $\tan\theta = \frac{2q_{01}}{q_{11}-q_{00}}$. Due to large E_J charge states are not good computational state. Instead the convenient choice is to bias the system at $q_x = \frac{1}{2}$, corresponding to $\theta = \frac{\pi}{2}$. Then $\sigma_3 = \sigma_x$ and the computational states are eigenstates of the current circulating in the loop, which is also the measured quantity .

A.2 Transmon

The transmon [2] is a superconducting qubit design with an Hamiltonian of the same form of the Quantronium and of the Cooper pair box but with a large value of $J = \frac{E_J}{E_C}$ ($J \sim 10^3 - 10^4$). It is possible to approximate the Hamiltonian with a power series to 4-th order of the potential $U(\phi) = E_J(1 - \cos\phi) \simeq -E_J + \frac{E_J}{2}\phi^2 - \frac{E_J}{24}\phi^4$, then the total Hamiltonian take the same form of that of the Harmonic oscillator with a quartic term. Writing this Hamiltonian in term of the ladder operator [3, 4]

$$H = \sqrt{2E_J E_C}(\hat{b}^\dagger \hat{b} + \frac{1}{2}) - \frac{E_J}{48}(\hat{b} + \hat{b}^\dagger)^4$$

(where a constant term E_J is neglected) it is evident that the quartic term, in the limit $E_J \gg E_C$ is perturbative, then the energy spectrum have the form

$$E_n = \sqrt{2E_J E_C}(n + \frac{1}{2}) - \frac{E_J}{16}(2n^2 + 2n + 1) \quad (\text{A.4})$$

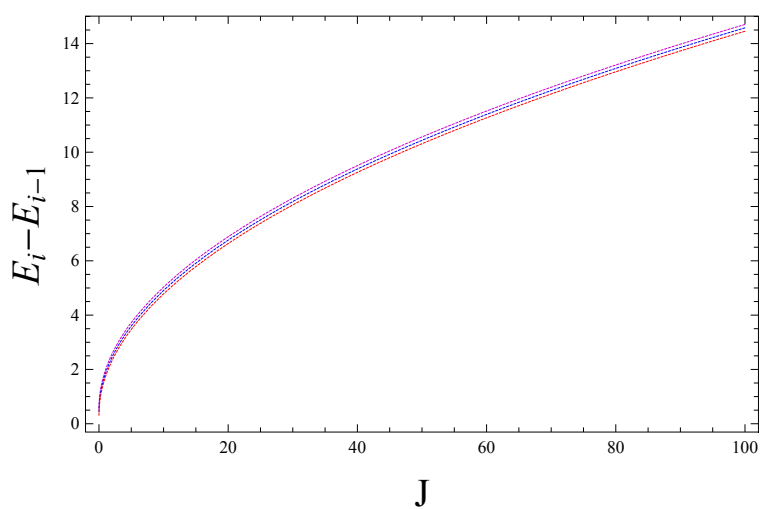


Figure A.2: Perturbative calculation of the energy splitting.

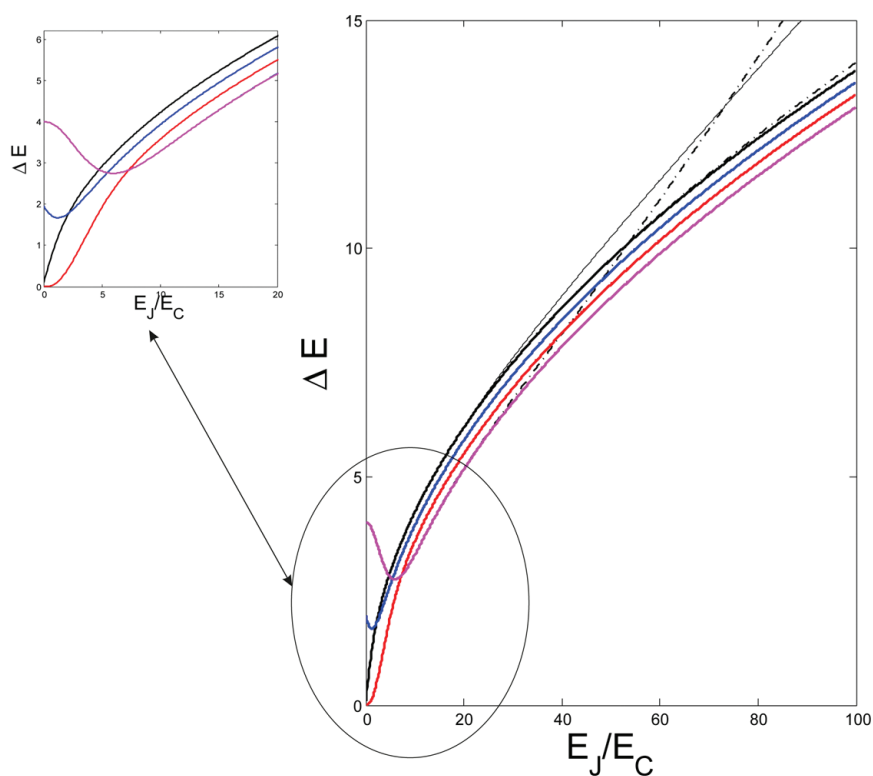


Figure A.3: Numerical calculation of the energy splitting.

where the last term in E_J guarantees the anharmonicity of the spectrum necessary for the purpose of using this device in quantum computation.

Bibliography

- [1] D. Vion, A. Aassime, A. Cottet, P. Joyez, H. Pothier, C. Urbina, D. Esteve, and M. H. Devoret. *Science*, **296**:886, 2002.
- [2] Jens Koch, Terri M. Yu, Jay Gambetta, A. A. Houck, D. I. Schuster, J. Majer, Alexandre Blais, M. H. Devoret, S. M. Girvin, and R. J. Schoelkopf. *Phys. Rev. A*, **76**:042319, 2007.
- [3] J. J. Sakurai. *Modern Quantum Mechanics (Revised Edition)*. Addison Wesley, 1 edition, 1993.
- [4] Claude Cohen-Tannoudji, Bernard Diu, Frank Laloe, and Bernard Dui. *Quantum Mechanics (2 vol. set)*. Wiley-Interscience, 2006.

Appendix B

Average Hamiltonian theory for three photon STIRAP

In this appendix we perform a more formal derivation of the eq.5.24. We start with the model Hamiltonian for the *three-photon* realization of the STIRAP process in RWA and with the resonant approximation.

$$H(t) = \begin{pmatrix} 0 & \frac{1}{2}\Omega_{p_1}^*(t)e^{i\phi_{p_1}(t)} & 0 \\ \frac{1}{2}\Omega_{p_1}(t)e^{i\phi_{p_1}(t)} & E_1 & \frac{1}{2}\Omega_{p_2}^*(t)e^{i\phi_{p_2}(t)} + \frac{1}{2}\Omega_s^*(t)e^{i\phi_s(t)} \\ 0 & \frac{1}{2}\Omega_{p_2}(t)e^{i\phi_{p_2}(t)} + \frac{1}{2}\Omega_s(t)e^{i\phi_s(t)} & E_2 \end{pmatrix} \quad (\text{B.1})$$

B.1 Appropriate reference frame for the model Hamiltonian

We perform a transformation to a rotating frame using an unitary transformation

$$U_{rf}(t) = e^{-i(\phi_{p_1}(t)P_{11} + \phi_{p_2}(t)P_2)} \quad (\text{B.2})$$

where $P_{ij} = |i\rangle\langle j|$. Then we prevent to the Hamiltonian

$$H_{rf}(t) = \begin{pmatrix} 0 & \frac{1}{2}\Omega_{p_1}^*(t) & 0 \\ \frac{1}{2}\Omega_{p_1}(t) & \delta_2 & \frac{1}{2}\Omega_{p_2}^*(t) + \frac{1}{2}\Omega_s^*(t)e^{i\phi(t)} \\ 0 & \frac{1}{2}\Omega_{p_2}(t) + \frac{1}{2}\Omega_s(t)e^{i\phi(t)} & \delta_p \end{pmatrix} \quad (\text{B.3})$$

where $\dot{\phi}(t) = \delta(t) - \delta_2(t)$ and $\delta(t) = \delta_p(t) - \delta_s(t)$. The amplitude envelope $\Omega_i(t)$ are adiabatic as in the traditional STIRAP than for the next calculation we will consider them constant in time. We perform the derivation with a method defined in the Average Hamiltonian theory [1]. To this end we perform an other unitary transformation

$$U(t) = e^{-i(\delta_2 t P_{11} + \delta_p t P_{22})} \quad (\text{B.4})$$

The effective Hamiltonian in this reference frame is

$$\tilde{H} = \frac{1}{2} \begin{pmatrix} 0 & \Omega_{p_1}^* e^{i\delta_2 t} & 0 \\ \Omega_{p_1}^* e^{i\delta_2 t} & 0 & \Omega_{p_2} e^{i(\delta_p - \delta_2)t} + \Omega_s e^{i\delta_s t} \\ 0 & \Omega_{p_2} e^{-i(\delta_p - \delta_2)t} + \Omega_s e^{-i\delta_s t} & 0 \end{pmatrix} \quad (\text{B.5})$$

B.2 Time evolution operator

In quantum mechanics the Hamiltonian is directly correlated to the time evolution operator. In fact it is possible write a formal relation for the time evolution operator that make use of the *time-ordering*

$$U(t) = \mathcal{T} \left\{ e^{-i \int_0^t H(t) dt} \right\} \quad (\text{B.6})$$

Despite it's simplicity in this formal expression some problem arise due to the presence of the *time-ordering* \mathcal{T} . In fact its presence stays for

$$\mathcal{U}(t) = \lim_{\Delta t_i \rightarrow 0} e^{-iH(t_N)\Delta t_N} e^{-iH(t_{N-1})\Delta t_{N-1}} \dots e^{-iH(t_2)\Delta t_2} e^{-iH(t_1)\Delta t_1} \quad (\text{B.7})$$

However the Magnus expansion help us to write an approximate form of such propagator. The Magnus expansion is

$$e^A e^B = e^C; \quad C = A + B - \frac{1}{2}[A, B] + \dots \quad (\text{B.8})$$

It's possible apply this relation to two consecutive term of eq.B.7

$$e^{-iH(t_1)\Delta t_1} + e^{-iH(t_2)\Delta t_2} = e^{-i(H(t_1)\Delta t_1 + H(t_2)\Delta t_2) + \frac{1}{2}[H(t_1), H(t_2)]\Delta t_1 \Delta t_2}$$

and iterating

$$\mathcal{U}(t) = e^{-i \sum H(t_i)\Delta t_i + \frac{1}{2} \sum_{i,j} [H(t_i), H(t_j)]\Delta t_i \Delta t_j}$$

then performing the limit $\lim_{\Delta t_i} \rightarrow 0$

$$\mathcal{U}(t) = e^{-i \int_0^t H(t') dt' - \frac{i}{2} \int_0^t dt' \int_0^{t'} dt'' [H(t''), H(t')]} \quad (\text{B.9})$$

The crucial idea of the average Hamiltonian theory is to approximate the exponent in the approximate propagator eq. B.9 performing a coarse graining and making the ansatz that the information on the initial Hamiltonian are lost due to the fast oscillation. Then it consist in the approximation of the propagator with

$$\mathcal{U}(t) = e^{-iH_{eff}t}; \quad H_{eff} = \int_0^{T_{cg}} \frac{dt'}{T_{cg}} H(t') - \frac{i}{2} \int_0^{T_{cg}} \frac{dt'}{T_{cg}} \int_0^{t'} [H(t''), H(t')] \quad (\text{B.10})$$

In our case we choose a coarse graining such that $\frac{1}{\delta_{s,p}} \ll T \ll \frac{1}{\delta_2}$ and $T \ll \frac{1}{\delta_2 - \delta_p}$. The Stokes term are treated in the term derivating from the first order of the Magnus expansion

$$H_{eff}^S = \int_0^{T_{cg}} \frac{dt'}{T_{cg}} H(t') \simeq \frac{1}{2} \begin{pmatrix} 0 & 0 & 0 \\ 0 & 0 & \Omega_s e^{i\delta_s t} \\ 0 & \Omega_s e^{i\delta_s t} & 0 \end{pmatrix} \quad (\text{B.11})$$

The rest of the effective Hamiltonian is derived from the second order term of the Magnus expansion

$$H_{eff}^2 = \frac{i}{2} \int_0^{T_{cg}} \frac{dt'}{T_{cg}} \int_0^{t'} [H(t''), H(t')] \simeq \begin{pmatrix} S_1 & 0 & \frac{1}{2}\tilde{\Omega}_p \\ 0 & \delta_2 - S_1 - S_2 & 0 \\ \frac{1}{2}\tilde{\Omega}_p & 0 & S_2 \end{pmatrix} \quad (\text{B.12})$$

where $S_i, \tilde{\Omega}_p$ are the same obtained from the correction to the adiabatic elimination in chapter 5.

Bibliography

- [1] U. Haebleren and J. S. Waugh. *Phys. Rev.*, **175**:453, 1968.

Bibliography

- [1] R. Fazio G.Falci. *Quantum Computer, Algorithms and Chaos.*, chapter Quantum computation with Josephson qubits, pages 363–413. B.L. Altshuler and V. Tognetti IOS Press The Netherlands.
- [2] Marlan O. Scully and M. Suhail Zubairy. Cambridge University Press, 1 edition, 1997.
- [3] C. Cohen-Tannoudji, J. Dupont-Roc, and G. Grynberg. *Atom-Photon Interactions.* Wiley, 1998.
- [4] Jens Siewert, Tobias Brandes, and G. Falci. *Phys. Rev. B*, **79**:024504, 2009.
- [5] G. Falci, A. D’Arrigo, A. Mastellone, and E. Paladino. *Phys. Rev. Lett.*, **94**:167002, 2005.
- [6] Ulrich Weiss. *Quantum Dissipative Systems (Series in Modern Condensed Matter Physics)*. World Scientific Publishing Company, 2008.
- [7] G Falci, M Berritta, A Russo, A D’Arrigo, and E Paladino. *Physica Scripta*, **2012**(T151):014020, 2012.
- [8] Gustavsson Yan F. Yoshihara F. Harrabi K. Fitch G. Cory D. G. Nakamura Y. Tsai J. Oliver W. D. Bylander, J. *Nat Phys*, **7**:565, 2011.
- [9] N. V. Vitanov, M. Fleischhauer, B. W. Shore, and K. Bergmann. *Adv. Atom. Mol. Opt. Phy.*, **46**:55, 2001.
- [10] D’Arrigo A. Paladino E. Berritta M. Falci G. La Cognata, A. *submitted to Phys. Rev. B*.
- [11] S. Saito, T. Meno, M. Ueda, H. Tanaka, K. Semba, and H. Takayanagi. *Phys. Rev. Lett.*, **96**:107001, 2006.

- [12] A. Lupaşcu, P. Bertet, E. F. C. Driessen, C. J. P. M. Harmans, and J. E. Mooij. *Phys. Rev. B*, **80**:172506, 2009.
- [13] U. Haeblerlen and J. S. Waugh. *Phys. Rev.*, **175**:453, 1968.
- [14] P. Caldara, A. La Cognata, D. Valenti, B. Spagnolo, M. Berritta, E. Paladino, and G. Falci. *International Journal of Quantum Information*, **09**:119, 2011.
- [15] K. S. Novoselov, A. K. Geim, S. V. Morozov, D. Jiang, Y. Zhang, S. V. Dubonos, I. V. Grigorieva, and A. A. Firsov. *Science*, **306**:666, 2004.
- [16] Gordon W. Semenoff. *Phys. Rev. Lett.*, **53**:2449, 1984.
- [17] G. Falci, M. Morello Baganella, M. Berritta, A. D'Arrigo, and E. Paladino. *Physica E: Low-dimensional Systems and Nanostructures*, **42**(3):584, 2010.
- [18] S. V. Syzranov, M. V. Fistul, and K. B. Efetov. *Phys. Rev. B*, **78**:045407, 2008.
- [19] J. J. Sakurai. *Modern Quantum Mechanics (Revised Edition)*. Addison Wesley, 1 edition, 1993.
- [20] Claude Cohen-Tannoudji, Bernard Diu, Frank Laloe, and Bernard Dui. *Quantum Mechanics (2 vol. set)*. Wiley-Interscience, 2006.
- [21] G. Mahler and V.A. Weberruss. *Quantum networks: dynamics of open nanostructures*. Springer, 1995.
- [22] G. Falci. Quantum dynamics. Notes for Ph.D. course on *Quantum dynamics* at the University of Palermo, 2009-2010.
- [23] Wojciech Hubert Zurek. *Rev. Mod. Phys.*, **75**:715, 2003.
- [24] Michael A. Nielsen and Isaac L. Chuang. *Quantum Computation and Quantum Information (Cambridge Series on Information and the Natural Sciences)*. Cambridge University Press, 1 edition, 2004.
- [25] William R. Frensley. *Rev. Mod. Phys.*, **62**:745, 1990.
- [26] A. O. Caldeira and A. J. Leggett. *Phys. Rev. Lett.*, **46**:211, 1981.
- [27] A.O Caldeira and A.J Leggett. *Annals of Physics*, 149(**2**):374, 1983.
- [28] Yu. Pashkin Y. Nakamura and J. S. Tsai. *Nature*, **398**:786, 1999.

- [29] K. Bergmann, H. Theuer, and B. W. Shore. *Rev. Mod. Phys.*, **70**:1003, 1998.
- [30] T. D. Ladd, F. Jelezko, R. Laflamme, Y. Nakamura, C. Monroe, and J. L. O'Brien. *Nature*, **464**:45, 2010.
- [31] J. Clarke and F.K. Wilhelm. *Nature*, **453**:1031, 2008.
- [32] R. J. Schoelkopf and S. M. Girvin. *Nature*, **451**:664, 2008.
- [33] D. Vion, A. Aassime, A. Cottet, P. Joyez, H. Pothier, C. Urbina, D. Esteve, and M. H. Devoret. *Science*, **296**:886, 2002.
- [34] Sankar Das Sarma, Michael Freedman, and Chetan Nayak. *Physics Today*, **59**:32, 2006.
- [35] Nori Franco You, J. Q. *Nature*, **474**:589, 2011.
- [36] E. Paladino, A. Mastellone, A. D'Arrigo, and G. Falci. *Phys. Rev. B*, **81**:052502, 2010.
- [37] F Chiarello, E Paladino, M G Castellano, C Cosmelli, A D'Arrigo, G Torrioli, and G Falci. *New Journal of Physics*, **14**:023031, 2012.
- [38] G. Ithier, E. Collin, P. Joyez, P. J. Meeson, D. Vion, D. Esteve, F. Chiarello, A. Shnirman, Y. Makhlin, J. Schrieffer, and G. Schön. *Phys. Rev. B*, **72**:134519, 2005.
- [39] F. Bloch. *Phys. Rev.*, **70**:460, 1946.
- [40] Alfred G. Redfield. *Phys. Rev.*, **98**:1787, 1955.
- [41] F. Bloch. *Phys. Rev.*, **105**:1206, 1957.
- [42] Melvin Lax. *Phys. Rev.*, **129**:2342, 1963.
- [43] Heinz-Peter Breuer and Francesco Petruccione. *The Theory of Open Quantum Systems*. Oxford University Press, USA, 2007.
- [44] C. W. Gardiner. *Quantum Noise: A Handbook of Markovian and Non-Markovian Quantum Stochastic Methods with Applications to Quantum Optics*. Springer Berlin Heidelberg, 2010.
- [45] E. Geva and R. Kosloff. *Journal of chemical physics*, **102**:8541, 1995.
- [46] Vittorio Gorini, Andrzej Kossakowski, and E. C. G. Sudarshan. *Journal of Mathematical Physics*, **17**:821, 1976.

- [47] G. Lindblad. *Communications in Mathematical Physics*, **48**:119, 1976.
- [48] A. La Cognata, P. Caldara, D. Valenti, B. Spagnolo, A. D'Aarrigo, E. Paladino, and G. Falci. *International Journal of Quantum Information*, **09**:1, 2011.
- [49] A. B. Zorin, F.-J. Ahlers, J. Niemeyer, T. Weimann, H. Wolf, V. A. Krupenin, and S. V. Lotkhov. *Phys. Rev. B*, **53**:13682, 1996.
- [50] Y. Nakamura, Yu. A. Pashkin, and J. S. Tsai. *Phys. Rev. Lett.*, **87**:246601, Nov 2001.
- [51] I. Chiorescu, Y. Nakamura, C. J. P. M. Harmans, and J. E. Mooij. *Science*, **299**:1869, 2003.
- [52] John M. Martinis, S. Nam, J. Aumentado, and C. Urbina. *Phys. Rev. Lett.*, **89**:117901, 2002.
- [53] Yang Yu, Siyuan Han, Xi Chu, Shih-I Chu, and Zhen Wang. *Science*, **296**:889, 2002.
- [54] A. J. Hoffman, S. J. Srinivasan, J. M. Gambetta, and A. A. Houck. *Phys. Rev. B*, **84**:184515, 2011.
- [55] Tatsuya Kutsuzawa, Hirotaka Tanaka, Shiro Saito, Hayato Nakano, Kouichi Semba, and Hideaki Takayanagi. *Applied Physics Letters*, **87**:073501, 2005.
- [56] I. Chiorescu, P. Bertet, K. Semba, Y. Nakamura, C. J. P. M. Harmans, and J. E. Mooij. *Nature*, **431**:159, 2004.
- [57] Jürgen Lisenfeld, Clemens Müller, Jared H. Cole, Pavel Bushev, Alexander Lukashenko, Alexander Shnirman, and Alexey V. Ustinov. *Phys. Rev. B*, **81**:100511, 2010.
- [58] V. I. Shnyrkov, D. Born, A. A. Soroka, and W. Krech. *Phys. Rev. B*, **79**:184522, 2009.
- [59] A. Fedorov, A. K. Feofanov, P. Macha, P. Forn-D'iaz, C. J. P. M. Harmans, and J. E. Mooij. *Phys. Rev. Lett.*, **105**:060503, 2010.
- [60] E. Arimondo. V coherent population trapping in laser spectroscopy. volume **35** of *Progress in Optics*, page 257. Elsevier, 1996.
- [61] B. W. Shore N. V. Vitanov, T. Halfmann and K. Bergmann. *Annu. Rev. Phys. Chem.*, **52**:763, 2001.

- [62] M. H. S. Amin, A. Yu. Smirnov, and Alec Maassen van den Brink. *Phys. Rev. B*, **67**:100508, 2003.
- [63] J. Siewert and T. Brandes. *Adv. Solid State Phys.*, **44**:181, 2004.
- [64] K. V. R. M. Murali, Z. Dutton, W. D. Oliver, D. S. Crankshaw, and T. P. Orlando. *Phys. Rev. Lett.*, **93**:087003, 2004.
- [65] Yu-xi Liu, J. Q. You, L. F. Wei, C. P. Sun, and Franco Nori. *Phys. Rev. Lett.*, **95**:087001, 2005.
- [66] M. J. Storz *et al.* M. Mariani. *arXiv:cond-mat/0509737v2*, 2005.
- [67] Katarina Cicak Fabio Altomare Jae I. Park Raymond W. Simmonds Mika A. Sillanpää Jian Li, G. S. Paraoanu and Pertti J. Hakonen. *Scientific Reports 2*, Art. num. 645, 2012. 1038/srep00645.
- [68] Ioannis Thanopoulos, Petr Král, and Moshe Shapiro. *Phys. Rev. Lett.*, **92**:113003, 2004.
- [69] F. Nori J.Q, You. **474**:589.
- [70] Yury P. Bliokh, Sergey Savel'ev, and Franco Nori. *Phys. Rev. Lett.*, **100**:244803, 2008.
- [71] Vitanov. *Manipulating Quantum Structures Using Laser Pulses*. Cambridge.
- [72] T. Brandes J. Siewert and G. Falci. *Opt. Comm.*, **264**:435, 2006.
- [73] Mika A. Sillanpää, Jian Li, Katarina Cicak, Fabio Altomare, Jae I. Park, Raymond W. Simmonds, G. S. Paraoanu, and Pertti J. Hakonen. *Phys. Rev. Lett.*, **103**:193601, 2009.
- [74] M. Baur, S. Filipp, R. Bianchetti, J. M. Fink, M. Göppl, L. Steffen, P. J. Leek, A. Blais, and A. Wallraff. *Phys. Rev. Lett.*, **102**:243602, 2009.
- [75] A. A. Abdumalikov, O. Astafiev, A. M. Zagoskin, Yu. A. Pashkin, Y. Nakamura, and J. S. Tsai. *Phys. Rev. Lett.*, **104**:193601, 2010.
- [76] R. Bianchetti, S. Filipp, M. Baur, J. M. Fink, C. Lang, L. Steffen, M. Boissonneault, A. Blais, and A. Wallraff. *Phys. Rev. Lett.*, **105**:223601, 2010.

- [77] William R. Kelly, Zachary Dutton, John Schlafer, Bhaskar Mookerji, Thomas A. Ohki, Jeffrey S. Kline, and David P. Pappas. *Phys. Rev. Lett.*, **104**:163601, 2010.
- [78] P. Joyez D. Esteve V. Bouchiat, D. Vion and M. H. Devoret. *Physica Scripta*, **T 76**:165, 1998.
- [79] T. Duty, D. Gunnarsson, K. Bladh, and P. Delsing. *Phys. Rev. B*, **69**:140503, 2004.
- [80] A. Blais L. Frunzio R.-S. Huang J. Majer S. Kumar S. M. Girvin & R. J. Schoelkopf A. Wallraff, D. I. Schuster. *Nature*, **421**:162, 2004.
- [81] Jens Koch, Terri M. Yu, Jay Gambetta, A. A. Houck, D. I. Schuster, J. Majer, Alexandre Blais, M. H. Devoret, S. M. Girvin, and R. J. Schoelkopf. *Phys. Rev. A*, **76**:042319, 2007.
- [82] E. Collin, G. Ithier, A. Aassime, P. Joyez, D. Vion, and D. Esteve. *Phys. Rev. Lett.*, **93**:157005, 2004.
- [83] Chad Rigetti, Jay M. Gambetta, Stefano Poletto, B. L. T. Plourde, Jerry M. Chow, A. D. Córcoles, John A. Smolin, Seth T. Merkel, J. R. Rozen, George A. Keefe, Mary B. Rothwell, Mark B. Ketchen, and M. Steffen. *Phys. Rev. B*, **86**:100506, 2012.
- [84] E. Paladino, L. Faoro, G. Falci, and Rosario Fazio. *Phys. Rev. Lett.*, **88**:228304, 2002.
- [85] Daniel Sank, R. Barends, Radoslaw C. Bialczak, Yu Chen, J. Kelly, M. Lenander, E. Lucero, Matteo Mariantoni, A. Megrant, M. Neeley, P. J. J. O'Malley, A. Vainsencher, H. Wang, J. Wenner, T. C. White, T. Yamamoto, Yi Yin, A. N. Cleland, and John M. Martinis. *Phys. Rev. Lett.*, **109**:067001, 2012.
- [86] P. A. Ivanov, N. V. Vitanov, and K. Bergmann. *Phys. Rev. A*, **70**:063409, 2004.
- [87] A. D'Arrigo G. Falci, A. Mastellone and E. Paladino. *Phys. Rev. Lett.*, **13**:323, 2006.
- [88] T. B̃ondo A. K̃uhn, M. H̃enrich and G. Rempe. *Appl. Phys. B*, **69**:373, 1999.
- [89] Q. Shi and E. Geva. *Journal of chemical physics*, **119**:11773, 2003.

- [90] C. J.P. M. Harmans I. Chiorescu, Y. Nakamura and J. E. Mooij. *Science*, **299**:1869, 2003.
- [91] O. Astafiev Y. Nakamura T. Yamamoto, Yu.A. Pashkin and J. S. Tsai. *Nature*, **425**:941, 2003.
- [92] A. C.J. ter Haar-C. J.P. M. Harmans J. B. Majer, F. G. Paaauw and J. E. Mooij. *Phys. Rev. Lett.*, **94**:090501, 2005.
- [93] L. M. K. Vandersypen and I. L. Chuang. *Rev. Mod. Phys.*, **76**:1037, 2005.
- [94] Heer R. Strasser G. Rakoczy, D. and Smoliner J. *Physica E*, **16**:129, 2003.
- [95] M. Hanggi P. Thorwart, M. Grifoni. *Annals of physics*, **293**:15, 2001.
- [96] S. Dorsey A. T. Fisher M. Garg A. Leggett, A. J. Chakravarty and W. Zwerger. *Rev. Mod. Phys.*, **59**:1, 1987.
- [97] M. Grifoni and P. Hanggi. *phys. Rep.*, **304**:229, 1998.
- [98] A. J. Leggett. *Phys. Rev. B*, **30**:1208, 1984.
- [99] Chung-Hsien Chou, Ting Yu, and B. L. Hu. *Phys. Rev. E*, **77**:011112, 2008.
- [100] M. Rosenau da Costa, A. O. Caldeira, S. M. Dutra, and H. Westfahl. *Phys. Rev. A*, **61**:022107, 2000.
- [101] N. V. Prokofev and P. C. E. Stamp. *Rep. Prog. Phys.*, **63**:669726, 2000.
- [102] Patel V. Chen W. Tolpygo S. K. Friedman, J. R. and J. E. Lukens. *Nature*, **406**:43, 2000.
- [103] F. Grossmann, T. Dittrich, P. Jung, and P. Hänggi. *Phys. Rev. Lett.*, **67**:516, 1991.
- [104] R. Löfstedt and S. N. Coppersmith. *Phys. Rev. Lett.*, **72**:1947, 1994.
- [105] Lorenza Viola, Emanuel Knill, and Seth Lloyd. *Phys. Rev. Lett.*, **82**:2417, 1999.
- [106] R.P Feynman and F.L Vernon Jr. *Annals of Physics*, **24**:118, 1963.
- [107] G. G. Engerholm D. O. Harris and W. D. Gwinn. *J. Chem. Phys.*, **43**:1515, 1965.

- [108] David O. Harris, Gail G. Engerholm, and William D. Gwinn. *The Journal of Chemical Physics*, **43**:1515, 1965.
- [109] Walter Greiner. *Relativistic Quantum Mechanics. Wave Equations*. Springer, 2000.
- [110] A. H. Castro Neto, F. Guinea, N. M. R. Peres, K. S. Novoselov, and A. K. Geim. *Rev. Mod. Phys.*, **81**:109, 2009.
- [111] Vincent Hakim and Vinay Ambegaokar. *Phys. Rev. A*, **32**:423, 1985.